UNIVERSITY OF OKLAHOMA

GRADUATE COLLEGE

APPLICATION OF KINETIC DOPING OF SILICA SOL-GEL THIN FILMS TO INTERNAL COATING OF CAPILLARY TUBES AND DOPING OF BRANCHED POLYETHYLENIMINE

A DISSERTATION

SUBMITTED TO THE GRADUATE FACULTY

in partial fulfillment of the requirements for the

Degree of

DOCTOR OF PHILOSOPHY

By

JESSICA JENSEN
Norman, Oklahoma
2020

APPLICATION OF KINETIC DOPING OF SILICA SOL-GEL THIN
FILMS TO INTERNAL COATING OF CAPILLARY TUBES AND
DOPING OF BRANCHED POLYETHYLENIMINE

A DISSERTATION APPROVED FOR THE

DEPARTMENT OF CHEMISTRY AND BIOCHEMISTRY

BY THE COMMITTEE CONSISTING OF

Dr. Wai Tak Yip, Chair

Dr. Charles V. Rice

Dr. Susan J. Schroeder

Dr. Daniel T. Glatzhofer

Dr. Lloyd A. Bumm

TABLE OF CONTENTS

ABSTRACT

The applications of kinetic doping in silica sol-gel thin films are a mostly under-developed area. Previously, our lab has demonstrated a high loading capacity for cationic dye and protein guest molecules in silica thin films coated on flat-surface coverslips. Expanding on this work, we hypothesized that doping of films internally on capillary tubes was possible, with the aim of developing protocols for loading enzymes on these substrates. Such devices could be very useful for biocatalysis in microfluidic devices. Additionally, we theorized that branched polyethylenimine (BPEI) could be loaded into a silica thin film with kinetic doping. An organic molecule with a cationic charge at neutral pH, BPEI was a good candidate for kinetic doping and could not be loaded via traditional methods. Loading of BPEI could produce films and coatings that are useful in heavy metal remediation or inhibition of biofilm formation.

In chapter three, kinetic doping is applied to loading internally coated capillary tubes. Parameters for internally doping capillary tubes were developed with rhodamine 6G, producing internally coated thin films with approximately 90 nm thickness. Horseradish peroxidase (HRP) was loaded into the thin films, with a 47000X increase in concentration over the loading solution. Activity of the loaded HRP was determined to be 0.019 ± 0.003 U/mg, and it was shown to have a stronger resistance to denaturation by methanol than surface-adsorbed HRP.

In chapter four, kinetic doping was utilized to functionalize silica thin films with 25000 MW BPEI. To our knowledge, this is the first time that a highly basic guest such as BPEI has been doped into silica thin films. Parameters for the kinetic doping of 1800 and 750000 MW BPEI into silica sol-gel thin films were developed in chapter 5. Solvent accessible amines were quantified: 25000 and 750000 MW BPEI doped films were found to have similar amounts of amines while 1800 MW BPEI doped films had significantly less. SEM images of the films revealed drastic morphology differences between the films.

Two applications of these films were tested. The 25000 MW films were tested for copper (II) sequestration to assess their potential for heavy metal sequestration, and showed high loading capacity of 10 ± 6 mmol/g. They proved to be reusable, with only a 6% reduction in the amount of copper (II) ions sequestered by the third use. The films were also stable against leaching over the course of one week in solution, with less than 1% of the original BPEI lost under various storage conditions. The efficacy of the 1800, 25000, and 750000 MW films against *S. epidermis* biofilms were tested with a crystal violet assay, and all films proved to be effective in inhibiting biofilm formation (*p*-value < 0.05). The best dopant, 25000 MW BPEI, caused an 89% reduction in biofilm growth and surpassed the performance of the clinical antibiotic gentamycin (*p*-value < 0.003).

Most of the results in chapters three and five are pending publication at this time. Most of the results in chapter four have been previously published in 2019 in ACS Omega (Jensen, J. M.; Yip, W. T., Amine Functionalization of Silica Sol–Gel Thin Films via Kinetic Doping: A Novel, Green Approach. *ACS Omega* 2019**,** *4* (20), 18545-18554.).

CHAPTER 1 - Sol Gel Chemistry

1.1 The Basics of Sol-Gel Chemistry

The term 'sol-gel' comes from the solution-gelation polymerization process whereby the initial solution reacts when left in open air to form a gel.[1] Silica sol-gel technology was discovered in the 19th century when it was observed that a silica alkoxide solution formed a gel when exposed to air.[2] Since then, extensive research has been conducted on silica sol-gel technology for various applications with untold number of modifications in precursors, coating or deposition technique, and post-synthesis modification.[3-12] One of the most popular types of materials made using sol-gel techniques is silica based, typically derived from tetralkyl orthosilicates like tetraethylorthosilicate (TEOS) or tetramethylorthosilicate (TMOS).[8, 13-14] In this dissertation, sol-gel with TEOS as the precursor is the only type studied.

The formation of silica sol-gels can be broken down into two separate steps: hydrolysis followed by condensation.[15] A schematic of these steps with TEOS as the precursor are shown below in Figure 1.1-3.

Step 1: Hydrolysis
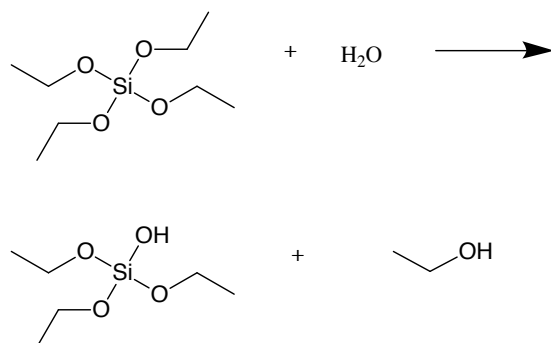
Figure 1 Hydrolysis, the first step in silica sol gel chemistry

Step 2: Condensation
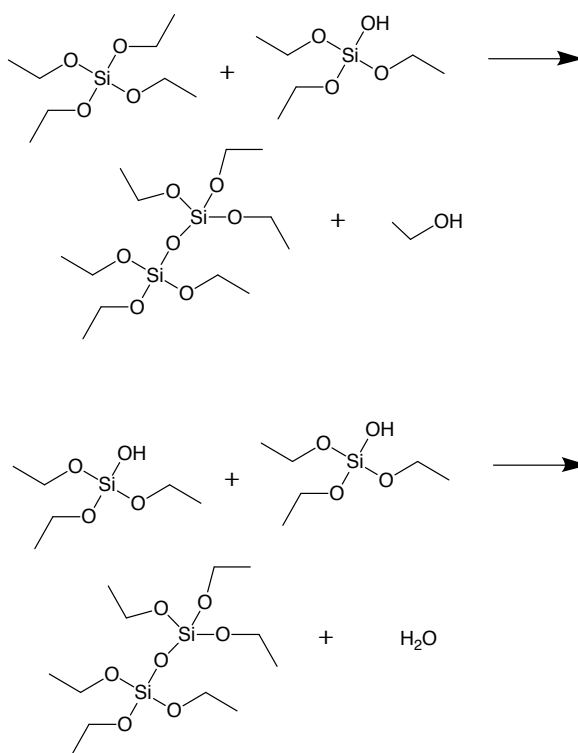
Figure 1.2 Condensation, the second step of silica sol gel chemistry. There are two reactions through which the sol can undergo condensation.
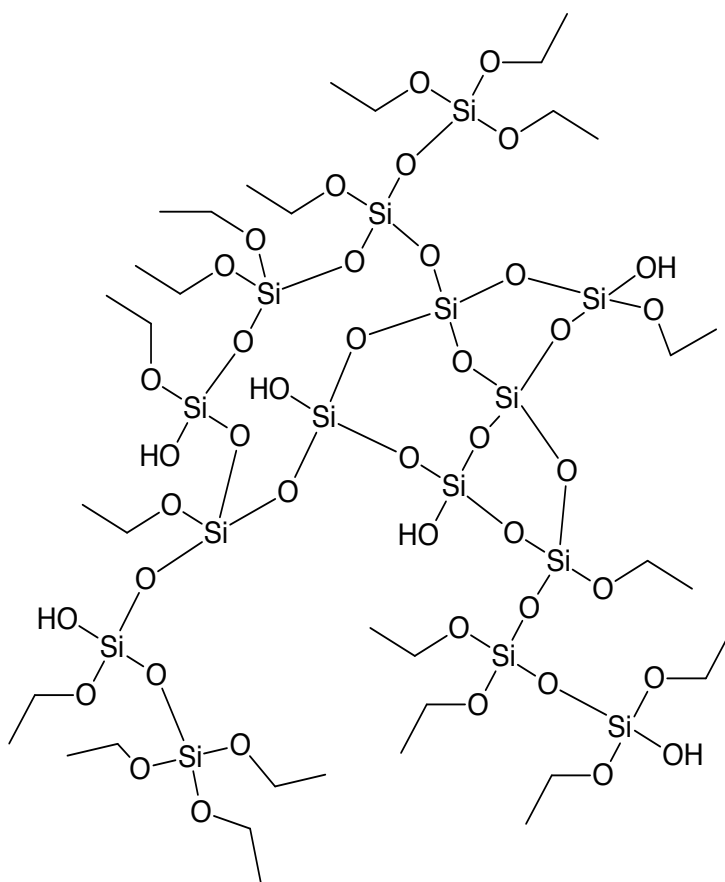
Figure 1.3 Eventually, through repeat hydrolysis and condensation, a 3-dimensional network of silica begins to form, and continues to form Si-O-Si bonds even after the liquid sol mixture has turned into a gel.

An acid or base is used to catalyze the hydrolysis step between a silicon alkoxide and water to produce silanols. Acids, such as phosphoric acid, are generally used to catalyze thin film or monolith formation,[16] while bases are used to catalyze the growth of silica nanoparticles, commonly known as the Stöber process.[17] The partially hydrolyzed precursors then undergo a condensation reaction where the individual silanols react, eliminating ethanol and water, to form a porous, solid, three-dimensional network of

silicon dioxide. These steps are most commonly performed at room temperature and pressure.

The exact mechanism by which the reaction proceeds depends on whether an acid or base is used as a catalyst. When an acid is the catalyst, an alkoxide group of the TEOS is protonated and then attacked by water to form a pentacoordinate transition state. This complex then undergoes decay by releasing ethanol. During the condensation step, a silanol is protonated and becomes electrophilic, making it susceptible to nucleophilic attack by another neutral silanol. This forms a siloxane bond and displaces a protonated water as a by-product. When a base is used as the catalyst, the hydrolysis step proceeds through a rapid dissociation of water into a hydroxyl anion, a nucleophile, which attacks the silicon atom in TEOS to form a pentacoordinated intermediate. The intermediate then decays through the release of an ethoxide anion. The condensation step proceeds through the deprotonation of a silanol that will attack a neutral silanol, forming a penta- or hexacoordinate transition state that will decay by the displacement of an ethoxide anion or hydroxide.

Additionally, pH affects the ratio of the rate of the hydrolysis step to the rate of the condensation step, influencing the resulting structure. Under low pH conditions, caused by using acid as the catalyst, the hydrolysis rate outstrips the rate of condensation, causing the final silica sol-gel to be a weakly branched polymer network. This favors linear polymers that easily form thin films and monoliths. With higher pH conditions, with a base catalyst, the rate of condensation is much faster than the rate of hydrolysis,

resulting in more uniform and closely networked particles. This favors the formation of uniform particles, which is why bases are used to catalyze nanoparticle formation. A neutral pH favors the formation of random aggregates.

After sufficient time, the steps of hydrolysis and polycondensation form macromolecules in the liquid. When the macromolecules are suspended in the solution mixture, the sol-gel is in the 'sol' state, as sol is defined as a colloidal suspension of solid particles in a liquid.[8] As they continue to react and join together to form aggregates, enough Si-O-Si linkages will eventually be formed causing the solution to lose its fluidity and become an elastic solid, hence the gel state. It is worth noting that the hydrolysis and condensation steps do not stop at this stage, continuing to form Si-O-Si bonds. The new bonds will strengthen the silica network, but can cause shrinkage and potential pore collapse.

Silica sol-gels can be categorized in several ways, as alcogels or hydrogels and as xerogels or aerogels. Alcogels and hydrogels are categorized by the dispersion medium used during their formation reaction. Alcogels are the more traditional method of creating sol-gels by using alcohol to mix with the alkoxysilane precursors and water. Alcohol is needed as a homogenizing agent, as water and alkoxysilanes are generally immiscible.[8] Alcogels generally result in silica sol-gels with a dense internal structure.[18] Sol-gels that only use water as the solvent, with no added alcohol to serve as a homogenizing agent, are known as hydrogels. Hydrogels were first proposed in 1987 when Avnir and Kaufman[19] found the alcohol produced as a by-product of the hydrolysis step was enough to homogenize the system with the addition of a buffer solution or growth medium into

the sol after the initial hydrolysis step has proceeded long enough. The ratio of the sol to the buffer solution affects the gelation time and pore size of the final sol-gel. While hydrogels are more labor intensive to synthesize than alcogels, requiring more steps, they are popular for being a more biocompatible process.[20-23]

The method used to dry the silica sol-gel also introduces another categorization: xerogels and aerogels. A xerogel is produced when a sol-gel is allowed to dry through natural evaporation. Producing an aerogel requires replacing the liquid phase of the gel with a gas, often through a supercritical drying process. While a xerogel is easier to produce, they show a much higher degree of shrinkage and a higher percentage of pore collapse as compared to aerogels.[24]

Conditions can be controlled to affect the final state of the silica sol-gel no matter what classification it is. Conditions including the precursor, the molar ratio of the silica precursor to water, the catalyst, the solvent, the reaction conditions like temperature or pressure, the pH, the presence of other molecules in the sol, and the age of the gel, which will continue to change the gel's properties because of the continuous formation of Si-O-Si bonds.[25-34] These factors can be used to control the pore size in the final gelled structure of the silica sol-gel, ranging from 1 nm in diameter up to 200 nm.[25-28, 35] Pore size is especially important when attempting to incorporate a dopant or guest molecule into the silica sol-gel structure. Addition of other molecules to the sol is one method that can induce drastic structural changes. Various types of hybrid sol-gels have been synthesized to tune or add to the properties of silica sol-gels.[36-45] Of particular relevance

to this dissertation is the use of enzymes[46-54] and polymers[55-59] as additives to silica sol-gels.

1.2   Guest-Molecules in a Sol-Gel Matrix

Materials created through the silica sol-gel process are mechanically strong, thermally stable, chemically inert, and largely immune to photodegradation. They utilize mostly mild conditions, are synthesized at room temperature and pressure and can have many of their specific properties chemically tuned. This creates considerable interest in their many potential applications, especially when consideration is given to the functionalization that can be achieved by guest molecules. The ability to load guest molecules in a sol-gel matrix was first made viable in 1984 when Avnir et al. first loaded the organic dye rhodamine 6G into a silica sol-gel matrix.[60] Since then, silica sol-gels that result in bulk materials,[61-63] powders,[64] and thin films[65-69] have all been studied as solid matrices for a wide variety of doped guest molecules.

One of the most popular uses of entrapped guest molecules is for biosensors or biological catalysts that utilize entrapped biological molecules in the silica sol-gel matrix. Many of the advantages of silica sol-gels can be exploited for these sensors, as long as the guest molecules continues to function once entrapped in the silica matrix. This was first achieved in 1984 by Venton et al. when they were able to entrap antiprogesterone antibodies within a monotlithic silica-poly(3-aminopropysiloxane) sol-gel.[70] The antibodies were still able to display the recognition and binding functions of the free antibodies while entrapped in the matrix. Expansion to enzymes came in 1985 when Glad

et al. entrapped glucose oxidase, horseradish peroxidase, living yeast cells, trypsin, and alkaline phosphatase in monolithic and thick-film organic-inorganic sol-gel matrices of silica-poly[N,N-bis(2-hydroxyethyl)-3-aminopropylsiloxane].[71] These entrapped enzymes were able to catalyze their respective substrates and release the products back into solution, but remain entrapped in the matrix.

The generally accepted explanation for guest molecule entrapment is that they are held in the pore spaces inside the silicon dioxide network.[72-74] The average size of the pores play a significant role in the local environment of the guest molecules, with the pore size having an effect on everything from guest molecule incorporation to behavior of the gel itself.[75-77] Additionally, the solvent has a large effect on the entrapped molecule, with many studies showing the environment in pores that are sufficiently large, or with guest molecules that are sufficiently small, is the same as that of a free solution with the same solvent.[78-82] In these cases, the properties of the solvent, notably the composition,[83-84] pH,[85] polarity,[68, 86] and viscosity,[87-88] play the primary role in determining the guest molecule's local environment. With smaller pores or larger molecules, some studies have shown that while enzymes retain enough mobility to remain active, they do exhibit restricted motion within the pores.[14, 68, 78, 85, 89]

Some conditions do not merely trap the guest molecule physically in the sol-gel pores, but instead hydrogen-bonding[90-92] or electrostatic interactions[85, 93] between the wall of the pore and the guest molecule further limit the freedom of the entrapped guest molecule.[94-96] No matter the method of entrapment, there are benefits of immobilization in a sol-gel

matrix, namely high reusability and higher chemical and thermal stability are usually observed from the entrapped guest molecules.[24, 46-47, 49-50, 53, 97-101]

1.3   Traditional Sol-Gel Doping Methods

Two main methods of loading guest molecules into silica sol-gels that do not involve subsequent chemical modification have been well-documented: pre-doping and post-doping.[15, 102] Pre-doping was the first loading method developed, as it was the method used by Avnir et al. when initially loading rhodamine 6G into a silica sol-gel film.[60] It is the most widely used technique for guest molecule loading, whereby the guest molecule is added directly to the precursor solution prior to gelation. This does present challenges for loading guest molecules, especially proteins. Most conventional sol-gel processes result in alcogels, which require the use of alcohol with the precursor at low pH, both of which can easily denature proteins. To load proteins, variations on the hydrogel process have been investigated, replacing alcohol and adding buffers or developing even more elaborate multi-step aqueous processes to protect the proteins from denaturation.[47, 49-51] This can lead to costlier and more labor intensive loading processes, which still pose additional challenges. Regardless of the methods, the amount of guest in the liquid sol must be balanced so that the sol can still properly gel, which imposes a significant constraint to the maximum amount of the guest molecule incorporated.[103-104]

Post-doping is an adsorption process, where the guest is allowed to adsorb onto the inner porous surfaces of an already formed sol-gel material.[105-106] This can result in much lower loading or the need for special selection or modification of the precursor to enhance

adsorption.[107-108] Post-doped films are also more prone to releasing the guest molecule

back into solution.[109] Techniques that chemically graft guest molecules to the sol may

also be considered post-doping, but they are often labor intensive and relatively costly.[110-111]

1.4 Kinetic Doping – A New Doping Approach

Recently, a third method for guest molecule loading was discovered in our laboratory,

called Kinetic Doping. The kinetic doping technique introduces the guest molecule to the

sol-gel matrix while it is still evolving, taking full advantage of the reaction kinetics of

the sol-gel process to enhance guest loading. A nascent film is introduced to a solution of

the desired guest molecule after deposition, when enough hydrolysis and condensation

has occurred to support the film structure, but well before all of the sol-gel reactions have

had time to complete. Loading at this stage of film formation, while the remainder of the

film is still growing, means that most of the alcohol has already been driven off, leading

to milder conditions for protein loading. These conditions are achieved without the

modifications reported in a number of methods that involve stabilizers or extra steps to

produce hybrid gels or hydrogels. [112] Additionally, molecules that may interfere with the

sol-gel chemistry when added to the precursor solution, like basic polymers, could

theoretically be loaded via kinetic doping, as the reaction has already proceeded

sufficiently downstream such that thin film formation will continue unabated even upon

contact with a base.

Campbell et al. has shown that kinetic doping is capable of loading rhodamine 6G at a

concentration many times higher than what was possible with either pre- or post-

doping.[113] Crosley demonstrated that kinetic doping could load enzymes into silica thin films at millimolar concentrations from very dilute loading solutions, resulting in 930X to 2600X increase in concentration.[53] Kinetic doping can also be used on both spin coated and dip coated films, expanding the potential shapes and sizes of substrates for wider applications.[54]

1.5 Drain Coating

There exist several methods to coat a sol-gel thin film on a substrate, with one of the most common being dip or drain coating.[8] Dip or drain coating is a well-studied method used with a variety of coating substances, and patent for drain coating can be found as early as 1910.[114] With dip or drain coating, a substrate is held, generally vertically, in a liquid sol and then either the substrate or the sol solution is removed at a constant speed. This deposits the solution on the surface of the substrate and once coated, the liquid sol will gradually turn into a solid thin film after undergoing the necessary hydrolysis and condensation reactions. The film thickness is mainly determined by solution composition and withdrawal speed.[115-116] Dip or drain coating allows the even coating of irregular surfaces. In this work, the sole method used to coat substrates is drain coating.

Drain coating using a coating solution with comparatively low viscosities (such as the sol prepared in this work) and a withdrawal speed between 1-10 mm/sec can be described by the Landau Levich equation:[117]

$$h_0 = 0.94 \, \frac{(\eta U_0)^{\frac{2}{3}}}{\gamma_{LV}^{1/6}(\rho g)^{1/2}}$$

h_0 is the film thickness, and

η is the viscosity of the liquid coating, and

U_0 is the drain speed, and

γ_{LV} is the ratio of viscous drag to liquid-vapor surface tension, and

ρ is the density of the liquid, and

g is gravitational acceleration.

This is the regime where most dip and drain coating takes place.[8] Using the same sol gel precursor materials as utilized in this work, Crosley found this model to estimate thickness of films within ±10 nm of their measured values.[118] Thus, it is the model used to estimate the thickness of flat-surface coated films for the dye concentration comparison to the internally coated glass capillary tubes reported in Chapter 3.

The same model cannot be directly applied to the results in Chapters 4 and 5, as they are coated at a much higher withdrawal speed. Instead, the general model for drain coating at this high speed can be described by:

$$h = c_1 \left(\frac{\eta U_o}{\rho g}\right)^{\frac{1}{2}}$$

where c_1 is a constant for the fluid being coated, about 0.8 for Newtonian liquids.[119] Unfortunately, films coated at high speed are often uneven,[8] so SEM images were taken to examine the thickness of the films instead and no initial thickness calculation was performed using this equation.

1.6 Internally Coated Glass Capillary Tubes: A Novel Substrate

Using dip-coating and expanding on Crosley's previous work, chapter 3 of this dissertation covers the internal doping of capillary tubes with horseradish peroxidase. Crosley focused on the development of flat-surface films, but there is also interest in devices based on glass capillary tubes or other tubing with internally coating enzymes or other biological materials.[120-122] These types of devices can either rely on capillary action or have solutions of interest driven through them by an external pump and use the loaded biological material as a sensor or catalyst. However, the internal coating of capillary tubes does present additional challenges for creating even internal coatings[123] and for loading, which may have led to less interest in internally coated capillary tubes despite their many desirable traits. To circumvent the challenges, a few research groups have inserted monoliths into capillaries or immobilized enzymes on capillary filters, instead of inside the capillaries themselves.[124-125] Chemical modification of the surfaces for immobilization of enzymes in devices is also commonly required,[126-129] increasing the difficulty and expense of such fabrications.

Based on the flat-surface coating techniques developed by Crosley et al., chapter three of this dissertation concerns the development of internally doped glass capillary tubes. Their

loading and activity were quantified, and the performance of capillary films was compared to that of flat-surface films. Horseradish peroxidase was shown to retain activity, although much reduced from the free enzyme or even that loaded in flat-surface films. However, a large degree of protection was imparted to the films from denaturation by ethanol and methanol.

Most of the results in chapter three are currently pending publication.

1.7 Branched Polyethylenimine: A Polymer With Myriad Uses

In addition to entrapping enzymes, surface functionalization of silica sol gel thin films provides great benefits and there is much interest about it in the literature. One of the biggest groups of interest for silica functionalization is amines, as surface functionalization of silica with various amine-containing compounds has shown anti-fouling effects,[130] increased heavy metal adsorption,[131] chromatography applications,[132] catalytic applications,[133] and more. One of the most interesting molecules for its potential in kinetic doping is branched polyethylenimine (BPEI), which is a polyamine that is commercially available in a wide-range of molecular weights. BPEI has shown great potential for environmental applications such as aqueous heavy metal removal[59, 134] and carbon dioxide capture[135] when attached to a solid substrate and has also shown antimicrobial activity both on its own[136] and as antibiotic potentiators.[137]

BPEI has been loaded into monoliths and nanoparticles, but it has never been successfully loaded into silica thin films, to the best of our knowledge. This is most likely

due to their very basic nature that may significantly impair thin film formation, as basic conditions typically favor nanoparticle formation.[17] Using pre-doping methods would probably be impossible with such a basic polymer. Post-doping methods have employed multiple synthetic steps often with environmentally harmful organic precursors or solvents, resulting in a labor intensive and costly process.[11, 138-139]

Using kinetic doping, we were able to load various molecular weights of BPEI into silica thin films and examine the effect of polymer size on kinetic doping. In chapter four, a 25000 molecular weight (MW) polymer was successfully loaded, but 600 MW BPEI was not. The ability of 25000 MW loaded films to sequester copper was examined and shown to be higher than commercially available products. In chapter five, the loading of 1800 and 750000 MW BPEI was achieved and the effect of molecular weight on the kinetic doping process was systematically examined. The ability of 1800, 25000, and 750000 MW BPEI films to inhibit biofilm formation was examined and compared. These results show the promise of silica functionalized with BPEI and detail an inexpensive, facile method for doing so.

Most of the results in chapter four have been published in 2019 in ACS Omega. (Jensen, J. M.; Yip, W. T., Amine Functionalization of Silica Sol–Gel Thin Films via Kinetic Doping: A Novel, Green Approach. *ACS Omega* 2019**, *4* (20), 18545-18554.)

Most of the results in chapter five are currently pending publication.

1.8   References

1.   Ciriminna, R.; Fidalgo, A.; Pandarus, V.; Beland, F.; Ilharco, L. M.; Pagliaro, M., The Sol-Gel Route to Advanced Silica-Based Materials and Recent Applications. *Chemistry Review (Washington, DC, U. S.)* **2013,** *113* (8), 6592-6620.

2.   Ebelmen, Untersuchungen über die Verbindungen der Borsäure und Kieselsäure mit Aether. *Justus Liebigs Annalen der Chemie* **1846,** *57* (3), 319-355.

3.   Danks, A. E.; Hall, S. R.; Schnepp, Z., The evolution of 'sol–gel' chemistry as a technique for materials synthesis. *Materials Horizons* **2016,** *3* (2), 91-112.

4.   Da'na, E., Adsorption of heavy metals on functionalized-mesoporous silica: A review. *Microporous Mesoporous Materials* **2017,** *247*, 145-157.

5.   Collino, R.; Therasse, J.; Chaput, F.; Boilot, J.-P.; Levy, Y., Biological activity of functionalized SiO2 thin films prepared by sol-gel method. *Journal of Sol-Gel Science and Technology* **1996,** *7* (1/2), 81-85.

6.   Ciriminna, R.; Cara, P. D.; Sciortino, M.; Pagliaro, M., Catalysis with Doped Sol-Gel Silicates. *Advanced Synthesis Catalysis* **2011,** *353* (5), 677-687.

7.   Chaudhuri, H.; Dash, S.; Sarkar, A., Fabrication of New Synthetic Routes for Functionalized Si-MCM-41 Materials as Effective Adsorbents for Water Remediation. *Industrial & Engineering Chemistry Research* **2016,** *55* (38), 10084-10094.

8.   Brinker, C. J.; Scherer, G. W., *Sol-Gel Science: The Physics and Chemistry of Sol-Gel Processing*. United States: Academic Press: 2013.

9.   Allen, J. J.; Rosenberg, E.; Johnston, E.; Hart, C., Sol-Gel Synthesis and Characterization of Silica Polyamine Composites: Applications to Metal Ion Capture. *ACS Applied Materials & Interfaces* **2012,** *4* (3), 1573-1584.

10.   Owens, G. J.; Singh, R. K.; Foroutan, F.; Alqaysi, M.; Han, C.-M.; Mahapatra, C.; Kim, H.-W.; Knowles, J. C., Sol–gel based materials for biomedical applications. *Progress in Materials Science* **2016,** *77*, 1-79.

11.   Kursunlu, A. N.; Guler, E.; Dumrul, H.; Kocyigit, O.; Gubbuk, I. H., Chemical modification of silica gel with synthesized new Schiff base derivatives and sorption studies of cobalt (II) and nickel (II). *Applied Surface Science* **2009,** *255* (21), 8798-8803.

12.   Islam, M. S.; Choi, W. S.; Lee, H.-J., Controlled Etching of Internal and External Structures of SiO2 Nanoparticles Using Hydrogen Bond of Polyelectrolytes. *ACS Applied Materials & Interfaces* **2014,** *6* (12), 9563-9571.

13.   Jeronimo, P. C. A.; Araujo, A. N.; Conceicao, B. S. M. M. M., Optical sensors and biosensors based on sol-gel films. *Talanta* **2007,** *72* (1), 13-27.

14.   Dunn, B.; Zink, J. I., Probes of Pore Environment and Molecule-Matrix Interactions in Sol-Gel Materials. *Chemical Materials* **1997,** *9* (11), 2280-2291.

15.   Dimitriev, Y.; Ivanova, Y.; Iordanova, R., History of sol-gel science and technology (review). *Journal of the University of Chemical Technology and Metallurgy* **2008,** *43* (2), 181-192.

16.   Hench, L. L.; West, J. K., The sol-gel process. *Chemical Reviews* **1990,** *90* (1), 33-72.

17.   Stöber, W.; Fink, A.; Bohn, E., Controlled growth of monodisperse silica spheres in the micron size range. *Journal of Colloid and Interface Science* **1968,** *26* (1), 62-69.

18.   Forest, L.; Gibiat, V.; Woignier, T., Chemical and structural evolution of silica alcogels during their formation: acoustical study. *Journal of Sol-Gel Science and Technology* **1998,** *13* (1/2/3), 329-333.

19.   Avnir, D.; Kaufman, V. R., Alcohol is an unnecessary additive in the silicon alkoxide sol-gel process. *Journal of Non-Crystalline Solids* **1987,** *92* (1), 180-2.

20.   Ferrer, M. L.; del Monte, F.; Levy, D., A Novel and Simple Alcohol-Free Sol-Gel Route for Encapsulation of Labile Proteins. *Chemical Materials* **2002,** *14* (9), 3619-3621.

21.   Li, F.; Lyu, D.; Liu, S.; Guo, W., DNA Hydrogels and Microgels for Biosensing and Biomedical Applications. *Advanced Materials* **2020,** *32* (3), 1806538.

22.   Khurana, B.; Gierlich, P.; Meindl, A.; Gomes-da-Silva, L. C.; Senge, M. O., Hydrogels: soft matters in photomedicine. *Photochemical & Photobiological Sciences* **2019,** *18* (11), 2613-2656.

23.   George, S. M.; Tandon, S.; Kandasubramanian, B., Advancements in Hydrogel-Functionalized Immunosensing Platforms. *ACS Omega* **2020,** *5* (5), 2060-2068.

24.   Ciriminna, R.; Fidalgo, A.; Pandarus, V.; Beland, F.; Ilharco, L. M.; Pagliaro, M., The Sol-Gel Route to Advanced Silica-Based Materials and Recent Applications. *Chemical Reviews (Washington, DC, U. S.)* **2013,** *113* (8), 6592-6620.

25.   Deshpande, R.; Hua, D. W.; Smith, D. M.; Brinker, C. J., Pore structure evolution in silica gel during aging/drying. III. Effects of surface tension. *Journal of Non-Crystalline Solids* **1992,** *144* (1), 32-44.

26.   Davis, P. J.; Deshpande, R.; Smith, D. M.; Brinker, C. J.; Assink, R. A., Pore structure evolution in silica gel during aging/drying. IV. Varying pore fluid pH. *Journal of Non-Crystalline Solids* **1994,** *167* (3), 295-306.

27.   Davis, P. J.; Brinker, C. J.; Smith, D. M., Pore structure evolution in silica gel during aging/drying. I. Temporal and thermal aging. *Journal of Non-Crystalline Solids* **1992,** *142* (3), 189-96.

28.   Davis, P. J.; Brinker, C. J.; Smith, D. M.; Assink, R. A., Pore structure evolution in silica gel during aging/drying. II. Effect of pore fluids. *Journal of Non-Crystalline Solids* **1992,** *142* (3), 197-207.

29.   Glaves, C. L.; Brinker, C. J.; Smith, D. M.; Davis, P. J., In situ pore structure studies of xerogel drying. *Chemical Materials* **1989,** *1* (1), 34-40.

30.   Scherer, G. W.; Pardenek, S. A.; Swiatek, R. M., Viscoelasticity in silica gel. *Journal of Non-Crystalline Solids* **1988,** *107* (1), 14-22.

31.   Smith, D. M.; Davis, P. J.; Brinker, C. J., In-situ pore structure analysis during aging and drying of gels. *Materials Research Society Symposium Proceedings* **1990,** *180* (Better Ceram. Chem. 4), 235-46.

32.   Scherer, G. W., Aging and drying of gels. *Journal of Non-Crystalline Solids* **1988,** *100* (1-3), 77-92.

33.   Wen, J.; Wilkes, G. L., Organic/Inorganic Hybrid Network Materials by the Sol-Gel Approach. *Chemical Materials* **1996,** *8* (8), 1667-1681.

34.   ILER, R. K., *The Colloid Chemistry of Silica and Silicates*. John Wiley & Sons, Inc.: New York, NY, 1979.

35.   Kato, M.; Sakai-Kato, K.; Toyo'oka, T., Silica sol-gel monolithic materials and their use in a variety of applications. *Journal of Separation Science* **2005,** *28* (15), 1893-1908.

36.   Zoriany, M. Y.; Nashaat, A.; El-Shaer, Y.; Naeem, I.; Elzahed, O.; Gobara, M., Optimized silica-based hybrid coatings for the protection of aluminum against chloride-rich environment. *Journal of Sol-Gel Science and Technology* **2020**, Ahead of Print.

37.   Salama, A.; Hesemann, P., Synthesis and characterization of N-guanidinium chitosan/silica ionic hybrids as templates for calcium phosphate mineralization. *International Journal of Biological Macromolecules* **2020,** *147*, 276-283.

38.   Pirzada, T.; Ashrafi, Z.; Xie, W.; Khan, S. A., Multifunctional Aerogels: Cellulose Silica Hybrid Nanofiber Aerogels: From Sol-Gel Electrospun Nanofibers to

Multifunctional Aerogels (Adv. Funct. Mater. 5/2020). *Advanced Functional Materials* **2020,** *30* (5), 2070031.

39.   Phillips, K. R.; Shirman, T.; Aizenberg, M.; England, G. T.; Vogel, N.; Aizenberg, J., Silica-titania hybrids for structurally robust inverse opals with controllable refractive index. *Journal of Materials Chemistry C* **2020,** *8* (1), 109-116.

40.   Liu, Z.-L.; Zhu, G.-P.; Wang, Z.-Y.; Zhao, L.-C.; Dong, B.; Dong, Y.-H.; Feng, W., Novel hybrid silica thin film based on bismuth vanadate and polyoxometalates system: visible-light photochromic behavior and mechanism. *Optoelectronics and Advanced Materials, Rapid Communications* **2019,** *13* (5-6), 320-325.

41.   Kapusuz, D., Sol-gel derived silica/polyethylene glycol hybrids as potential oligonucleotide vectors. *Journal of Materials Research* **2019,** *34* (22), 3787-3797.

42.   Heshmati, M. R.; Amiri, S.; Hosseini-Zori, M., Synthesis and characterization of superhydrophobic-superoleophobic and anti-corrosion coatings via sol-gel process. *Open Journal of Organic Polymer Materials* **2020,** *10* (1), 1-15.

43.   Benvenuti, J.; Giraldi Fisch, A.; Zimnoch Dos Santos, J. H.; Gutterres, M., Hybrid sol-gel silica adsorbent material based on grape stalk applied to cationic dye removal. *Environmental Progress and Sustainable Energy* **2020**, Ahead of Print.

44.   Ballarre, J.; Aydemir, T.; Liverani, L.; Roether, J. A.; Goldmann, W. H.; Boccaccini, A. R., Versatile bioactive and antibacterial coating system based on silica, gentamicin, and chitosan: Improving early stage performance of titanium implants. *Surface Coating Technology* **2019**, Ahead of Print.

45.   Ahmadi, H.; Abdollahi, M., Synthesis and structural characterization of lignin/silica hybrid nanoparticles functionalized with sulfonic acid-terminated polyamidoamine. *Wood Science and Technology* **2020**, Ahead of Print.

46.   Pierre, A. C., The Sol-Gel Encapsulation of Enzymes. *Biocatalysis & Biotransformation* **2004,** *22* (3), 145-170.

47.   Bhatia, R. B.; Brinker, C. J.; Gupta, A. K.; Singh, A. K., Aqueous Sol-Gel Process for Protein Encapsulation. *Chemical Materials* **2000,** *12* (8), 2434-2441.

48.   Gupta, R.; Chaudhury, N. K., Entrapment of biomolecules in sol-gel matrix for applications in biosensors: Problems and future prospects. *Biosensors and Bioelectronics* **2007,** *22* (11), 2387-2399.

49.   Gill, I.; Ballesteros, A., Bioencapsulation within synthetic polymers (Part 1): sol-gel encapsulated biologicals. *Trends in Biotechnology* **2000,** *18* (7), 282-296.

50.   Gill, I.; Ballesteros, A., Encapsulation of biologicals within silicate, siloxane, and hybrid sol-gel polymers: an efficient and generic approach. *Journal of the American Chemical Society* **1998,** *120* (34), 8587-8598.

51.   Ellerby, L. M.; Nishida, C. R.; Nishida, F.; Yamanaka, S. A.; Dunn, B.; Valentine, J. S.; Zink, J. I., Encapsulation of proteins in transparent porous silicate glasses prepared by the sol-gel method. *Science (Washington, D. C., 1883-)* **1992,** *255* (5048), 1113-15.

52.   Crosley, M. S.; Yip, W. T., Multienzyme, Multistep Biosensor Produced through Kinetic Doping. *Journal of Physical Chemistry B* **2019,** *123* (18), 3962-3967.

53.   Crosley, M. S.; Yip, W. T., Silica Sol-Gel Optical Biosensors: Ultrahigh Enzyme Loading Capacity on Thin Films via Kinetic Doping. *Journal of Physical Chemistry B* **2017,** *121* (9), 2121-2126.

54.   Crosley, M. S.; Yip, W. T., Kinetically Doped Silica Sol-Gel Optical Biosensors: Expanding Potential Through Dip-Coating. *ACS Omega* **2018,** *3* (7), 7971-7978.

55.   Karamikamkar, S.; Behzadfar, E.; Naguib, H. E.; Park, C. B., Insights into in-situ sol-gel conversion in graphene modified polymer-based silica gels for multifunctional aerogels. *Chemical Engineering Journal* **2019**, Ahead of Print.

56.   Jung, H. K.; Jung, B. M.; Choi, U. H., Synthesis and Characterization of Silica Aerogel-Polymer Hybrid Materials. *Molecular Crystals and Liquid Crystals* **2019,** *687* (1), 97-104.

57.   Fidalgo, A.; Farinha, J. P. S.; Martinho, J. M. G.; Ilharco, L. M., Nanohybrid silica/polymer aerogels: The combined influence of polymer nanoparticle size and content. *Materials & Design* **2020,** *189*, 108521.

58.   Alhooshani, K., Determination of chlorinated hydrocarbons in milk samples using sol-gel based polymer coated silica sorbent for stir-bar supported micro-solid-phase extraction coupled with gas chromatography mass-spectrometry. *Journal of Saudi Chemical Society* **2019**, Ahead of Print.

59.   Thakur, A. K.; Nisola, G. M.; Limjuco, L. A.; Parohinog, K. J.; Torrejos, R. E. C.; Shahi, V. K.; Chung, W.-J., Polyethylenimine-modified mesoporous silica adsorbent for simultaneous removal of Cd(II) and Ni(II) from aqueous solution. *Journal of Industrial and Engineering Chemistry (Amsterdam, Neth.)* **2017,** *49*, 133-144.

60.   Avnir, D.; Levy, D.; Reisfeld, R., The nature of the silica cage as reflected by spectral changes and enhanced photostability of trapped Rhodamine 6G. *Journal of Physical Chemistry* **1984,** *88* (24), 5956-9.

61.   Brinker, C. J.; Keefer, K. D.; Schaefer, D. W.; Ashley, C. S., Sol-gel transition in simple silicates. *Journal of Non-Crystalline Solids* **1982,** *48* (1), 47-64.

62.   Hench, L. L.; Simmons, J. H.; Zhu, B. F.; Ochoa, R. Laser dye impregnated silica sol-gel monoliths. US5222092A, 1993.

63.   Clavier, C. W.; Rodman, D. L.; Sinski, J. F.; Allain, L. R.; Im, H.-J.; Yang, Y.; Clark, J. C.; Xue, Z.-L., A method for the preparation of transparent mesoporous silica sol-gel monoliths containing grafted organic functional groups. *Journal of Materials Chemistry* **2005,** *15* (24), 2356-2361.

64.   Wu, X.; Choi, M. M. F.; Xiao, D., A glucose biosensor with enzyme-entrapped sol-gel and an oxygen-sensitive optode membrane. *Analyst (Cambridge, U. K.)* **2000,** *125* (1), 157-162.

65.   Sakka, S.; Kamiya, K.; Makita, K.; Yamamoto, Y., Formation of sheets and coating films from alkoxide solutions. *Journal of Non-Crystalline Solids* **1984,** *63* (1-2), 223-35.

66.   Sivakumar, S.; Van Veggel, F. C. J. M.; May, P. S., Near-Infrared (NIR) to Red and Green Up-Conversion Emission from Silica Sol-Gel Thin Films Made with La0.45Yb0.50Er0.05F3 Nanoparticles, Hetero-Looping-Enhanced Energy Transfer (Hetero-LEET): A New Up-Conversion Process. *Journal of the American Chemical Society* **2007,** *129* (3), 620-625.

67.   Juergen-Lohmann, D. L.; Nacke, C.; Simon, L. C.; Legge, R. L., Effect of sol-gel hydrophobicity on the distribution and structure of different proteins in organically modified sol-gel thin films. *Journal of Sol-Gel Science and Technology* **2009,** *52* (3), 370-381.

68.   Gilliland, J. W.; Yokoyama, K.; Yip, W. T., Solvent Effect on Mobility and Photostability of Organic Dyes Embedded inside Silica Sol-Gel Thin Films. *Chemical Materials* **2005,** *17* (26), 6702-6712.

69.   Abuin, M.; Serrano, A.; Llopis, J.; Garcia, M. A.; Carmona, N., Silica doped with lanthanum sol-gel thin films for corrosion protection. *Thin Solid Films* **2012,** *520* (16), 5267-5271.

70.   Venton, D. L.; Cheesman, K. L.; Chatterton, R. T., Jr.; Anderson, T. L., Entrapment of a highly specific antiprogesterone antiserum using polysiloxane copolymers. *Biochimica et Biophysica Acta, General Subjects* **1984,** *797* (3), 343-7.

71.   Glad, M.; Norrloew, O.; Sellergren, B.; Siegbahn, N.; Mosbach, K., Use of silane monomers for molecular imprinting and enzyme entrapment in polysiloxane-coated porous silica. *Journal of Chromatography* **1985,** *347* (1), 11-23.

72. Zhou, Y.; Yip, W. T., Balance between Coulombic Interactions and Physical Confinement in Silica Hydrogel Encapsulation. *Journal of Physical Chemistry B* **2009,** *113* (17), 5720-5727.

73. Pouxviel, J. C.; Dunn, B.; Zink, J. I., Fluorescence study of aluminosilicate sols and gels doped with hydroxy trisulfonated pyrene. *Journal of Physical Chemistry* **1989,** *93* (5), 2134-9.

74. Kaufman, V. R.; Avnir, D.; Pines-Rojanski, D.; Huppert, D., Water consumption during the early stages of the sol-gel tetramethylorthosilicate polymerization as probed by excited state proton transfer. *Journal of Non-Crystalline Solids* **1988,** *99* (2-3), 379-86.

75. Kunarti, E. S.; Moran, G., Effect of glycerol on the activity of α-chymotrypsin encapsulated in sol-gel derived silica monoliths. *Asian Journal Chemistry* **2011,** *23* (9), 3940-3944.

76. Hernandez, A.; Esquivel-Ferrino, P.; Gomez, I.; Cantu, L., Effect of the Sol-Gel Synthesis Parameters on the Incorporation of an Anti-inflammatory Drug in a Ceramic Material. *Materials Research Society Symposium Proceedings* **2007,** *1007* (Organic/Inorganic Hybrid Materials), No pp. given, Paper #: 1007-S08-02.

77. Daiko, Y.; Kasuga, T.; Nogami, M., Pore size effect on proton transfer in sol-gel porous silica glasses. *Microporous Mesoporous Materials* **2004,** *69* (3), 149-155.

78. Dave, B. C.; Soyez, H.; Miller, J. M.; Dunn, B.; Valentine, J. S.; Zink, J. I., Synthesis of Protein-Doped Sol-Gel SiO2 Thin Films: Evidence for Rotational Mobility of Encapsulated Cytochrome c. *Chemistry of Materials* **1995,** *7* (8), 1431-4.

79.   Husing, N.; Reisler, E.; Zink, J. I., Allosteric regulation of enzymatic reactions in a transparent inorganic sol-gel material. *Journal of Sol-Gel Science and Technology* **1999,** *15* (1), 57-61.

80.   Brennan, J. D., Using intrinsic fluorescence to investigate proteins entrapped in sol-gel derived materials. *Applied Spectroscopy* **1999,** *53* (3), 106A-121A.

81.   Hartnett, A. M.; Ingersoll, C. M.; Baker, G. A.; Bright, F. V., Kinetics and Thermodynamics of Free Flavins and the Flavin-Based Redox Active Site within Glucose Oxidase Dissolved in Solution or Sequestered within a Sol-Gel-Derived Glass. *Analytical Chemistry* **1999,** *71* (6), 1215-1224.

82.   Edmiston, P. L.; Wambolt, C. L.; Smith, M. K.; Saavedra, S. S., Spectroscopic characterization of albumin and myoglobin entrapped in bulk sol-gel glasses. *Journal of Colloid Interface Science* **1994,** *163* (2), 395-406.

83.   Dunn, B.; Zink, J. I., Optical properties of sol-gel glasses doped with organic molecules. *Journal of Materials Chemistry* **1991,** *1* (6), 903-13.

84.   Nishida, F.; McKiernan, J. M.; Dunn, B.; Zink, J. I.; Brinker, C. J.; Hurd, A. J., In situ fluorescence probing of the chemical changes during sol-gel thin film formation. *Journal of the American Ceramics Society* **1995,** *78* (6), 1640-8.

85.   Gilliland, J. W.; Yokoyama, K.; Yip, W. T., Effect of Coulombic Interactions on Rotational Mobility of Guests in Sol-Gel Silicate Thin Films. *Chemistry of Materials* **2004,** *16* (20), 3949-3954.

86.   Rottman, C.; Grader, G. S.; De Hazan, Y.; Avnir, D., Sol-Gel Entrapment of ET(30) in Ormosils. Interfacial Polarity-Fractality Correlation. *Langmuir* **1996,** *12* (23), 5505-5508.

87.   Narang, U.; Jordan, J. D.; Bright, F. V.; Prasad, P. N., Probing the Cybotactic Region of PRODAN in Tetramethylorthosilicate-Derived Sol-Gels. *Journal of Physical Chemistry B* **1994,** *98* (33), 8101-7.

88.   Narang, U.; Wang, R.; Prasad, P. N.; Bright, F. V., Effects of aging on the dynamics of rhodamine 6G in tetramethyl orthosilicate-derived sol-gels. *Journal of Physical Chemistry B* **1994,** *98* (1), 17-22.

89.   Gottfried, D. S.; Kagan, A.; Hoffman, B. M.; Friedman, J. M., Impeded Rotation of a Protein in a Sol-Gel Matrix. *Journal of Physical Chemistry B* **1999,** *103* (14), 2803-2807.

90.   Wang, H.; Zhang, J.; Zhang, W.; Yang, Y., Host-guest interactions of 5-fluorouracil in supramolecular organogels. *European Journal of Pharmaceutics and Biopharmaceutics* **2009,** *73* (3), 357-60.

91.   Madhu, S.; Sanjayan, G. J.; Madhu, S.; Sanjayan, G. J.; Gonnade, R. G.; Das, T.; Vanka, K., Twelve-Armed Hexaphenylbenzene-Based Giant Supramolecular Framework for Entrapping Guest Molecules. *Chempluschem* **2018,** *83* (11), 1032-1037.

92.   Tleugabulova, D.; Sui, J.; Ayers, P. W.; Brennan, J. D., Evidence for Rigid Binding of Rhodamine 6G to Silica Surfaces in Aqueous Solution Based on Fluorescence Anisotropy Decay Analysis. *Journal of Physical Chemistry B* **2005,** *109* (16), 7850-7858.

93.   Wu, Y.; Liang, J.; Horkay, F.; Libera, M., Antimicrobial loading into and release from poly(ethylene glycol)/poly(acrylic acid) semi-interpenetrating hydrogels. *Journal of Polymer Science, Part B: Polymer Physics* **2016,** *54* (1), 64-72.

94.   Zheng, X.-Y.; Wachi, M.; Harata, A.; Hatano, Y., Acidity effects on the fluorescence properties and adsorptive behavior of rhodamine 6G molecules at the air-water interface studied with confocal fluorescence microscopy. *Spectrochimica Acta, Part A* **2004,** *60A* (5), 1085-1090.

95.   Zheng, X. Y.; Harata, A.; Ogawa, T., Study of the adsorptive behavior of water-soluble dye molecules (rhodamine 6G) at the air-water interface using confocal fluorescence microscope. *Spectrochimica Acta, Part A* **2001,** *57A* (2), 315-322.

96.   Chen, Z.; Tang, Y.-J.; Xie, T.-T.; Chen, Y.; Li, Y.-Q., Fluorescence spectral properties of rhodamine 6G at the silica/water interface. *Journal of Fluorescence* **2008,** *18* (1), 93-100.

97.   Ryu, Y. H.; Yeo, K. B.; Ki, M.-R.; Kim, Y. J.; Pack, S. P., Improved stability and reusability of endoglucanase from Clostridium thermocellum by a biosilica-based auto-encapsulation method. *Biochemical Engineering Journal* **2016,** *105* (Part_A), 144-149.

98.   Ellerby, L. M.; Nishida, C. R.; Nishida, F.; Yamanaka, S. A.; Dunn, B.; Valentine, J. S.; Zink, J. I., Encapsulation of proteins in transparent porous silicate glasses prepared by the sol-gel method. *Science* **1992,** *255* (5048), 1113-5.

99.   Braun, S.; Rappoport, S.; Zusman, R.; Avnir, D.; Ottolenghi, M., Biochemically active sol-gel glasses: the trapping of enzymes. *Materials Letters* **1990,** *10* (1-2), 1-5.

100.   Jeronimo, P. C. A.; Araujo, A. N.; Montenegro, M. C. B. S. M., Optical sensors and biosensors based on sol-gel films. *Talanta* **2007,** *72* (1), 13-27.

101.   Zhang, F.; Wang, M.; Liang, C.; Jiang, H.; Shen, J.; Li, H., Thin-layer polymer wrapped enzymes encapsulated in hierarchically mesoporous silica with high activity and enhanced stability. *Scientific Reports* **2014,** *4*, article 4421.

102.   Mackenzie, J. D., Sol-gel research - Achievements since 1981 and prospects for the future. *Journal of Sol-Gel Science and Technology* **2003,** *26* (1/2/3), 23-27.

103.   Lim, M. H.; Stein, A., Comparative Studies of Grafting and Direct Syntheses of Inorganic-Organic Hybrid Mesoporous Materials. *Chemical Materials* **1999,** *11* (11), 3285-3295.

104.   Angelome, P. C.; Soler-Illia, G. J. d. A. A., Organically Modified Transition-Metal Oxide Mesoporous Thin Films and Xerogels. *Chemical Materials* **2005,** *17* (2), 322-331.

105.   Reisfeld, R.; Zigansky, E.; Saraidarov, T., Steady state spectroscopy and stability of tris(8-hydroxy quinoline) aluminum and ruthenium tris bipyridile chloride in sol-gel glasses. *Optical Materials (Amsterdam, Neth.)* **2008,** *30* (11), 1706-1709.

106.   Reisfeld, R.; Levchenko, V.; Saraidarov, T.; Rysiakiewicz-Pasek, E.; Baranowski, M.; Podhorodecki, A.; Misiewicz, J.; Antropova, T., Steady state and femtosecond spectroscopy of Perylimide Red dye in porous and sol-gel glasses. *Chemical Physical Letters* **2012,** *546*, 171-175.

107. Biswas, A.; Friend, C. S.; Maciel, G. S.; Prasad, P. N., Optical properties of europium doped gels during densification. *Journal of Non-Crystalline Solids* **2000,** *261* (1-3), 9-14.

108. V. Deshpande, A.; Kumar, U., Molecular forms coumarin 307 in sol-gel glasses. *Journal of Fluorescence* **2006,** *16* (5), 679-687.

109. Czarnobaj, K.; Lukasiak, J., In vitro release of cisplatin from sol-gel processed porous silica xerogels. *Drug Delivery* **2004,** *11* (6), 341-4.

110. Schramm, C.; Kitzke, A.; Tessadri, R., Cobalt chloride-based humidity sensor attached to sol-gel modified cellulosic material. *Cellular Chemical Technology* **2017,** *51* (3-4), 273-282.

111. Jiang, H.-p.; Wang, X.-c.; Zhong, F.-c.; Hao, X.-f., Preparation and surface chemical modification of the monodisperse SiO2 nanoparticles. *Guangzhou Huagong* **2011,** *39* (8), 36-39.

112. Livage, J.; Coradin, T.; Roux, C., Encapsulation of biomolecules in silica gels. *Journal of Physics: Condensed Matter* **2001,** *13* (33), R673-R691.

113. Campbell, A. L. O.; Lei, Q.; Tak Yip, W., Kinetic approach to hyper-doped optical quality thin films. *Chemical Communications (Cambridge, U. K.)* **2014,** *50* (66), 9321-9324.

114. Munroe, C. E., Coating Sounding Tubes. *Chemical Engineering Science* **1910,** *10*, 50.

115.   ten Elshof, J. E., 4 - Chemical solution deposition techniques for epitaxial growth of complex oxides. In *Epitaxial Growth of Complex Metal Oxides*, Koster, G.; Huijben, M.; Rijnders, G., Eds. Woodhead Publishing: 2015; pp 69-93.

116.   Lončarević, D.; Čupić, Ž., Chapter 4 - The perspective of using nanocatalysts in the environmental requirements and energy needs of industry. In *Industrial Applications of Nanomaterials*, Thomas, S.; Grohens, Y.; Pottathara, Y. B., Eds. Elsevier: 2019; pp 91-122.

117.   L. Landau, V. L., Dragging of a Liquid by a Moving Plate. *Acta Physicochim U.R.S.S.* **1942,** *17*, 42-54.

118.   Crosley, M., KINETIC DOPING OF SILICA SOL-GEL THIN FILMS AND APPLICATION AS BIOSENSORS. Yip, W. T.; Hansmann, U.; Rice, C.; White, R.; Bumm, L., Eds. 2019.

119.   Brinker, C. J.; Frye, G. C.; Hurd, A. J.; Ashley, C. S., Fundamentals of sol-gel dip coating. *Thin Solid Films* **1991,** *201* (1), 97-108.

120.   Tan, X.; Khaing Oo, M. K.; Gong, Y.; Li, Y.; Zhu, H.; Fan, X., Glass capillary based microfluidic ELISA for rapid diagnostics. *Analyst* **2017,** *142* (13), 2378-2385.

121.   Jannat, M.; Yang, K.-L., Immobilization of Enzymes on Flexible Tubing Surfaces for Continuous Bioassays. *Langmuir* **2018,** *34* (47), 14226-14233.

122.   Besanger, T. R.; Hodgson, R. J.; Green, J. R. A.; Brennan, J. D., Immobilized enzyme reactor chromatography: Optimization of protein retention and enzyme activity in monolithic silica stationary phases. *Analytica Chimica Acta* **2006,** *564* (1), 106-115.

123.   Jing, C.; Zhao, X.; Han, J.; Zhu, K.; Liu, A.; Tao, H., A new method of fabricating internally sol-gel coated capillary tubes. *Surface Coating Technology* **2003,** *162* (2-3), 228-233.

124.   Molinari, R.; Santoro, M. E.; Drioli, E., Study and Comparison of Two Enzyme Membrane Reactors for Fatty Acids and Glycerol Production. *Industrial & Engineering Chemistry Research* **1994,** *33* (11), 2591-9.

125.   Giorno, L.; Drioli, E.; Carvoli, G.; Cassano, A.; Donato, L., Study of an enzyme membrane reactor with immobilized fumarase for production of L-malic acid. *Biotechnology and Bioengineering* **2001,** *72* (1), 77-84.

126.   Lian, X.; Fang, Y.; Joseph, E.; Wang, Q.; Li, J.; Banerjee, S.; Lollar, C.; Wang, X.; Zhou, H.-C., Enzyme-MOF (metal-organic framework) composites. *Chemical Society Reviews* **2017,** *46* (11), 3386-3401.

127.   Zhu, Y.; Chen, Q.; Shao, L.; Jia, Y.; Zhang, X., Microfluidic immobilized enzyme reactors for continuous biocatalysis. *Reaction Chemistry & Engineering* **2020,** *5* (1), 9-32.

128.   Honda, T.; Yamaguchi, H.; Miyazaki, M., Development of Enzymatic Reactions in Miniaturized Reactors. *Advance Biotechnology* **2017,** *5* (Applied Bioengineering), 99-166.

129.   Britton, J.; Majumdar, S.; Weiss, G. A., Continuous flow biocatalysis. *Chemical Society Reviews* **2018,** *47* (15), 5891-5918.

130.   Tauhardt, L.; Pretzel, D.; Gottschaldt, M.; Schubert, U. S. In *Surface coating of sensor materials using poly(2-ethyl-2-oxazoline) based polymers for the prevention of biofilm formation*, American Chemical Society: 2013; pp COLL-459.

131.   Aguado, J.; Arsuaga, J. M.; Arencibia, A.; Lindo, M.; Gascón, V., Aqueous heavy metals removal by adsorption on amine-functionalized mesoporous silica. *Journal of Hazardous Materials* **2009,** *163* (1), 213-221.

132.   Bagheri, H.; Babanezhad, E.; Khalilian, F., A novel sol-gel-based amino-functionalized fiber for headspace solid-phase microextraction of phenol and chlorophenols from environmental samples. *Analytica Chimica Acta* **2008,** *616* (1), 49-55.

133.   Shabir, J.; Garkoti, C.; Surabhi; Sah, D.; Mozumdar, S., Development of Amine Functionalized Wrinkled Silica Nanospheres and Their Application as Efficient and Recyclable Solid Base Catalyst. *Catalysis Letters* **2018,** *148* (1), 194-204.

134.   Wang, J.; Li, Z., Enhanced selective removal of Cu(II) from aqueous solution by novel polyethylenimine-functionalized ion imprinted hydrogel: Behaviors and mechanisms. *Journal of Hazardous Materials* **2015,** *300*, 18-28.

135.   Zhang, W.; Liu, H.; Sun, C.; Drage, T. C.; Snape, C. E., Capturing CO2 from ambient air using a polyethyleneimine–silica adsorbent in fluidized beds. *Chemical Engineering Science* **2014,** *116*, 306-316.

136.   Gibney, K.; Sovadinova, I.; Lopez, A. I.; Urban, M.; Ridgway, Z.; Caputo, G. A.; Kuroda, K., Poly(ethylene imine)s as antimicrobial agents with selective activity. *Macromolecular Bioscience* **2012,** *12* (9), 1279-1289.

137.   Foxley, M. A.; Friedline, A. W.; Jensen, J. M.; Nimmo, S. L.; Scull, E. M.; King, J. B.; Strange, S.; Xiao, M. T.; Smith, B. E.; Thomas, K. J., III; Glatzhofer, D. T.; Cichewicz, R. H.; Rice, C. V., Efficacy of ampicillin against methicillin-resistant Staphylococcus aureus restored through synergy with branched poly(ethylenimine). *Journal of Antibiotics* **2016,** *69* (12), 871-878.

138.   Zhu, M.; Lerum, M. Z.; Chen, W., How To Prepare Reproducible, Homogeneous, and Hydrolytically Stable Aminosilane-Derived Layers on Silica. *Langmuir* **2012,** *28* (1), 416-423.

139.   Al-Oweini, R.; El-Rassy, H., Synthesis and characterization by FTIR spectroscopy of silica aerogels prepared using several Si(OR)4 and R"Si(OR')3 precursors. *Journal of Molecular Structure* **2009,** *919* (1-3), 140-145.

CHAPTER 2 - Techniques and Instrumentation

2.1   Abstract

The experimental techniques, procedures, and primary instrumentation used in the

research section of this work are discussed in this chapter. A list of relevant materials is

provided and any modification of materials as received is noted. The process for creating

the sol precursor solution used in the sol-gel process and the preparation of the loading

solutions used for kinetic doping are detailed. Variations in sol preparation and loading

solution parameters for various guest molecules are included. Experimental rationale for

the guest molecules chosen is discussed. The preparation of all assay solutions is also

detailed. Data gathered by collaborators is noted. The experimental set-up for the primary

method for data acquisition, UV-Vis spectroscopy, is discussed.

2.2   Introduction

Silica sol-gel technology was discovered in the 19th century when it was observed that a

silica alkoxide solution formed a gel when exposed to air.[1] Since then, extensive research

has been conducting on silica sol-gel technology for various applications,[2] including as a

solid matrix for guest molecules. Silica sol-gels that result in bulk materials,[3-5] powders,[6]

and thin films[7-11] have been studied, and guest molecules have been trapped with pre- and

post-doping techniques.[12-15] Based on protocols the published by Higgins[16] and Zink[17] lab groups, a new doping technology was developed by the Yip lab group. Campbell[18] and Crosley[19-21] developed kinetic doping techniques in silica sol-gel for both spin- and dip-coating, loading both dye and enzymes.

Based on this work, kinetic doping of silica sol-gel was expanded for use in internally coated glass capillary tubes. Parameters were developed to load previously studied guest molecules into thin films coated internally on glass capillary tubes, which presents new challenges for both initial loading of dopants and characterization thereof. UV-Vis spectroscopy was used to quantify the loading of rhodamine 6G dye and the loading and activity of horseradish peroxidase (HRP) enzymes. Scanning electron microscopy (SEM) was used to characterize the films.

Additionally, parameters to load a new dopant molecule, branched polyethylenimine (BPEI), were developed. Characterization techniques for quantifying loaded molecules, copper (II) sequestration capability of the loaded films, and solvent-accessible primary and secondary amines were developed using UV-Vis spectroscopy. UV-Vis spectroscopy was also used to quantify the film's ability to inhibit biofilm formation. Scanning electron microscopy (SEM) was also used to characterize the films.

2.3 Materials

For capillary tube loading, tetraethylorthosilicate (TEOS), rhodamine 6G (R6G), and hydrochloric acid were purchased from Sigma-Aldrich. Phosphoric acid was purchased

from EMD Millipore. Horseradish peroxidase (HRP) was purchased from Gold Technology. Glass capillary tubes (25 μL Drummond Wiretrol Calibrated Micropipets). All chemicals and materials were used as received, with the exception of the glass capillary tubes, which were cleaned prior to use.

For loading of flat surface films, tetraethylorthosilicate (TEOS); rhodamine 6G (R6G); sodium hydroxide; and 600, 1800, 25000, and 750000 MW branched polyethylenimine (BPEI) were purchased from Sigma-Aldrich. 85% phosphoric acid was purchased from EMD Millipore. Premium grade glass coverslips (25 mm × 25 mm × 170 μm and 22 mm × 22 mm × 170 μm) were purchased from Fisher Scientific. All chemicals and materials were used as received, with the exception of the glass coverslips, which were cleaned prior to use.

For film assays, 95% ethanol, 99% methanol, crystal violet dye and bacterial growth media were purchased from Sigma-Aldrich. Hydrogen peroxide (30% solution) were purchased from EMD Millipore. Guaiacol was purchased from Cayman Chemical Company. Methicillin-resistant *Staphylococcus epidermidis* (MRSE) bacteria were purchased from the American Type Culture Collection (ATCC 35984). All chemicals and materials were used as received.

2.4 Preparation of Glass Coverslips for Coating Purposes

A procedure developed by Campbell and Lei was used to clean the glass coverslips for flat surface film coating.[22] To remove any organic contaminants on the glass coverslip

surface, the coverslips were sonicated in an acetone bath for 30 minutes and rinsed with Millipore water three times to remove all residual acetone. The coverslips were then sonicated in 10% w/v NaOH for another 30 minutes and rinsed with Millipore water five times to remove all residual NaOH. The coverslips went through a final sonication in Millipore water for 30 minutes. The coverslips were then stored in Millipore water until use.

2.5   Preparation of Glass Capillary Tubes for Coating Purposes

The procedure for cleaning glass coverslips was modified for preparation of the glass capillary tubes. To remove any organic contaminants on the capillary tube inner-surface, 95% ethanol was pumped through each capillary for 5 minutes. Ethanol was chosen over acetone to avoid degradation of the tubing and pump mechanism after both solvents showed comparable abilities to remove organic contaminants. Deionized (DI) water was then pumped through each capillary for 5 minutes. To remove aqueous contaminants, 10% HCl was subsequently pumped through each tube for 5 minutes. HCl was chosen over NaOH to avoid contamination from any base during coating, which would catalyze aggregate, not thin film, formation. Finally, deionized water was then pumped through each capillary for 5 minutes. The capillaries were stored in deionized water until use.

2.6   Preparation of Silica Sol-Gel Precursor

Silica sol was prepared by mixing a 1:8:7 molar ratio of TEOS:ethanol:water with phosphoric acid acting as a catalyst. A mixture of 28 mL of TEOS, 55.9 mL of ethanol,

15.9 mL of deionized water and 0.31 mL of 1% v/v phosphoric acid at room temperature were prepared for capillary tube coatings. A mixture of 55.9 mL of TEOS, 111.8 mL of ethanol, 31.7 mL of deionized water and 0.62 mL of 1% v/v phosphoric acid at room temperature were prepared for flat surface coatings. For both types of substrate, the sol was then allowed to age for 20 hours at room temperature before use.

TEOS, whose molecular structure can be seen in Figure 2.1, was chosen as the silicon alkoxide precursor because it has been extensively studied with kinetic doping by Adam Campbell and Matthew Crosley. They initially chose it for its well documented reactions[23] and ability to load guest molecules with no extra reactants or post-reaction modifications.
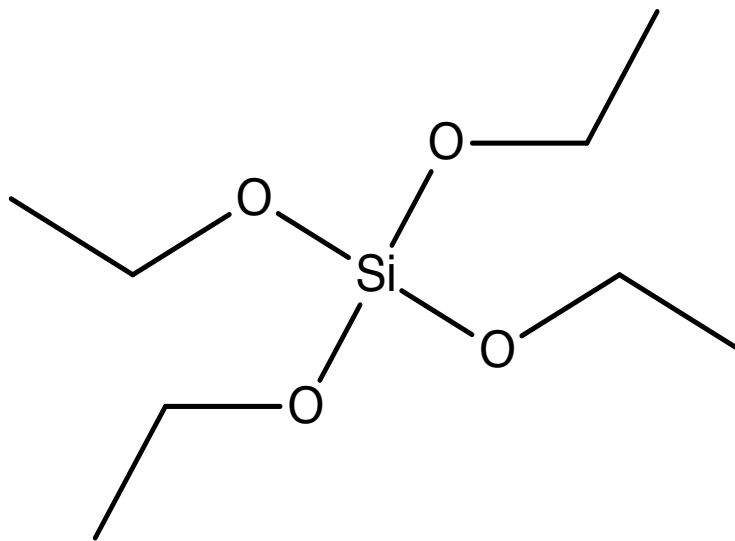
Figure 2.1 Tetraethylorthosilicate (TEOS) chemical structure

2.7   Preparation of Loading Solutions

Stock 100 mM pH 7.4 phosphate buffer solution was prepared by dissolving sodium

phosphate monobasic in DI water, and the final pH was adjusted with concentrated

phosphoric acid. This solution was refrigerated and stored in an airtight container. When

needed, 10 mM pH 7.4 phosphate buffer was prepared by diluting this stock solution with

DI water. For unloaded films, 10 mM pH 7.4 phosphate buffer was used in the same

volume and for the same loading time as the loading solutions for the loaded samples in

question.

The solution used to load Rhodamine 6G was prepared by dissolving R6G in 10 mM pH

7.4 phosphate buffer to a final concentration of 1 mM R6G. This solution was

refrigerated and stored in an airtight container for a period of no more than six months. 3

mL of this solution was transferred to a small test tube when capillary tubes were loaded, and 10 mL was transferred to 50 mL beakers when flat surface films were loaded.

Rhodamine 6G, the molecular structure of which can be seen in Figure 2.2, was chosen because of Crosley's characterization of it in flat-surface dip-coated films. It was initially chosen as a model dye for its positive charge at the loading pH of 7.4,[24] which is ideal for kinetic doping,[22] and high molar extinction coefficient in ethanol,[25-27] making its loading easily quantifiable.
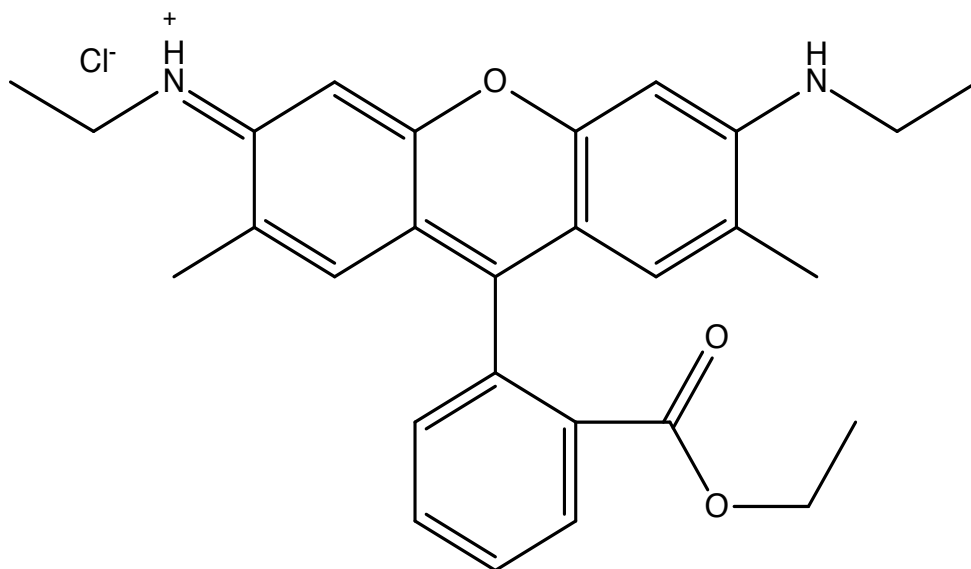
Figure 2.2 Chemical structure of Rhodamine 6G (R6G) at pH 7 or above.

A 0.1 mg/mL solution of horseradish peroxidase for enzyme loading in capillary tubes was prepared by adding the solid enzyme powder to 10 mM pH 7.4 phosphate buffer solution. The solutions were prepared at the time of loading from the enzyme, stored at -

20 ˚C as recommended by the manufacturer, and a stock solution of 100 mM pH 7.4 phosphate buffer solution diluted with DI water. 3 mL of this solution was transferred to a small test tube when capillary tubes were loaded.

HRP, whose protein structure is shown in Figure 2.3 below,[28] was also chosen as the model enzyme guest molecule because of Crosley's characterization of it in flat-surface dip-coated films. This allowed a comparison of the loading and activity of the enzyme when coated on different surfaces. Crosley initially chose it for its robust nature and the volume of research available concerning its reactions.[28-33]
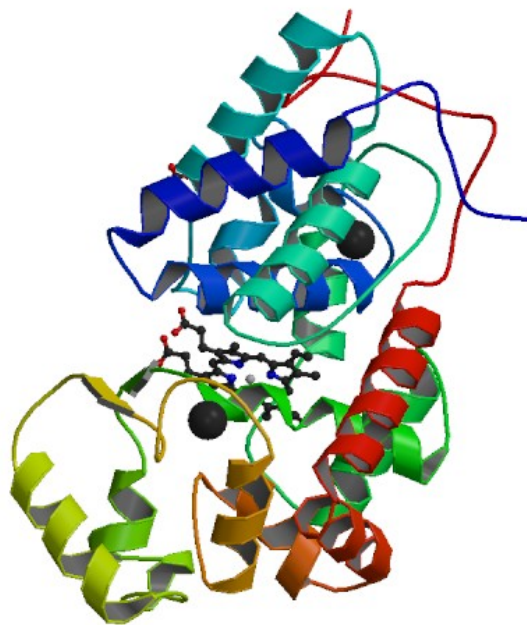
Figure 2.3 Crystal structure of ferrous horseradish peroxidase C1A. (PDB ID: 1h58)

1 mM solutions of 600 and 1800 MW branched polyethylenimine were prepared by adding the pure reagents to 10 mM pH 7.4 phosphate buffer solution and adjusting their

pH back to 7.4 with concentrated phosphoric acid. A 1 mM solution of 25,000 MW BPEI

was prepared by adding the pure reagent to DI water and adjusting the pH to 7.4. A 0.01

mM 750,000 MW solution was prepared by diluting the stock 50% w/v reagent with DI

water and adjusting the pH to 7.4. Phosphate buffer was not used for the 25,000 and

750,000 MW solutions due to the salting out effect observed with higher molecular

weight BPEI polymers.

BPEI was chosen as a possible guest molecule due to its organic nature, positive charge

at the optimal loading pH of 7.4,[34] and myriad uses including environmental applications

such as aqueous heavy metal removal,[35-36] carbon dioxide capture[37] when attached to a

solid substrate, and antimicrobial activity both on their own[38] and as antibiotic

potentiators.[39] The polymer's structure is shown in Figure 2.4 below.

Figure 2.4 Structure of branched polyethylenimine, with repeating units shown.

2.8   Dip-Coating Process for Flat-Surface Films

Flat surface thin films were prepared by drain coating with a sol solution inside a beaker, based on the drain coated film preparation method of Crosley et al.[21] After aging for 20 hours, the silica sol solution was transferred to a 250 mL beaker, elevated by a jack stand. A clean coverslip was dried with compressed air and immersed in the aged silica sol-gel coating solution while suspended from above. The sol solution was then drained at a rate of 1.36 cm/sec for BPEI films and 0.09 cm/sec for R6G films. Immediately after the silica sol solution was drained, the jack stand was lowered until the newly coated coverslip was completely exposed to ambient air. The thin film was allowed to age in ambient air (the delay time) before it was transferred to a loading solution, where the guest molecule was allowed to load into the film via kinetic doping for a specific time period (loading time). Delay and loading times vary for each guest molecule. After loading, films were rinsed with DI water, dried with house air, then immediately used or stored dry for future use.

2.9   Dip-Coating Process for Capillary Tubes

The process for dip-coating capillary tubes is based on the same procedure. After aging for 20 hours, the silica sol solution was transferred to a 50 mL round-bottom glass centrifuge tube, elevated by a jack stand. A clean capillary tube was purge dried with compressed air and immersed in the aged silica sol-gel coating solution while suspended from above. The capillary was positioned so that sol was pulled up into the tube by capillary action to the 25 μL mark. The sol solution in the centrifuge tube was then

drained at a rate of 0.09 cm/sec. The capillary was allowed to age on the drain coating

set-up in ambient air for 5 minutes. It was then transferred to a hose with house air

running through it at 3 LPM for a defined period of time (the drying time). The outside of

the capillary was then wiped to remove any externally coated thin film. It was then placed

in a test tube with loading solution, where the loading solution was drawn into the tube

through capillary action, again to the 25 μL mark. R6G was allowed to load into the film

via kinetic doping for one hour, and HRP was allowed to load into the film for one week.

2.10 Preparation of Bradford Assay Solutions

Attempts were originally made to quantify the mass of HRP loaded in capillary tubes

using a modified Bradford assay developed by Crosley et al.[20] based on the original

Bradford assay.[40] 100 mg of Coomassie Brilliant Blue Dye G-250 was dissolved in 50

mL ethanol, which was then added to 100 mL concentrated phosphoric acid, then diluted

to 1 L with DI water. The assay solution was refrigerated and stored for in an airtight

container for no longer than 2 months.

Coomassie Brilliant Blue, whose chemical structure is shown in Figure 2.5, has two

forms; the absorption of the blue form (maximum at approximately 495 nm) increases in

the presence of proteins, while the unbound form (maximum at approximately 465 nm)

decreases. The spectrum of the dye, showing its two peaks of bound and unbound dye, is

shown in Figure 2.6.
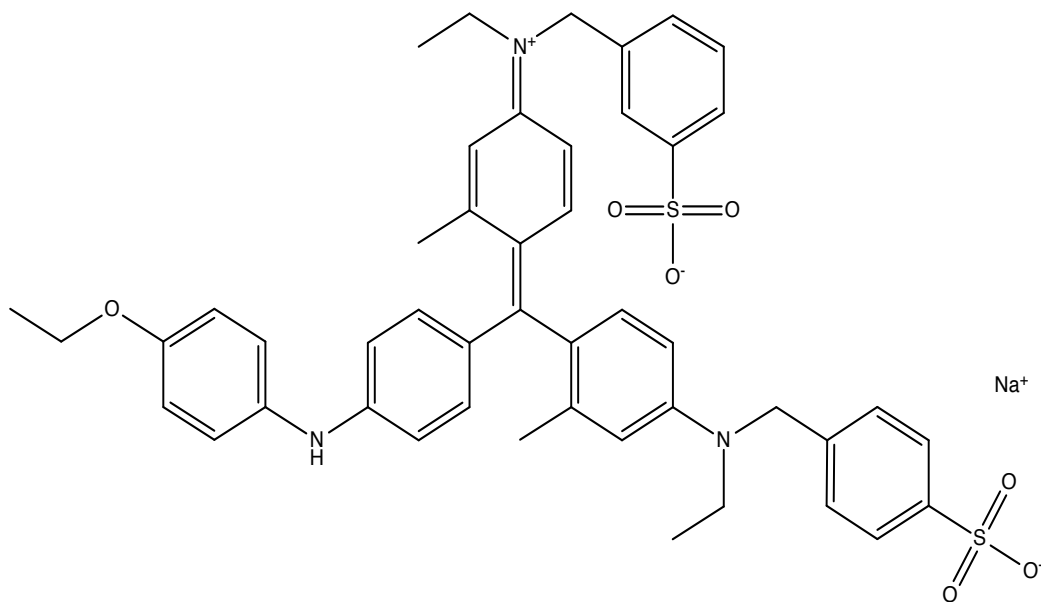
Figure 2.5 Coomassie Brilliant Blue G-250 structure
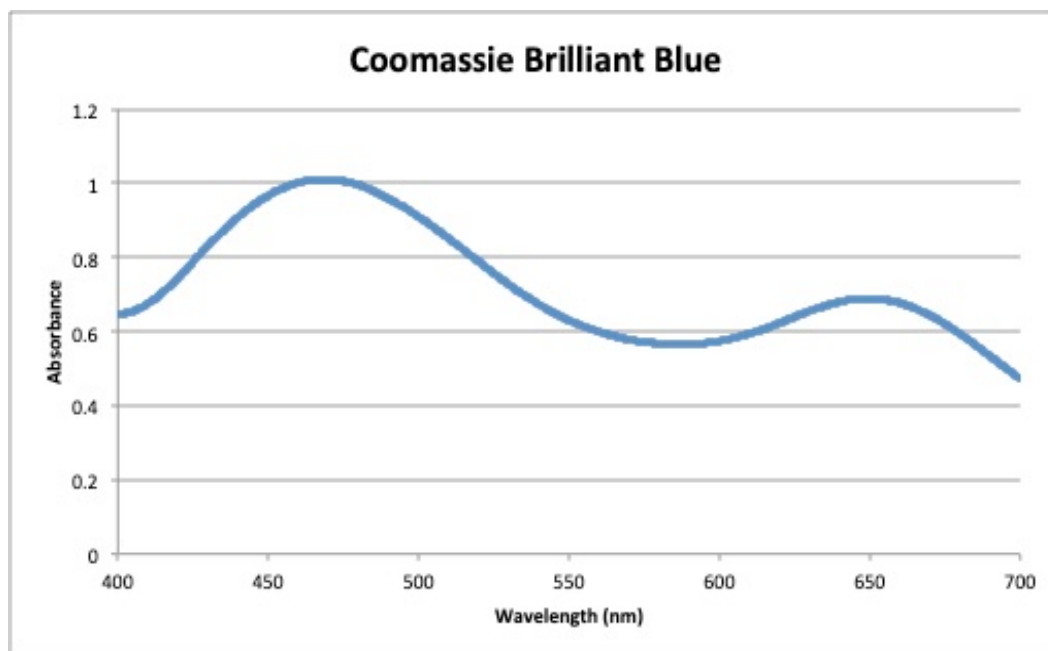
Figure 2.6 Spectrum of Coomassie Brilliant Blue

2.11 Preparation of Ninhydrin Assay Solutions

The mass of HRP loaded in capillary tubes was quantified via the ninhydrin method of protein quantification, based on the procedure developed by Troll et al.[41] Solutions of 500 mg of ninhydrin in 10 mL of absolute ethanol and 80 mg of phenol in 20 mL absolute ethanol were made by dissolving the solid powder in absolute ethanol. 2 mL of 0.01 M KCN in 100 mL pyridine was prepared by dissolving the KCN solid in absolute ethanol, then diluting it with pyridine. These solutions were stored in airtight containers at room temperature for no more than a month. 2 mL of the phenol, 2 mL of the KCN, and 0.4 mL of the ninhydrin solutions were used to test 1 mL of the protein solution.

Solvent accessible primary and secondary amines were quantified via the ninhydrin method of amine quantification, based on the procedure developed by Kaiser et al.[42] Solutions of 500 mg of ninhydrin in 10 mL of absolute ethanol and 80 mg of phenol in 20 mL absolute ethanol were made by dissolving the solid powder in absolute ethanol. 2 mL of 0.001 M KCN in 100 mL pyridine was prepared by dissolving the KCN solid in absolute ethanol, then diluting it with pyridine. These solutions were stored in airtight containers at room temperature for no more than a month. 750 μL each of the phenol, KCN, and ninhydrin solutions were used to test one 22 x 22 mm BPEI loaded coverslip.

Ninhydrin (2,2-dihydroxyindane- 1,3-dione), whose chemical structure is shown in Figure 2.7, is a compound that reacts with primary and secondary amines to produce Ruhemann's purple, which can be detected colormetrically.[43-45] It is commonly used to in amino acid analysis of proteins. Because of its reaction with amines, Ruhemann's purple

is used for detecting the solvent-accessible primary and secondary amines in loaded

BPEI. It was also used for quantifying the amino acids produced when the capillary thin

films were dissolved with sodium hydroxide to release degraded HRP into solution. A

spectrum showing the Ruhemann's purple product is included as Figure 2.8.
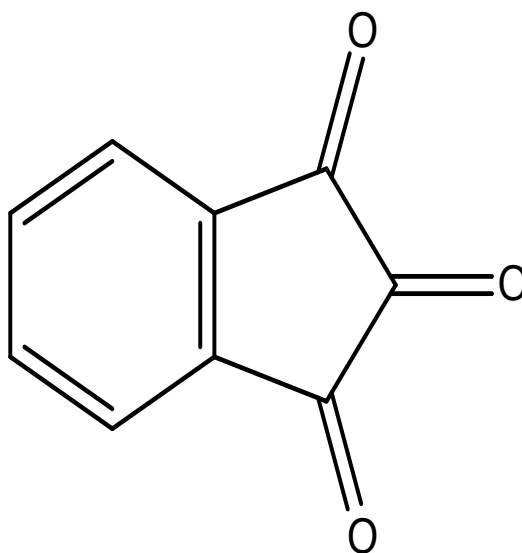
Figure 2.7 Chemical structure of ninhydrin (2,2-dihydroxyindane- 1,3-dione)
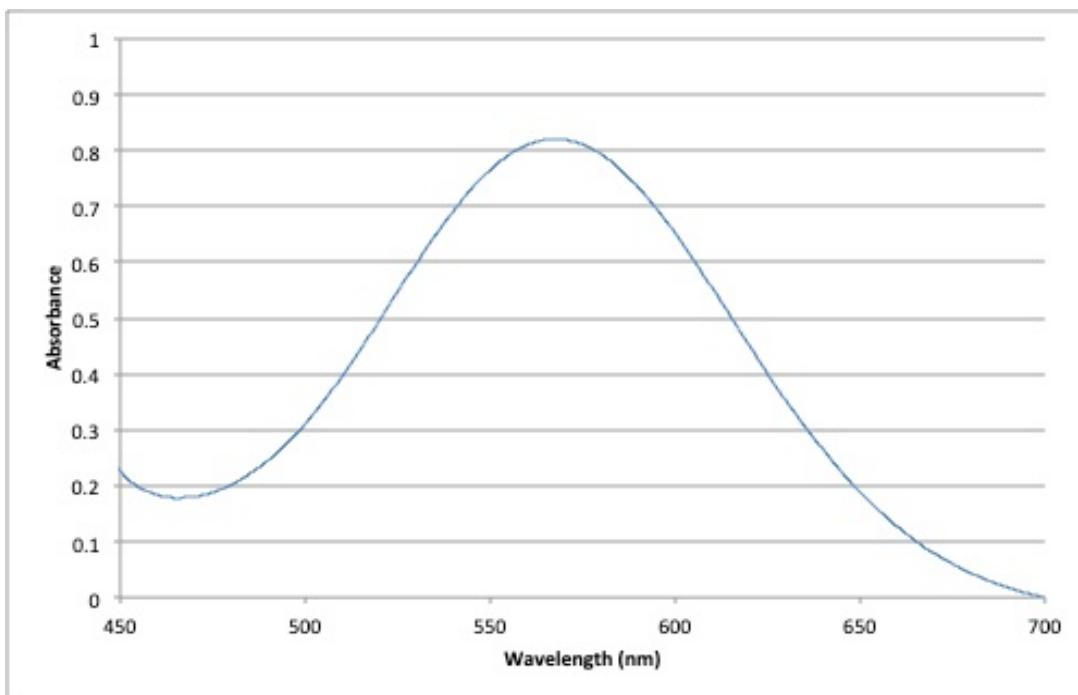
Figure 2.8 Spectrum of ninhydrin product after reaction with HRP

2.12 Preparation of Guaiacol Assay

Activity of the entrapped HRP was assessed through an HRP/guaiacol assay. A 100 mL solution of 3.3 μL liquid guaiacol and 1.4 μL 30% hydrogen peroxide in pH 7.4 10 mM phosphate buffer was prepared. This results in a 140 μM hydrogen peroxide and 300 μM guaiacol solution. The assay solution was prepared immediately before use. Hydrogen peroxide was stored at -20 °C and guaiacol was stored at room temperature, as recommended by the manufacturers.

Guaiacol, whose chemical structure is shown in Figure 2.9, was chosen to measure the activity of horseradish peroxidase due to its well-studied and easily detectable product.[46-49] The spectrum of the quinone product is shown in Figure 2.10.
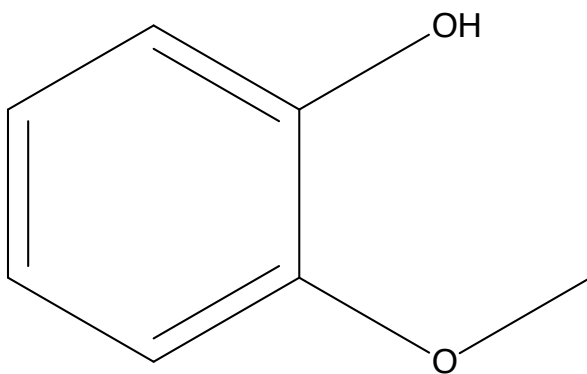
Figure 2.9 Chemical structure of guaiacol
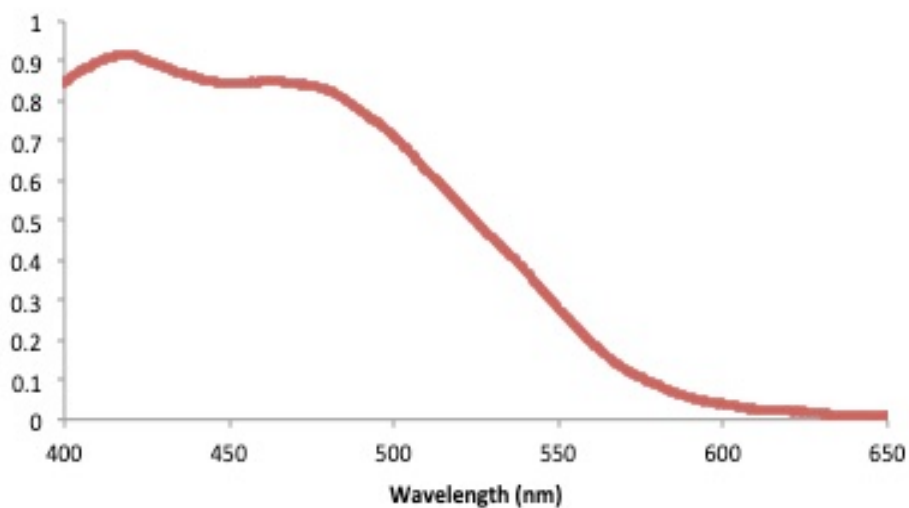
Figure 2.10 Spectrum of the product of HRP and guaiacol after 1 minute of reaction

2.13 UV-Vis Absorption Spectroscopy

Absorption spectra were taken with a Shimadzu UV-2101PC UV-Vis scanning spectrophotometer in a parallel two-beam configuration. Quantification of Rhodamine 6G loading in both capillary and flat surface films was performed spectroscopically via ethanol extraction. 25,000 MW BPEI loading was done with a spectroscopic copper (II) assay. Copper (II) sequestration by 25,000 MW BPEI thin films was quantified with a similar assay. Quantification of horseradish peroxidase in capillary tubes was initially attempted with a modified Bradford, which showed poor correlation and was deemed unreliable. Instead ninhydrin assays, through spectroscopic measurement of Ruhemann's purple, was used to quantify both loaded horseradish peroxidase in capillary tubes and solvent-accessible primary and secondary amines in 1800, 25,000, and 750000 MW thin films. Horseradish peroxidase activity in capillary tubes was quantified with a guaiacol/hydrogen peroxide assay. All assays used solution measurements, requiring no modification of the spectrophotometer or special protocols.

2.14 Antibiofilm Assays

Crystal violet assays were performed by Anh K. Lam in the Rice laboratory using their materials and UV-Vis spectrophotometer. Lam grew the biofilms on loaded films provided by us, dyed the biofilms, re-dissolved the crystal violet, and measured the results herself.

2.15 Scanning Electron Microscope (SEM)

A JEOL JSM-880 scanning electron microscope with a 5 nm Au-Pd sputter-coated layer was used to obtain images of thin films. All images were collected by Dr. Preston Larson at the University of Oklahoma. Cross-sectional images of internally-coated capillary tubes and flat surface thin films were collected in magnifications ranging from 2,500-100,000X to determine film thickness and examine film properties. Top-down images of BPEI loaded films were collected at 25,000X magnification to examine surface properties.

2.16 References

1.   Ebelmen, Untersuchungen über die Verbindungen der Borsäure und Kieselsäure mit Aether. *Justus Liebigs Annalen der Chemie* **1846,** *57* (3), 319-355.

2.   Danks, A. E.; Hall, S. R.; Schnepp, Z., The evolution of 'sol–gel' chemistry as a technique for materials synthesis. *Materials Horizons* **2016,** *3* (2), 91-112.

3.   Brinker, C. J.; Keefer, K. D.; Schaefer, D. W.; Ashley, C. S., Sol-gel transition in simple silicates. *Journal of Non-Crystalline Solids* **1982,** *48* (1), 47-64.

4.   Hench, L. L.; Simmons, J. H.; Zhu, B. F.; Ochoa, R. Laser dye impregnated silica sol-gel monoliths. US5222092A, 1993.

5.   Clavier, C. W.; Rodman, D. L.; Sinski, J. F.; Allain, L. R.; Im, H.-J.; Yang, Y.; Clark, J. C.; Xue, Z.-L., A method for the preparation of transparent mesoporous silica sol-gel monoliths containing grafted organic functional groups. *Journal of Materials Chemistry* **2005,** *15* (24), 2356-2361.

6.   Wu, X.; Choi, M. M. F.; Xiao, D., A glucose biosensor with enzyme-entrapped sol-gel and an oxygen-sensitive optode membrane. *Analyst (Cambridge, U. K.)* **2000,** *125* (1), 157-162.

7.   Sakka, S.; Kamiya, K.; Makita, K.; Yamamoto, Y., Formation of sheets and coating films from alkoxide solutions. *Journal of Non-Crystalline Solids* **1984,** *63* (1-2), 223-35.

8.   Sivakumar, S.; Van Veggel, F. C. J. M.; May, P. S., Near-Infrared (NIR) to Red and Green Up-Conversion Emission from Silica Sol-Gel Thin Films Made with La0.45Yb0.50Er0.05F3 Nanoparticles, Hetero-Looping-Enhanced Energy Transfer (Hetero-LEET): A New Up-Conversion Process. *Journal of the American Chemical Society* **2007,** *129* (3), 620-625.

9.   Juergen-Lohmann, D. L.; Nacke, C.; Simon, L. C.; Legge, R. L., Effect of sol-gel hydrophobicity on the distribution and structure of different proteins in organically modified sol-gel thin films. *Journal of Sol-Gel Science and Technology* **2009,** *52* (3), 370-381.

10.   Gilliland, J. W.; Yokoyama, K.; Yip, W. T., Solvent Effect on Mobility and Photostability of Organic Dyes Embedded inside Silica Sol-Gel Thin Films. *Chemical Materials* **2005,** *17* (26), 6702-6712.

11.   Abuin, M.; Serrano, A.; Llopis, J.; Garcia, M. A.; Carmona, N., Silica doped with lanthanum sol-gel thin films for corrosion protection. *Thin Solid Films* **2012,** *520* (16), 5267-5271.

12.   Nicole, L.; Boissiere, C.; Grosso, D.; Quach, A.; Sanchez, C., Mesostructured hybrid organic-inorganic thin films. *Journal of Materials Chemistry* **2005,** *15* (35-36), 3598-3627.

13.   Lim, M. H.; Stein, A., Comparative Studies of Grafting and Direct Syntheses of Inorganic-Organic Hybrid Mesoporous Materials. *Chemical Materials* **1999,** *11* (11), 3285-3295.

14.   Dimitriev, Y.; Ivanova, Y.; Iordanova, R., History of sol-gel science and technology (review). *Journal of the University of Chemical Technology and Metallurgy* **2008,** *43* (2), 181-192.

15.   Mackenzie, J. D., Sol-gel research - Achievements since 1981 and prospects for the future. *Journal of Sol-Gel Science and Technology* **2003,** *26* (1/2/3), 23-27.

16.   Wang, H.; Bardo, A. M.; Collinson, M. M.; Higgins, D. A., Microheterogeneity in Dye-Doped Silicate and Polymer Films. *Journal of Physical Chemistry B* **1998,** *102* (37), 7231-7237.

17.   Ellerby, L. M.; Nishida, C. R.; Nishida, F.; Yamanaka, S. A.; Dunn, B.; Valentine, J. S.; Zink, J. I., Encapsulation of proteins in transparent porous silicate glasses prepared by the sol-gel method. *Science (Washington, D. C., 1883-)* **1992,** *255* (5048), 1113-15.

18.   Yip, W. T.; Campbell, A.; Lei, Q. Kinetically controlled sol-gel doping method where the dopant is added during the gelation stage. US20160332194A1, 2016.

19.   Crosley, M. S.; Yip, W. T., Multienzyme, Multistep Biosensor Produced through Kinetic Doping. *Journal of Physical Chemistry B* **2019,** *123* (18), 3962-3967.

20.   Crosley, M. S.; Yip, W. T., Silica Sol-Gel Optical Biosensors: Ultrahigh Enzyme Loading Capacity on Thin Films via Kinetic Doping. *Journal of Physical Chemistry B* **2017,** *121* (9), 2121-2126.

21.   Crosley, M. S.; Yip, W. T., Kinetically Doped Silica Sol-Gel Optical Biosensors: Expanding Potential Through Dip-Coating. *ACS Omega* **2018,** *3* (7), 7971-7978.

22.   Campbell, A. L. O.; Lei, Q.; Tak Yip, W., Kinetic approach to hyper-doped optical quality thin films. *Chemical Communications (Cambridge, U. K.)* **2014,** *50* (66), 9321-9324.

23.   Young, S. K., Sol-gel science for ceramic materials. *Material Matters (Milwaukee, WI, U. S.)* **2006,** *1* (3), 8-10.

24.   J. Buckingham, F. M., *Dictionary of Organic Compounds*. 6 ed.; Chapman & Hall: 1995; Vol. 1-9.

25.   Laboratory, E. K. C.; Division, R. P., *Kodak Laser Dyes*. Laboratory and Research Products Division, Eastman Kodak Company: 1987.

26.   Kauffman, J. M., Laser dye structures and synonyms. *Applied Optics* **1980,** *19* (20), 3431-3435.

27.   Hammond, P., Spectra of the lowest excited singlet states of rhodamine 6G and rhodamine B. *IEEE Journal of Quantum Electronics* **1979,** *15* (7), 624-632.

28.   Berglund, G. I.; Carlsson, G. H.; Smith, A. T.; Szoeke, H.; Henriksen, A.; Hajdu, J., The catalytic pathway of horseradish peroxidase at high resolution. *Nature (London, U. K.)* **2002,** *417* (6887), 463-468.

29.   Zollner, H., *Handbook of Enzyme Inhibitors*. Second ed.; Wiley: 1993.

30.   Welinder, K. G., Amino acid sequence studies of horseradish peroxidase. Amino and carboxyl termini, cyanogen bromide and tryptic fragments, the complete sequence, and some structural characteristics of horseradish peroxidase C. *European Journal of Biochemistry* **1979,** *96* (3), 483-502.

31.   Shannon, L. M.; Kay, E.; Lew, J. Y., Peroxidase isozymes from horseradish roots. I. Isolation and physical properties. *Journal of Biological Chemistry* **1966,** *241* (9), 2166-72.

32.   Veitch, N. C., Horseradish peroxidase: a modern view of a classic enzyme. *Phytochemistry (Elsevier)* **2004,** *65* (3), 249-259.

33.   Takahashi, H.; Li, B.; Sasaki, T.; Miyazaki, C.; Kajino, T.; Inagaki, S., Catalytic Activity in Organic Solvents and Stability of Immobilized Enzymes Depend on the Pore Size and Surface Characteristics of Mesoporous Silica. *Chemical Materials* **2000,** *12* (11), 3301-3305.

34.   von Harpe, A.; Petersen, H.; Li, Y.; Kissel, T., Characterization of commercially available and synthesized polyethylenimines for gene delivery. *Journal of Controlled Release* **2000,** *69* (2), 309-322.

35.   Thakur, A. K.; Nisola, G. M.; Limjuco, L. A.; Parohinog, K. J.; Torrejos, R. E. C.; Shahi, V. K.; Chung, W.-J., Polyethylenimine-modified mesoporous silica adsorbent for simultaneous removal of Cd(II) and Ni(II) from aqueous solution. *Journal of Industrial and Engineering Chemistry (Amsterdam, Neth.)* **2017,** *49*, 133-144.

36.   Wang, J.; Li, Z., Enhanced selective removal of Cu(II) from aqueous solution by novel polyethylenimine-functionalized ion imprinted hydrogel: Behaviors and mechanisms. *Journal of Hazardous Materials* **2015,** *300*, 18-28.

37.   Zhang, W.; Liu, H.; Sun, C.; Drage, T. C.; Snape, C. E., Capturing CO2 from ambient air using a polyethyleneimine–silica adsorbent in fluidized beds. *Chemical Engineering Science* **2014,** *116*, 306-316.

38.   Gibney, K.; Sovadinova, I.; Lopez, A. I.; Urban, M.; Ridgway, Z.; Caputo, G. A.; Kuroda, K., Poly(ethylene imine)s as antimicrobial agents with selective activity. *Macromolecular Bioscience* **2012,** *12* (9), 1279-1289.

39.   Foxley, M. A.; Friedline, A. W.; Jensen, J. M.; Nimmo, S. L.; Scull, E. M.; King, J. B.; Strange, S.; Xiao, M. T.; Smith, B. E.; Thomas, K. J., III; Glatzhofer, D. T.; Cichewicz, R. H.; Rice, C. V., Efficacy of ampicillin against methicillin-resistant Staphylococcus aureus restored through synergy with branched poly(ethylenimine). *Journal of Antibiotics* **2016,** *69* (12), 871-878.

40.   Bradford, M. M., A rapid and sensitive method for the quantitation of microgram quantities of protein utilizing the principle of protein-dye binding. *Analytical Biochemistry* **1976,** *72*, 248-54.

41.   Troll, W.; Cannan, R. K., A modified photometric ninhydrin method for the analysis of amino and imino acids. *Journal of Biological Chemistry* **1953,** *200*, 803-11.

42.   Kaiser, E.; Colescott, R. L.; Bossinger, C. D.; Cook, P. I., Color test for detection of free terminal amino groups in the solid-phase synthesis of peptides. *Analytical Biochemistry* **1970,** *34* (2), 595-598.

43.   Yemm, E. W.; Cocking, E. C., Determination of amino acids with ninhydrin. *Analyst* **1955,** *80*, 209-13.

44.   Moore, S.; Stein, W. H., A modified ninhydrin reagent for the photometric determination of amino acids and related compounds. *Journal of Biological Chemistry* **1954,** *211*, 907-13.

45.   Moore, S.; Stein, W. H., Photometric ninhydrin method for use in the chromatography of amino acids. *Journal of Biological Chemistry* **1948,** *176*, 367-88.

46.   Smith, K.; Silvernail, N. J.; Rodgers, K. R.; Elgren, T. E.; Castro, M.; Parker, R. M., Sol-Gel Encapsulated Horseradish Peroxidase: A Catalytic Material for Peroxidation. *Journal of the American Chemical Society* **2002,** *124* (16), 4247-4252.

47.   Amako, K.; Chen, G.-X.; Asada, K., Separate assays specific for ascorbate peroxidase and guaiacol peroxidase and for the chloroplastic and cytosolic isoenzymes of ascorbate peroxidase in plants. *Plant Cell Physiology* **1994,** *35* (3), 497-504.

48.   Lemon, H. W., The effect of alkali on the ultraviolet absorption spectra of hydroxyaldehydes, hydroxyketones and other phenolic compounds. *Journal of the American Chemical Society* **1947,** *69* (12), 2998-3000.

49.   Tonami, H.; Uyama, H.; Nagahata, R.; Kobayashi, S., Guaiacol oxidation products in the enzyme-activity assay reaction by horseradish peroxidase catalysis. *Chemistry Letters* **2004,** *33* (7), 796-797.

2.17

CHAPTER 3 - Enzyme Loading in Internally Coated Capillary Tubes Via Kinetic Doping

3.1 Abstract

Development of capillary tubes internally doped with enzymes is of great interest for microfluidic reactions, and kinetic doping could provide a facile, inexpensive method for their manufacture. Kinetic doping has previously been demonstrated to have a high loading capacity with thin films coated on flat-surface coverslips. Dip coating of these surfaces was developed with the eventual intention to coat different shapes and sizes of substrates. In this study, we expand the use of kinetic doping to internally coated capillary tubes. Parameters for internally doping capillary tubes were developed with rhodamine 6G which produced internally coated thin films with a 90 nm thickness. Horseradish peroxidase was then loaded into the thin films, with a 47000X increase in concentration over the loading solution. Activity of the loaded HRP was determined to be 0.019 ± 0.003 U/mg, and shown to have a stronger resistance to denaturation by methanol.

3.2 Introduction

Many researchers have investigated the encapsulation of enzymes in silica in order to gain the benefits of immobilization, namely high reusability and higher chemical and thermal stability.[1-11] Sol-gel based technologies are especially promising, with their ease of synthesis and high loading capacity.[9, 12] Devices containing sol-gel immobilized enzymes in silica could be inexpensively and easily fabricated for biosensing or catalysis purposes. Additionally, immobilized enzymes have shown resistant to, and even catalytic activity in, organic solvents.[13-14] This potential for microfluidic applications and catalysis in different solvents means immobilization of enzymes in silica has great potential.

Microfluidic and flow-through reactions catalyzed by immobilized enzymes have begun to receive increased attention from researchers in recent years,[15-18] despite the loss of activity that generally comes from immobilization.[19-21] Flow-through reactions mainly rely on enzymes immobilized on beads,[22-23] and much of the research in microfluidic devices is focused on 'lab on a chip' technologies, where a 'chip' or very small device is developed for specific microfluidic reactions.[24-27] However, there is also interest in devices based on glass capillary tubes[28-29] or other tubing that allows flow through reactions.[30] These types of devices can either rely on capillary action, like many 'lab on a chip' technologies or have substrate driven through them by an external pump, providing a level of versatility in design. Of special interest, some of these devices are reconfigurable, allowing for multiple types of reactions to be performed with a single device, making them even more versatile.[31]

The internal coating of capillary tubes does present certain challenges, however, leading to some authors using very involved methods to obtain a continuous film, like the manufacture of specialized equipment for the elevation-evacuation of sol within the capillary without vibrational distrubances,[32] which may have led to less interest in internally coated capillary tubes despite their many desirable traits. Chemical modification of the surfaces for immobilization of enzymes in devices is also commonly required,[15-18] increasing the difficulty and expense of production. Overcoming these barriers to enable inexpensive and facile manufacturing of glass capillary tubes with high concentrations of immobilized enzymes could be of great benefit.

To that aim, we have extended the kinetic doping technique developed by our group to internally coat capillary tubes with silica thin films with entrapped horseradish peroxidase (HRP). Kinetic doping is a doping method that utilizes a window of opportunity in the gelation process of silica thin films where the ethanol has been mostly driven off, but cross-linking has not significantly proceeded, where proteins can be entrapped by the film without being denatured by the ethanol solvent often used in silica sol-gel chemistry. Kinetic doping has been shown to exhibit a high dopant capacity, produce films with a good retention of enzyme activity, and nearly instantaneous response time.[33] This could lead to an inexpensive manufacturing process for enzyme coated glass capillary tubes that is low on both material and labor cost, which is significant for potential commercialization. Additionally, this method could be extended to smaller diameter capillaries, leading to inexpensive microfluidic devices.

Here, we report a facile, inexpensive method for entrapping horseradish peroxidase internally in silica thin films on glass capillary tubes using kinetic doping. The method was developed using a dye, rhodamine 6G (R6G), then applied to the enzyme horseradish peroxidase. The activity of the entrapped horseradish peroxidase in the capillary tubes was measured, and a method for measuring the quantity of entrapped enzyme was developed. Additionally, observations were made on the resistance of entrapped enzymes to normally denaturing ethanol and methanol. To our knowledge, this is the first time that an entrapped enzyme has been internally coated onto a capillary tube using the sol-gel method.

3.3 Methods

3.3.1 Materials and General Methods

Tetraethylorthosilicate (TEOS), Rhodamine 6G (R6G), 95% ethanol, and 99% methanol were purchased from Sigma-Aldrich. Phosphoric acid and hydrogen peroxide (30% solution) were purchased from EMD Millipore. Horseradish peroxidase (HRP) was purchased from Gold Technology. Guaiacol was purchased from Cayman Chemical Company. Glass capillary tubes (25 μL Drummond Wiretrol Calibrated Micropipets) were purchased from Fisher Scientific. All chemicals and materials were used as received, with the exception of the glass capillary tubes and coverslips, which were cleaned prior to use. All UV−vis spectra were obtained via a Shimadzu UV-2101PC UV−vis spectrometer. Scanning electron microscopy (SEM) images were obtained via a JEOL JSM-880 instrument with a 5 nm Au−Pd sputter-coated layer to examine the morphology of the thin film and measure the film thickness.

3.3.2   Preparation of Glass Capillary Tubes

To remove any organic contaminants on the capillary tube inner-surface, 95% ethanol was pumped through each capillary for 5 minutes. Deionized water was then pumped through each capillary for 5 minutes. To remove aqueous contaminants, 10% HCl was subsequently pumped through each tube for 5 minutes. Finally, deionized water was then pumped through each capillary for 5 minutes. The capillaries were stored in deionized water until use.

3.3.3   Preparation of Silica Sol

Silica sol was prepared by mixing a 1:8:7 molar ratio of TEOS:ethanol:water with phosphoric acid acting as a catalyst. A mixture of 55.9 mL of TEOS, 111.8 mL of ethanol, 31.7 mL of deionized water and 0.62 mL of 1% v/v phosphoric acid at room temperature were prepared for most coatings. The sol was then allowed to age for 20 hours at room temperature before use.

3.3.4   Preparation of Internally-Doped Silica Sol-Gel Thin Films in Capillary Tubes

Thin films were prepared by drain coating with a sol solution inside a centrifuge tube, based on the drain coated film preparation method of Crosley et al.[33] After aging for 20 hours, the silica sol solution was transferred to a 50 mL round-bottom glass centrifuge tube, elevated by a jack stand. A clean capillary tube was purge dried with compressed air and immersed in the aged silica sol-gel coating solution while suspended from above.

The capillary was positioned so that sol was pulled up into the tube by capillary action to the 25 μL mark. The sol solution in the centrifuge tube was then drained at a rate of 0.09 cm/sec. The capillary was allowed to age on the drain coating set-up in ambient air for 5 minutes, subsequently referred to as the delay time. It was then transferred to a hose with house air running through it at 3 LPM for 1 minute, subsequently referred to as the drying time. The outside of the capillary was then wiped to remove any externally coated thin film. It was then placed in a test tube with loading solution, where the loading solution was drawn into the tube through capillary action, again to the 25 μL mark.

R6G was allowed to load into the film via kinetic doping for one hour, and HRP was allowed to load into the film for one week. The loading solution consisted of 1 mM R6G in 10 mM phosphate buffer, adjusted to pH 7.4 with phosphoric acid or 0.1 mg/mL HRP in 10 mM phosphate buffer, adjusted to pH 7.4 with phosphoric acid. After loading, capillaries were removed from solution, rinsed with DI water to remove all of the adsorbed R6G or most of the adsorbed HRP, dried with house air, and tested or stored for future use. Post-doped controls, where HRP is immobilized via simple surface adsorption, were made by extending the delay time to 15 minutes and the dry time to 10 minutes, then submerging the tubes in 10 mM phosphate buffer, pH 7.4, for one hour. The capillaries were then removed, rinsed, and dried, and placed in the same loading solution for the same amount of time as the kinetically doped samples for comparison.

3.3.5 Quantitative Determination of R6G Loading

R6G loading was determined by alcohol extraction of R6G. Capillary tubes loaded with R6G were submerged in 95% ethanol for 24 hours, to allow all trapped dye to escape into solution. For comparison, flat surface films were submerged in 95% ethanol for multiple days, with sonication and addition of fresh solvent three times, in an attempt to extract all solvent accessible dye from the silica film. The absorbance of these solutions was then measured at 532 nm. Thickness of the flat surface films was calculated using the Landau-Levich equation[34] to determine the original R6G concentration in the films.

3.3.6 Quantitative Determination of HRP Loading

HRP loading in capillary tubes was quantified via the ninhydrin method of protein quantification, based on the procedure developed by Troll et al.[35] Briefly, solutions of 500 mg of ninhydrin dissolved in 10 mL of absolute ethanol, 80 mg of phenol dissolved in 20 mL absolute ethanol, and 2 mL of 0.01 M KCN in 100 mL pyridine were prepared. Capillary tubes that had been loaded with HRP were allowed to sit in 2 mL of 2 M NaOH for two weeks to dissolve the thin film and release the encapsulated HRP, then the solution was brought to approximately pH 7 with concentrated HCl. 1 mL of this solution was then combined with 2 mL of the phenol and 2 mL of the KCN solutions in a test tube. The test tube was then stoppered and placed into a boiling water bath and allowed to equilibrate. 0.4 mL of the ninhydrin solution was then added and the reaction was allowed to proceed for 5 minutes. The absorbance of this solution was then measured at 571 nm. A standard curve was constructed by dissolving known quantities of HRP in 2 M

NaOH and following the same procedure (see Figure 3.1). The samples were compared to the standard curve to determine the amount of HRP in solution, and the original amount of HRP in the capillary tubes was then calculated. The absorbance of the sample solutions did not increase when the capillary tubes were allowed to sit in NaOH more than two weeks, so all HRP was assumed to be released into solution in two weeks.
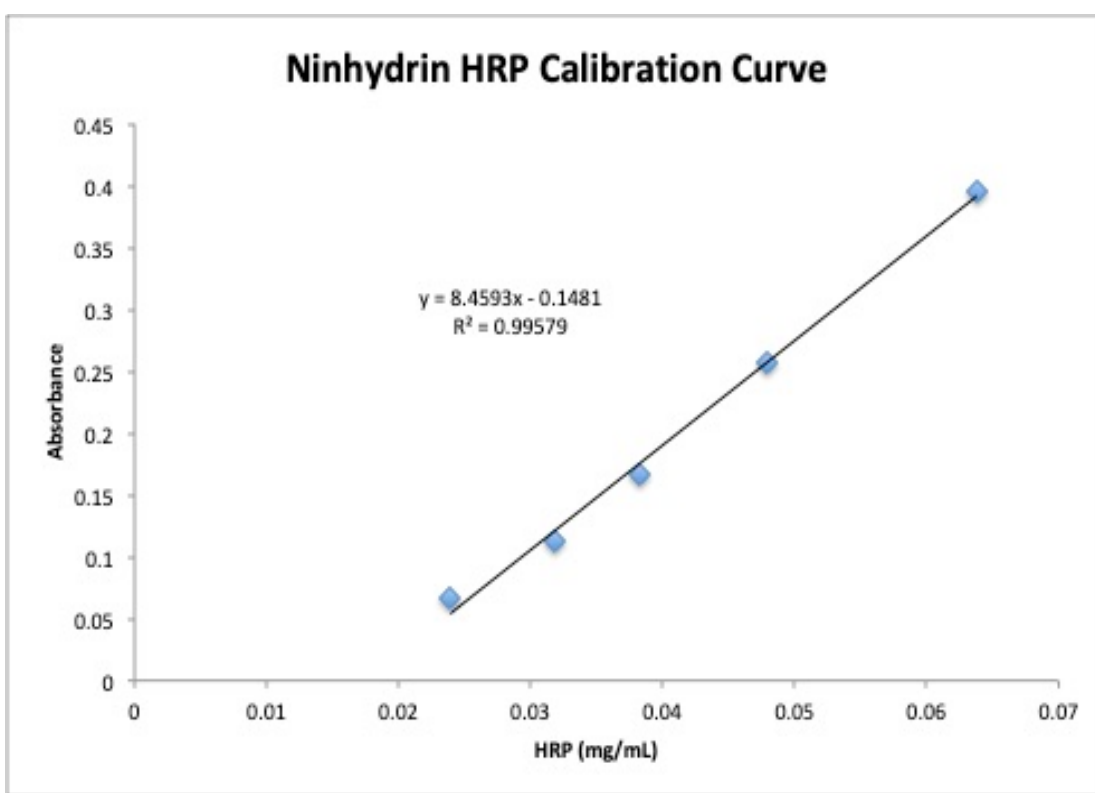
Figure 3.1 Calibration curve constructed with horseradish peroxidase in solution, which had been denatured with sodium hydroxide. A ninhydrin assay was then performed on the samples to determine the linear response portion.

3.3.7 Quantitative Determination of HRP Activity

Activity of the entrapped HRP was assessed through an HRP/guaiacol assay. The formation of the quinone product was monitored through UV-vis absorption at 436 nm. A 100 mL solution of 3.3 μL liquid guaiacol and 1.4 μL 30% hydrogen peroxide in pH 7.4

10 mM phosphate buffer was pumped into capillary tubes for differing time periods, then

pumped back into a cuvette for absorption measurement. Due to adsorbed HRP washing

off of the tubes and continuing to react in the cuvettes, the formation of the quinone was

monitored for several minutes and the concentration at the time the solution was pumped

out of the capillaries was obtained by extrapolation (see Figure 3.2 for an example of this

data). The enzyme activity could then be calculated using the initial rate method, as all

measured time points fell into the initial linear rate portion of the reaction (see Figure

3.3).
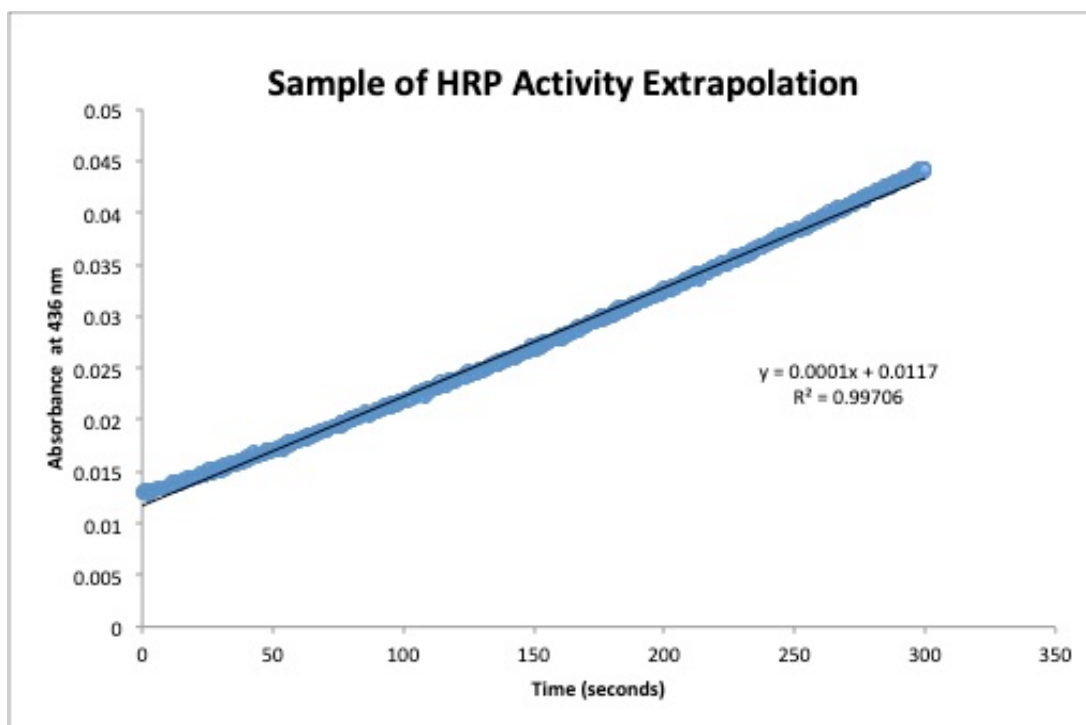
Figure 3.2 Example of one of the samples used to determine HRP activity. Adsorbed HRP came off into solution when measuring activity, causing the reaction to continue outside of the capillary tube. In order to extrapolate what the initial absorbance measurement was, the time it took to transfer the solution from the capillary to the cuvette was recorded and the reaction was allowed to continue for 5 minutes while being recorded. A linear fit was then applied and the absorbance of the product at the time of transfer was calculated.
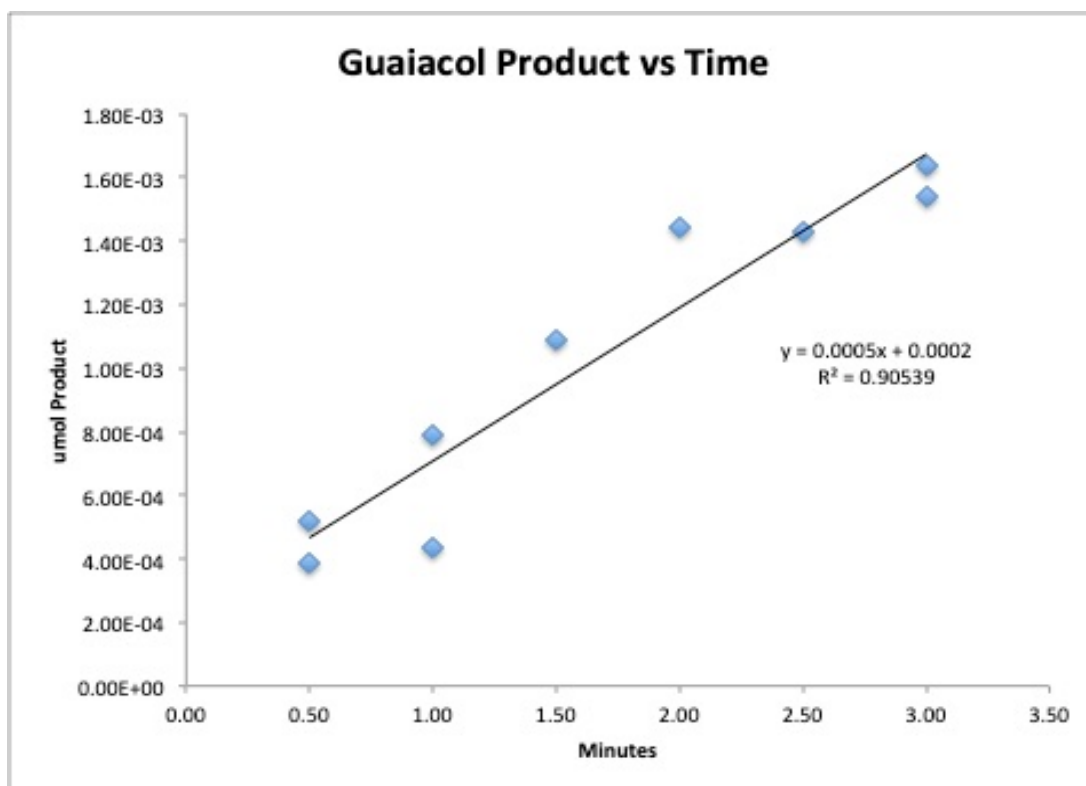
Figure 3.3 Micromole of the quinone product of guaiacol (as measured with absorbance readings at 436 nm) plotted versus time of the guaiacol in contact with the HRP loaded capillaries to determine activity of the enzyme.

3.4 Results and Discussion

3.4.1 Parameter Optimization with Rhodamine 6G

Internally coating a capillary tube with a silica thin film using the sol-gel method presents unique challenges as compared to flat surface coating. The sol gel process works through two main reactions: hydrolysis and polycondensation. These reactions release ethanol and water into the surrounding air as the film gels. The formation of the films requires the evaporation of these by-products. The enclosure inherent in capillary tubes impedes this evaporation, slowing the formation of the films. Additionally, exposure to the sol vapors is known to negatively affect flat surface films, damaging the structural integrity of the

film.[33] Instead of a continuous film, exposure to vapors results in sparse aggregates. This can be seen by the loading of R6G, which only loads into the coated silica aggregates (as shown by the faint, mottled loading in Figure 3.4A) and does not adhere to the glass substrate after washing.
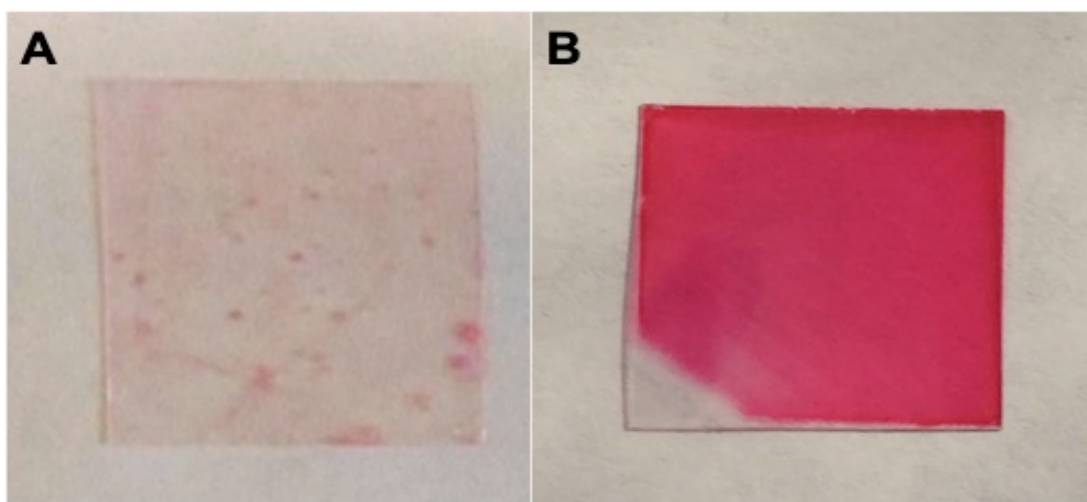
Figure 3.4 A) Photograph of film that was exposed to the vapors from the sol while aging. Sparse aggregates loaded with R6G can be seen on the film. B) Photograph of film that was not exposed to vapors while aging. The continuous film loaded with R6G, excepting the corner that is not dipped into the sol during coating, can be seen.

To prevent this, house air was forced through the capillary tubes after drain coating. Initially, capillary tubes were drained of sol, and then put immediately onto a hose with an attached air regulator. This resulted in films that were, to the eye, evenly coated with R6G (see Figure 3.5A). However, as SEM images reveal, the sol had formed aggregates, instead of films, on the inside of the capillary tubes (see Figure 3.5B). This is likely due to vibrations introduced when moving the capillary from the drain coating set-up to the purge drying set-up. The vibrations disrupt the film development and compromise its structural integrity before there is sufficient polycondensation to set the film, thereby breaking the nascent film into aggregates.
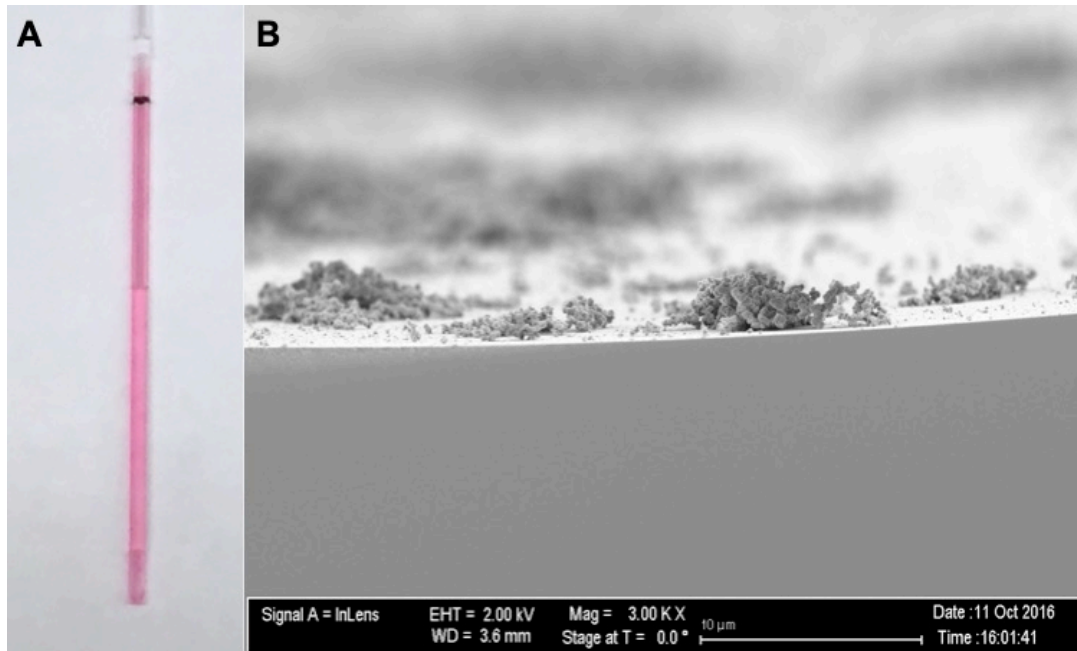
Figure 3.5 A) Photograph of capillary tube with no delay time and 1 minute drying time at 3 LPM air flow, loaded with R6G. B) SEM of a capillary tube made using the same parameters, showing aggregates instead of a thin film.
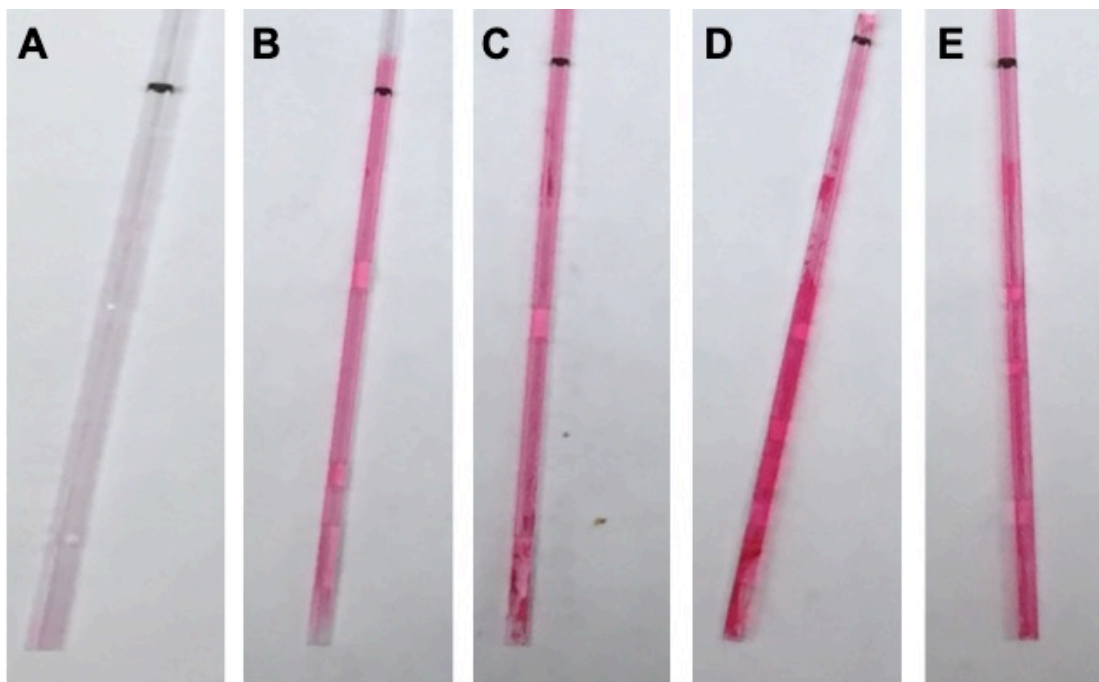
Figure 3.6 Capillary tubes loaded with R6G with a delay time of 5 minutes, dried at 3 LPM for A) 0 minutes, B) 1 minute, C) 2 minutes, D) 5 minutes, E) 10 minutes.

Drying time is also necessary, however, as films that had a 5 minute delay time but were

not purge dried showed no loading (see Figure 3.6). One minute of purge drying at 3 LPM was enough to enable loading, so several delay times from 5 minutes to 15 minutes were tested with a 1 minute drying time at 3 LPM after all delay times. While the capillary tubes looked visually similar to the capillaries without a delay time, the SEM images showed a thin film, instead of aggregates (see Figure 3.7). While these films were not even, and some aggregates could still be seen attached to the film surface, they were consistent for all delay times with an average thickness of 90 nm. Thus, a delay time of 5 minutes was chosen for further coating. With parameters for an intact film determined,
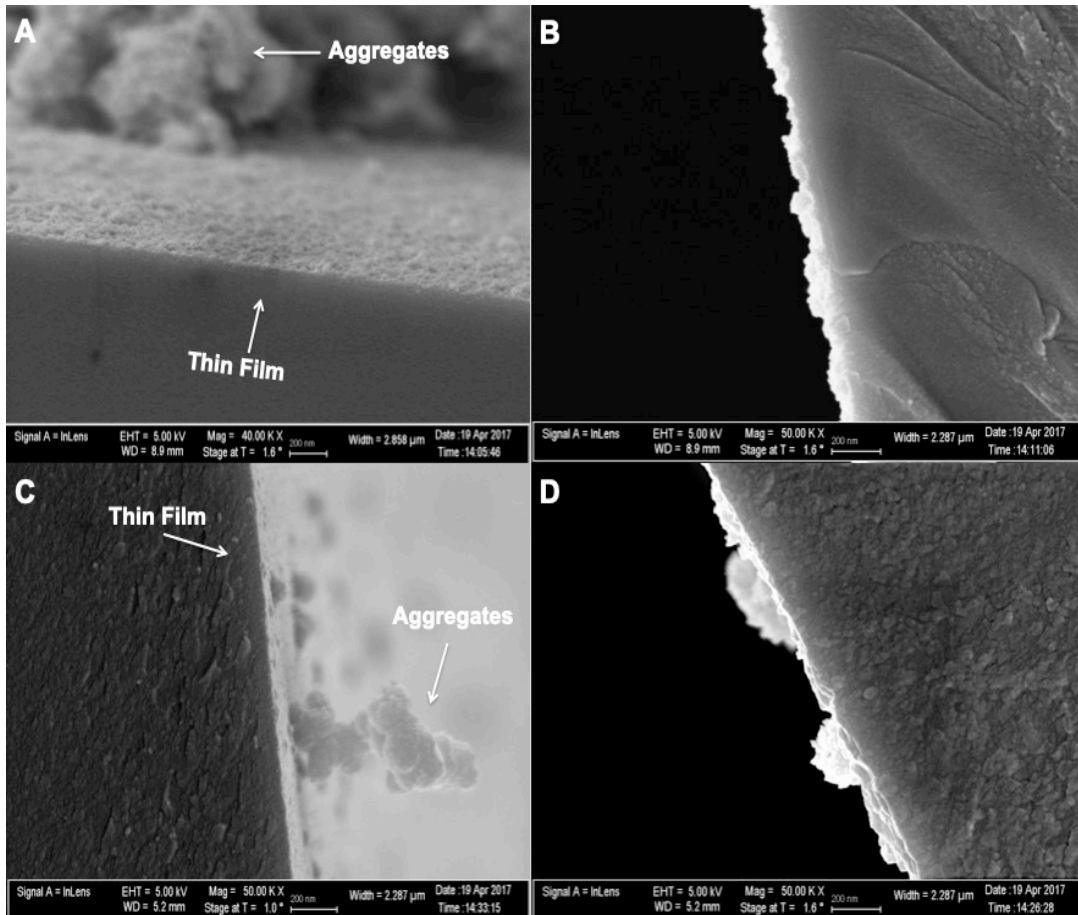
Figure 3.7 SEM images of capillary tubes loaded with R6G, with a dry time of 1 minute and a delay time of A&B) 5 minutes and C&D) 15 minutes. Both films are approximately 90 nm thick, although thickness of film is highly variable for both delay times.

subsequent loading was done with horseradish peroxidase.

3.4.2 Quantitative Determination of Horseradish Peroxidase Loading

Using the parameters determined from R6G loading, horseradish peroxidase (HRP) was loaded into the capillary tubes. After loading, the same guaiacol assay that was used for flat-surface films was used to check for enzyme activity, but an assay had to be developed to quantify the amount of protein loaded into the capillaries first.

The internally-coated thin films were dissolved by incubating the tubes with 2 M sodium hydroxide for two weeks. A ninhydrin assay was then performed on the dissolved films, which was compared to a standard curve made from free HRP denatured in 2 M sodium hydroxide. Using this curve, the films were determined to have an average of 0.051 ± 0.007 mg of the protein loaded. Using the 90 nm average thickness, a concentration of approximately 0.11 M or 4700 mg/mL, a 47000X increase from the loading solution, is calculated. The capillary tubes also had a large amount of adsorbed HRP on the internal surface, which could not be easily washed off. Post-doped controls, which should have very little kinetic doping and instead have predominantly surface adsorbed HRP, showed loading of 3700 mg/mL, which is 79% of the total loading. Kinetic doping would thus account for 985 mg/mL of HRP loaded into the film; a 9850X increase over the initial loading solution.

This is an even larger increase over the initial loading solution than seen with flat surface loading, which has an increase of 2400X; it is worth noting, however, the modified Bradford assay used on flat surface loading was only able to quantify the solvent

accessible HRP and was thought to underestimate the amount of total HRP loaded, due to the size of the Coomassie blue dye limiting its diffusion into the thin film.[33] The modified Bradford assay developed by Crosley et al.[8] to quantify the amount of HRP loaded onto flat-surface coverslips could not be used for capillary tubes. The results obtained from such measurements in the capillary tube exhibited poor correlation for both the decrease of the unbound form or the increase of the bound form of the Coomassie blue dye and thus deemed unreliable for this work. The ninhydrin assay here works with the dissolved thin film, so all loaded protein, not just the solvent-accessible protein, is quantified.

The HRP that was kinetically doped did differ from the post-doped HRP as demonstrated by denaturation of the protein with ethanol and methanol. Both kinetically doped and post-doped capillaries showed activity after soaking in a 30% ethanol for one week or after pumping 95% ethanol through the capillaries for 48 hours. This exposure to ethanol would denature free HRP in solution. Additionally, kinetically doped capillaries kept activity when 99% methanol was pumped through the tubes for 15 seconds, but the methanol stopped the activity of the post-doped controls. Pumping 99% methanol through either the kinetically doped or post-doped capillaries for longer than 15 seconds deactivated all HRP. Images of these tubes, with kinetically doped tubes that were and were not exposed to methanol and a post-doped control that has been exposed to methanol, are seen in Figure 3.8. This resistance seems to mean that both types of doping provide a large degree of protection from ethanol which is not uncommon for enzymes trapped in solid state.[36] However, the kinetically doped HRP was afforded additional protection from even methanol. The additional protection provided by kinetic doping

over post-doped controls means kinetically doped internally coated capillary tubes have the potential to utilize enzymes to catalyze reactions in non-aqueous solutions or to be sterilized for possible medical applications more so than a more traditional method of entrapping proteins on a flat surface as they are more resistant to denaturing solvents.
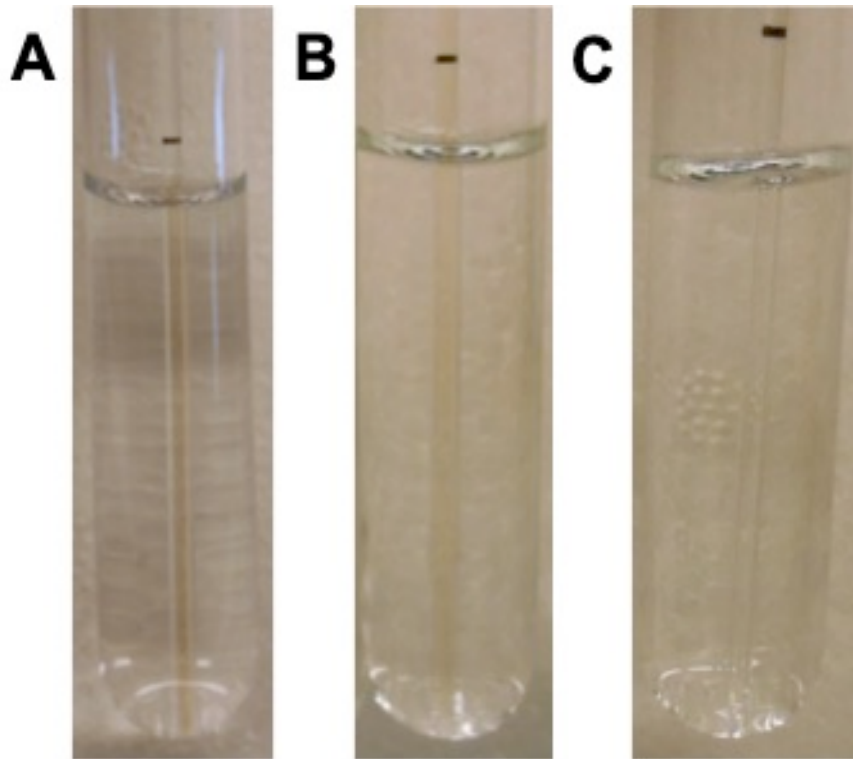
Figure 3.8 A) Capillary tube kinetically doped with HRP exposed to the guaiacol/hydrogen peroxide assay, showing the dark brown quinone product. This product indicates the enzymes are still active after loading. B) Capillary tube kinetically doped with HRP exposed to the guaiacol/hydrogen peroxide assay after being exposed to methanol for 15 seconds, still showing the dark brown quinone product. This product indicates the enzymes are still active after methanol exposure. C) Capillary tube post-doped with HRP exposed to the guaiacol/hydrogen peroxide assay after being exposed to methanol for 15 seconds, with the dark brown quinone product no longer being produced. The lack of this product indicates the enzymes are no longer active.

3.4.3   Activity Determination of Horseradish Peroxidase

After determination of the amount of HRP loaded into the thin films, activity of the enzyme had to be determined to assess the application potential of the internally coated capillary tubes. The ability of the enzyme to catalyze guaiacol was quantified through monitoring the appearance of the quinone product by UV-vis spectroscopy in a series of time points. Using the activity and the amount of HRP loaded into the film, the activity per milligram of protein was calculated to be 0.019 ± 0.003 U/mg. This is a marked decrease from the activity of free HRP, 35.4 ± 0.8 U/mg, or HRP loaded onto a flat-surface substrate, 3.7 ± 0.2 U/mg.[33]

The low activity may be partially explained by the method of protein quantification used here, versus the modified Bradford assay used to quantify the loading in flat surface samples. In this work, all protein, even that which is not accessible to solution, is quantified by dissolving the film. Only solvent accessible HRP was quantified by the Bradford assay, which is the only HRP that could interact with the substrate. Any HRP that is not solvent accessible would artificially deflate the activity of the capillary tubes. The increase in concentration over the loading solution is 490% higher in the capillary tubes than on a flat surface, but it seems unlikely such a similar doping protocol would yield such different results. More likely, much of the protein quantified in the capillary thin films is not solvent accessible, increasing the amount quantified but not the amount available to interact with the substrate. Moreover, the surface area of a capillary tube is approximately 95% less than that of the flat surface samples. If more HRP is loaded into the film in capillary tubes, then it would by necessity be solvent-inaccessible due to the

decreased surface area. Given the decrease in surface area, and the marked increase in concentration in the film, the decrease in activity is likely not due to any additional denaturing or restriction of the enzyme in the capillaries versus the coverslips, but due to the solvent-inaccessibility of the majority of the enzymes. This could be remedied by using a different silica alkoxide precursor with larger alkoxide groups, which should increase pore size and thus accessibility of the enzymes.

This is further supported by a comparison of the solvent accessible dye between the capillary tubes and flat surface films. Internally coated films have a solvent-accessible R6G concentration of 0.58 ± 0.04 M, while flat surface films, with the same loading parameters and using the same quantification method, have a concentration of 1.0 ± 0.2 M, almost double the amount in the capillaries. The higher loading of dye in the flat surface films over the internally coated capillary tubes suggests the amount of HRP loaded should also be higher in the flat surface films if the same quantification method could be used.

Additionally, the measured activity of the HRP in the capillary tubes, even with the likely underestimation, is still comparable to that achieved in covalently bonded HRP in packed bed columns.[23] This means that flow-through reactions can be carried out with approximately the same efficiency in the internally coated capillaries, but with much smaller amounts of substrate and solvent.

3.5   Conclusions

In this study, we demonstrate the ability to kinetically dope internally coated capillary tubes with silica thin films by the sol-gel method. This method is less complex than previous methods used to internally coat capillary tubes by the sol-gel method and has a high enzyme loading capacity, resulting in a 47000X increase in HRP concentration in the thin film over the loading solution. While the activity of the enzyme is markedly decreased by entrapment, its resistance to denaturing methanol is increased compared to post-doped controls. This is the first time, to our knowledge, that enzymes have been loaded into internally coated thin films using the sol-gel method. The method to load these internally coated capillary tubes developed here represents a step toward the facile and inexpensive development of reconfigurable devices that could be used to enable complex reaction schemes in microfluidic devices.

3.6 References

1.   Ryu, Y. H.; Yeo, K. B.; Ki, M.-R.; Kim, Y. J.; Pack, S. P., Improved stability and reusability of endoglucanase from Clostridium thermocellum by a biosilica-based auto-encapsulation method. *Biochemical Engineering Journal* **2016,** *105* (Part_A), 144-149.

2.   Ellerby, L. M.; Nishida, C. R.; Nishida, F.; Yamanaka, S. A.; Dunn, B.; Valentine, J. S.; Zink, J. I., Encapsulation of proteins in transparent porous silicate glasses prepared by the sol-gel method. *Science* **1992,** *255* (5048), 1113-5.

3.   Braun, S.; Rappoport, S.; Zusman, R.; Avnir, D.; Ottolenghi, M., Biochemically active sol-gel glasses: the trapping of enzymes. *Materials Letters* **1990,** *10* (1-2), 1-5.

4.   Gill, I.; Ballesteros, A., Encapsulation of biologicals within silicate, siloxane, and hybrid sol-gel polymers: an efficient and generic approach. *Journal of the American Chemical Society* **1998,** *120* (34), 8587-8598.

5.   Gill, I.; Ballesteros, A., Bioencapsulation within synthetic polymers (Part 1): sol-gel encapsulated biologicals. *Trends in Biotechnology* **2000,** *18* (7), 282-296.

6.   Bhatia, R. B.; Brinker, C. J.; Gupta, A. K.; Singh, A. K., Aqueous Sol-Gel Process for Protein Encapsulation. *Chemical Materials* **2000,** *12* (8), 2434-2441.

7.   Pierre, A. C., The Sol-Gel Encapsulation of Enzymes. *Biocatalysis & Biotransformation* **2004,** *22* (3), 145-170.

8.   Crosley, M. S.; Yip, W. T., Silica Sol-Gel Optical Biosensors: Ultrahigh Enzyme Loading Capacity on Thin Films via Kinetic Doping. *Journal of Physical Chemistry B* **2017,** *121* (9), 2121-2126.

9.   Jeronimo, P. C. A.; Araujo, A. N.; Montenegro, M. C. B. S. M., Optical sensors and biosensors based on sol-gel films. *Talanta* **2007,** *72* (1), 13-27.

10.   Ciriminna, R.; Fidalgo, A.; Pandarus, V.; Beland, F.; Ilharco, L. M.; Pagliaro, M., The Sol-Gel Route to Advanced Silica-Based Materials and Recent Applications. *Chemical Reviews (Washington, DC, U. S.)* **2013,** *113* (8), 6592-6620.

11.   Zhang, F.; Wang, M.; Liang, C.; Jiang, H.; Shen, J.; Li, H., Thin-layer polymer wrapped enzymes encapsulated in hierarchically mesoporous silica with high activity and enhanced stability. *Scientific Reports* **2014,** *4*, article 4421.

12.   Crosley, M. S.; Yip, W. T., Multienzyme, Multistep Biosensor Produced through Kinetic Doping. *Journal of Physical Chemistry B* **2019,** *123* (18), 3962-3967.

13.   Takahashi, H.; Li, B.; Sasaki, T.; Miyazaki, C.; Kajino, T.; Inagaki, S., Catalytic Activity in Organic Solvents and Stability of Immobilized Enzymes Depend on the Pore Size and Surface Characteristics of Mesoporous Silica. *Chemical Materials* **2000,** *12* (11), 3301-3305.

14.   Takahashi, H.; Li, B.; Sasaki, T.; Miyazaki, C.; Kajino, T.; Inagaki, S., Immobilized enzymes in ordered mesoporous silica materials and improvement of their stability and catalytic activity in an organic solvent. *Microporous and Mesoporous Materials* **2001,** *44-45*, 755-762.

15.   Lian, X.; Fang, Y.; Joseph, E.; Wang, Q.; Li, J.; Banerjee, S.; Lollar, C.; Wang, X.; Zhou, H.-C., Enzyme-MOF (metal-organic framework) composites. *Chemical Society Reviews* **2017,** *46* (11), 3386-3401.

16.   Zhu, Y.; Chen, Q.; Shao, L.; Jia, Y.; Zhang, X., Microfluidic immobilized enzyme reactors for continuous biocatalysis. *Reaction Chemistry & Engineering* **2020,** *5* (1), 9-32.

17.   Honda, T.; Yamaguchi, H.; Miyazaki, M., Development of Enzymatic Reactions in Miniaturized Reactors. *Advance Biotechnology* **2017,** *5* (Applied Bioengineering), 99-166.

18.   Britton, J.; Majumdar, S.; Weiss, G. A., Continuous flow biocatalysis. *Chemical Society Reviews* **2018,** *47* (15), 5891-5918.

19.   Monton, M. R. N.; Forsberg, E. M.; Brennan, J. D., Tailoring Sol–Gel-Derived Silica Materials for Optical Biosensing. *Chemistry of Materials* **2012,** *24* (5), 796-811.

20.   Heller, J.; Heller, A., Loss of Activity or Gain in Stability of Oxidases upon Their Immobilization in Hydrated Silica: Significance of the Electrostatic Interactions of Surface Arginine Residues at the Entrances of the Reaction Channels. *Journal of the American Chemical Society* **1998,** *120* (19), 4586-4590.

21.   Zoungrana, T.; Findenegg, G. H.; Norde, W., Structure, stability, and activity of adsorbed enzymes. *Journal of Colloid and Interface Science* **1997,** *190* (2), 437-448.

22.	Heinzler, R.; Fischoeder, T.; Elling, L.; Franzreb, M., Toward automated enzymatic glycan synthesis in a compartmented flow microreactor system. *Advanced Synthetic Catalysis* **2019,** *361* (19), 4506-4516.

23.	Bilal, M.; Iqbal, H. M. N.; Hussain Shah, S. Z.; Hu, H.; Wang, W.; Zhang, X., Horseradish peroxidase-assisted approach to decolorize and detoxify dye pollutants in a packed bed bioreactor. *Journal of Environmental Management* **2016,** *183*, 836-842.

24.	Liao, Z.; Wang, J.; Zhang, P.; Zhang, Y.; Miao, Y.; Gao, S.; Deng, Y.; Geng, L., Recent advances in microfluidic chip integrated electronic biosensors for multiplexed detection. *Biosensors and Bioelectronics* **2018,** *121*, 272-280.

25.	Zhou, W.; Le, J.; Chen, Y.; Cai, Y.; Hong, Z.; Chai, Y., Recent advances in microfluidic devices for bacteria and fungus research. *Trends in Analytical Chemistry* **2019,** *112*, 175-195.

26.	Mukherji, S.; Mondal, D., Lab-on-chip (LOC) devices for point of care (POC) applications. *Woodhead Publishing Series in Biomaterials* **2017,** *118* (Medical Biosensors for Point of Care (POC) Applications), 99-131.

27.	Li, N.; Zhang, W.; Li, Y.; Lin, J.-M., Analysis of cellular biomolecules and behaviors using microfluidic chip and fluorescence method. *Trends in Analytical Chemistry* **2019,** *117*, 200-214.

28.	Tan, X.; Khaing Oo, M. K.; Gong, Y.; Li, Y.; Zhu, H.; Fan, X., Glass capillary based microfluidic ELISA for rapid diagnostics. *Analyst* **2017,** *142* (13), 2378-2385.

29.   Besanger, T. R.; Hodgson, R. J.; Green, J. R. A.; Brennan, J. D., Immobilized enzyme reactor chromatography: Optimization of protein retention and enzyme activity in monolithic silica stationary phases. *Analytica Chimica Acta* **2006,** *564* (1), 106-115.

30.   Jannat, M.; Yang, K.-L., Immobilization of Enzymes on Flexible Tubing Surfaces for Continuous Bioassays. *Langmuir* **2018,** *34* (47), 14226-14233.

31.   Bandulasena, M. V.; Vladisavljevic, G. T.; Benyahia, B., Versatile reconfigurable glass capillary microfluidic devices with Lego inspired blocks for drop generation and micromixing. *Journal of Colloid and Interface Science* **2019,** *542*, 23-32.

32.   Jing, C.; Zhao, X.; Han, J.; Zhu, K.; Liu, A.; Tao, H., A new method of fabricating internally sol-gel coated capillary tubes. *Surface Coating Technology* **2003,** *162* (2-3), 228-233.

33.   Crosley, M. S.; Yip, W. T., Kinetically Doped Silica Sol-Gel Optical Biosensors: Expanding Potential Through Dip-Coating. *ACS Omega* **2018,** *3* (7), 7971-7978.

34.   L. Landau, V. L., Dragging of a Liquid by a Moving Plate. *Acta Physicochim U.R.S.S.* **1942,** *17*, 42-54.

35.   Troll, W.; Cannan, R. K., A modified photometric ninhydrin method for the analysis of amino and imino acids. *Journal of Biological Chemistry* **1953,** *200*, 803-11.

36.   Kunkel, J.; Asuri, P., Function, Structure, and Stability of Enzymes Confined in Agarose Gels. *PLOS ONE* **2014,** *9* (1), e86785.

3.7

CHAPTER 4 - Amine-Functionalization of Silica Sol-Gel Thin Films via Kinetic Doping

4.1   Abstract

Amine-fuctionalized thin films are highly desirable technologies for analytical, materials, and biochemistry applications. Current functionalization procedures can be costly, environmentally unfriendly, and require many synthetic steps. Here, we present an inexpensive and facile way to functionalize a silica thin film with 25000 MW branched polyethylenimine (BPEI), consistent with green chemistry principles. Using UV-vis spectroscopy and scanning electron microscopy, BPEI was determined to be loaded into the film at approximately 0.5 M concentration, which is a 500X increase from the loading solution used. The films were also tested for copper (II) sequestration to assess their potential for heavy metal sequestration, and showed high loading capacity of 10 ± 6 mmol/g. Films proved to be reusable, using EDTA to chelate copper and regenerate the films, with only a 6% reduction in the amount of copper (II) ions sequestered by the third use. The films also proved stable against leaching over the course of one week in solution, with less than 1% of the original BPEI lost under various storage conditions (i.e. storage in DI water, storage in dilute BPEI solution, storage in DI water after annealing). These films show promise for multiple applications, from heavy metal sequestration to anti-fouling applications, while being inexpensive, facile, and environmentally friendly to

synthesize. To our knowledge, this is the first time that BPEI has been doped into silica thin films.

4.2 Introduction

Surface functionalization of silica is of great interest in many different fields, with the ability to change the surface chemistry of silica particles, monoliths, and thin films a highly desirable technology. Functionalization can drastically change the behavior of the silane groups that are typically found on the surface of silica gels.[1-5] Surface functionalization of silica with various amine-containing compounds has shown increased adsorption of proteins,[6] anti-fouling effects,[7] increased heavy metal adsorption,[8] chromatography applications,[9] catalytic applications,[10] and more.

One polyamine of great interest for functionalization of silica solid substrates is branched polyethylenimine (BPEI). BPEIs are polymers of variable molecular weights, rich in primary, secondary, and tertiary amine groups. They have shown great potential for environmental applications such as aqueous heavy metal removal[11-12] and carbon dioxide capture[13] when attached to a solid substrate. They have also shown antimicrobial activity both on their own[14] and as antibiotic potentiators.[15]

While BPEI has been loaded into monoliths and nanoparticles, to the best of our knowledge, they have never been successfully loaded into silica thin films, most likely due to their very basic nature that may significantly impair thin film formation, as basic conditions tend to favor nanoparticle formation.[16] Thus, there is a distinct possibility that

the incorporation of BPEI may adversely influence the structural integrity of a sol-gel thin film. Amine-functionalized thin films present expanded application possibilities, such as anti-bio-fouling coatings or coatings for heavy metal remediation.

To this end, many authors have employed multiple synthetic steps often with environmentally harmful organic precursors or solvents,[17-19] and there is much interest in developing more generic, robust, and 'green' technologies where the reduction in usage of harmful solvents is strongly encouraged.[20,21] Kinetic doping utilizes aqueous solutions for loading the BPEI guest molecules into the silica thin films, eliminating the need for any organic solvents relative to other competing surface functionalization technologies.[17-19] Using aqueous solutions with low concentrations of BPEI to functionalize silica thin films, the need for environmentally hazardous solvents to generate precursors or perform post-coating surface modification can be effectively eliminated, resulting in a much more 'green' technique.

Silica thin films with amine functionalization can be made with organosilane precursors that contain an amino functional group,[22] but this limits the size of the amine groups that can be introduced into the film. Additionally, every new amine compound requires the synthesis of a new organosilane precursor, adding another layer of complexity to the functionalization process. Amine containing polymers alone can be used to create thin films, but they lack the benefits of silica, like high surface areas, and many exhibit poor stability in water.[23] Plasma polymerization can be used to graft amine groups onto existing thin films,[24] but the high cost of plasma polymerization is prohibitive to wide

spread commercial applications. It is possible to functionalize silica thin films with polyethylenimine, as certain synthetic pathways have been demonstrated to functionalize the surface of silica gels, but they require multiple steps and environmentally hazardous chemicals.[25-26] Here we present a facile, inexpensive synthesis of silica sol gel thin films with doped BPEI that provides amine functionalization with high loading efficiency using relatively green chemistry principles.

Doping of BPEI into a silica sol-gel thin film, instead of synthetic functionalization of the surface, would allow for a facile, green synthesis with very few synthetic steps involved. However, polymers with high molecular mass present a challenge for both the traditional pre- and post-doping approaches to thin film loading, as too much polymer included in pre-doping, which is a technique that introduces dopants to the sol before depositing the film on a substrate,[27] will likely degrade the structural integrity of the resulting silica film. Whereas due to poor diffusion, a high molecular weight polymer is never an ideal candidate for post-doping, which involves adsorbing the dopant to porous surfaces,[28] due to poor diffusion. Kinetic doping is a technique for loading guest molecules into sol-gel thin films that involves introducing guest molecules into a still-evolving film, allowing them to be entrapped by the growing silica network.[29] This technique is well suited to overcome the challenges posed by BPEI to the more widely used doping techniques. Additionally, kinetic doping has previously been studied with positively charged organic dyes[29] and enzymes[30] as the dopant molecule, making BPEI, with its organic nature and high positive charge density at neutral pH, an ideal candidate for kinetic doping.

Here, we attempt to dope silica sol gel thin films with 600 and 25,000 MW BPEI. Using scanning electron microscopy (SEM) and UV-vis spectroscopy, the quality of the thin films and amount of doped BPEI was quantified. The resultant films are structurally sound with BPEI concentrations in the millimolar range with minimal leaching of the BPEI observed. Preliminary results indicate that these films are able to sequester 10 mmol of copper (II) ions per gram of film from solution, an approximately five-fold or more increase over most available amine-functionalized gel technologies.[12, 25, 31-33] Soaking in ethylenediaminetetraacetic acid (EDTA) solution in a subsequent step can remove these ions, regenerating the film which can be reused, with only a 6% decrease in copper (II) ion sequestration efficacy after 3 uses. This lends preliminary support for the use of these films in heavy metal removal with good reusability. It is also, to our knowledge, the first time that BPEI has been loaded as a guest molecule in silica sol gel thin films.

4.3 Methods

4.3.1 Materials and General Methods

Tetraethylorthosilicate (TEOS) and 600 and 2500 MW branched polyethylenimine (BPEI) were purchased from Sigma-Aldrich. The 600 MW BPEI has a primary:secondary:tertiary amine ratio of 1:2:1, respectively, and 25000 MW BPEI has a ratio of 1:1.2:0.76. Phosphoric acid was purchased from EMD Millipore. Premium grade glass coverslips (25 mm × 25 mm × 170 μm) were purchased from Fisher Scientific. All chemicals and materials were used as received, with the exception of the glass coverslips,

which were cleaned prior to use. All UV−vis spectra were obtained via a Shimadzu UV-2101PC UV−vis spectrometer.

4.3.2   Preparation of Glass Coverslips

To remove any organic contaminants on the glass coverslip surface, the coverslips were sonicated in an acetone bath for 30 minutes and rinsed with Millipore water three times to remove all residual acetone. The coverslips were then sonicated in 10% w/v NaOH for another 30 minutes and rinsed with Millipore water five times to remove all residual NaOH. The coverslips then went through a final sonication in Millipore water for 30 minutes. The coverslips were then stored in Millipore water until use.

4.3.3   Preparation of Silica Sol

Silica sol was prepared by mixing a 1:8:7 molar ratio of TEOS:ethanol:water with phosphoric acid acting as a catalyst. A mixture of 55.9 mL of TEOS, 111.8 mL of ethanol, 31.7 mL of deionized water and 0.62 mL of 1% v/v phosphoric acid at room temperature were prepared for most coatings. The sol was then allowed to age for 20 hours undisturbed at room temperature before use.

4.3.4   Preparation of BPEI-Doped Silica Sol-Gel Thin Films

Thin films were prepared by drain coating with a sol solution inside a beaker, based on the drain coated film preparation method of Crosley et al.[34] After aging for 20 hours, the

silica sol solution was transferred to a 250 mL beaker, elevated by a jack stand. A clean

coverslip was dried with compressed air and immersed in the aged silica sol-gel coating

solution while suspended from above. The sol solution was then drained at a rate of 1.36

cm/sec; the entire drain coating is complete in less than 2 seconds. Immediately after the

silica sol solution was drained, the jack stand was lowered until the newly coated

coverslip was completely exposed to ambient air. The thin film was allowed to age in

ambient air for 7.5 minutes before it was transferred to a loading solution, where BPEI

was allowed to load into the film via kinetic doping for one week. The loading solution

consisted of 1 mM 25000 MW BPEI in 10 mM phosphate buffer, adjusted to pH 7.4 with

phosphoric acid.

4.3.5   Quantitative Determination of BPEI Loading

Detection of BPEI in the film was done qualitatively with a procedure based on the

method for copper detection with BPEI by Wen et al.[35] using the sequestration of copper

(II) by BPEI. This produced a dark blue color that could be seen on the film with the

naked eye. Quantification of BPEI loading was measured separately, based on the same

interaction with copper (II) ions.

The basic amine functional groups in BPEI reacted visibly with the sol-gel film as the

film was lowered into the BPEI loading solution, often resulting in a slightly opaque film.

The effect is especially prominent around the corner and edges of the films. Due to the

degradation in film transparency, the depletion of BPEI from the loading solution was

used to quantify the amount of BPEI loaded. Films were removed from the loading solution after one week of loading time, and the loading solution was saved for testing. Excess loading solution, stored under the same conditions without exposure to any film, was also saved as a reference for testing.

Concentration of BPEI in the dopant solution, both with and without exposure to thin films, was then determined spectroscopically by complex formation with a known quantity of copper (II); the resulting complex exhibited two peaks, one intense peak in the UV region (276 nm) and one weaker peak in the visible region (638 nm). The UV peak was chosen for determination of BPEI loading, as the peak at 638 nm was too weak to quantify the small depletion of BPEI in the loading solution. The solutions could be minimally diluted such that the absorbance would fall in the linear range of the peak at 276 nm. The difference in copper (II) concentration for the solutions that had been used to load films and the solution that had not was used to calculate the number of moles of BPEI loaded into the film. A control experiment was performed by placing a clean glass coverslip into the dopant solution for one week, and the same difference method was used to show that BPEI was depleted noticeably from the loading solution only in the presence of a silica sol-gel thin film.

4.3.6 Quantitative Determination of Copper (II) Sequestration and Reusability

Sequestration of copper (II) ions was also measured based on the method of Wen et al.[35] A concentration curve was made with varying amounts of copper (II) chloride and constant 1 mM BPEI at 638 nm. The peak at 638 nm proved more suitable than the 276

nm peak in this measurement due to the relatively high concentration of copper ions, as it showed linearity in the concentration range being tested. Five identically prepared BPEI loaded films were placed into a solution of 20 mM copper (II) chloride and allowed to equilibrate for 30 minutes. The 5 BPEI loaded silica films were then removed from the copper (II) solution and the concentration of copper (II) remaining in solution was measured at 638 nm after the addition of 1 mM BPEI. This was compared to the original 20 mM copper (II) chloride solution, and the decrease in copper (II) ion concentration was calculated. An average mass for the films, obtained from 15 samples, was then used to calculate the amount of copper (II) sequestered per gram of film.

To examine the reusability, the five films that had been tested for copper (II) sequestration were then put into a 10 mM EDTA solution for 30 minutes. The films were rinsed, dried, and put back into a fresh 20 mM copper (II) chloride solution. The films were again allowed to equilibrate for 30 minutes, the concentration of copper (II) remaining in the solution was measured again to assess the copper (II) sequestration efficiency of the films. This cycle was repeated until a significant decrease in copper (II) sequestration was observed.

4.4   Results and Discussion

4.4.1   Optimal Loading Parameters for Branched Polyethylenimine (BPEI)

As shown in previous studies, there are several loading parameters that need to be examined for optimal kinetic doping. Film thickness and delay time (time between the end of drain coating and introduction of the film to the loading solution) are important

factors that influence optimal loading. Dopants that do not disrupt film structure have been shown to have an optimal delay time of 5 minutes for drain coating.[34] This may be different for BPEI, as the extent of polycondensation of the silica network increases with the delay time. Due to its basic nature, BPEI may load better into a thin film that has different levels of condensation than dopants that are relatively neutral. Drain speed can change the thickness of the film and possibly the absolute amount of BPEI loaded into the film. The film must be thick enough to quantify the amount of BPEI loaded, as thicker films are expected to host more BPEI molecules. Too thick films will lead to increasing thickness variations across the film, due to the forces that dominate drain coating in the high speed regime.[36]

Two molecular weights of BPEI, a lighter 600 MW and a heavier 25000 MW, were tested, to determine if identical loading parameters would work for BPEI with different molecular weights. They were tested, as BPEI of different sizes are known to react differently with many different chemicals, including silica.[37-39]

4.4.1.1 Molecular Weight

BPEI is a polymer that comes in many molecular weights. Different molecular weights have different properties; for example, the cytotoxicity of BPEI increases with increasing molecular weight.[40] Thus, it is desirable to explore the possibilities to produce silica films with BPEI of different molecular weights, hence with different cytotoxicity. Consequently, loading of a low and a high molecular weight, 600 and 25000 MW, BPEI were both attempted. However, none of the parameters that were tested, including drain

speed, delay time, and pH of loading solution, could be optimized to allow kinetic doping of the 600 MW BPEI. Any attempt to load within the kinetic doping window led to complete film destruction and visible silica particle aggregates formed in the solution. It was possible to load the higher molecular weight, 25000, and loading parameters for that weight were further refined.

BPEI and TEOS are known to form nanoparticles[41], which may act as an undesirable competing process with kinetic doping of BPEI into silica thin films, the speed of which seems to vary with varying molecular weight. Kinetic doping is thought to work because the poly-condensation of the liquid sol is still progressing during the doping stage and the dopant can still be entrapped by the evolving and growing silica network.[29] The only films that stayed intact upon contact with the 600 MW BPEI loading solution appeared to have passed this window of doping opportunity and did not allow much loading of the 600 MW BPEI, despite the smaller molecular weight. Different molecular weights of branched or linear polyethylenimines are known to react with silicon sources differently,[37] so this difference in behavior is not entirely unprecedented. We postulate that this is due to the chemical reaction between BPEI and the TEOS molecules that have not undergone polycondensation. Based on experimental evidence, 600 MW BPEI is likely to react more quickly than 25000 MW BPEI, so quickly that it outcompetes the polycondensation reaction so that kinetic doping is effectively inhibited.

The observation that different molecular weights of BPEI react with the film differently may prove to be a useful way to control film properties once BPEI of other molecular

weights are thoroughly examined. A thorough investigation of the effect of different

BPEI molecular weights on kinetic doping is contained in chapter 5.

4.4.1.2 Drain Speed

Film thickness was qualitatively examined for its affect on mechanical stability of the

film and the amount of BPEI that remained solvent accessible. Thicker films, created

with faster drain speeds, take longer to complete the evaporation process that is

responsible for the growth of a 3D network through the polycondensation reaction to

produce a mature thin film. Although a thicker film allows more entrapment of BPEI, the

slower evaporation process means more uncondensed TEOS molecules remain to

undergo undesirable side reactions with BPEI. Films that are too thick will additionally

drain coat in a different regime, leading to increasing thickness variations on the surface

of the film itself.[36]

Figure 4.1 shows a series of films that were loaded with a delay time of 5 minutes. To

vary film thickness, films were prepared with drain speeds from 0.67 to 1.50 cm/sec; all

film coatings were completed in less than 4 seconds, regardless of drain speed. Thinner

films (those coated at a lower drain speed) showed relatively poor loading of BPEI. As

drain speed increased, loading became more apparent as indicated by the more intense

blue color on the thin film due to complex formation with copper (II) ions. It is also

apparent that the highly loaded films exhibited a more significant mechanical
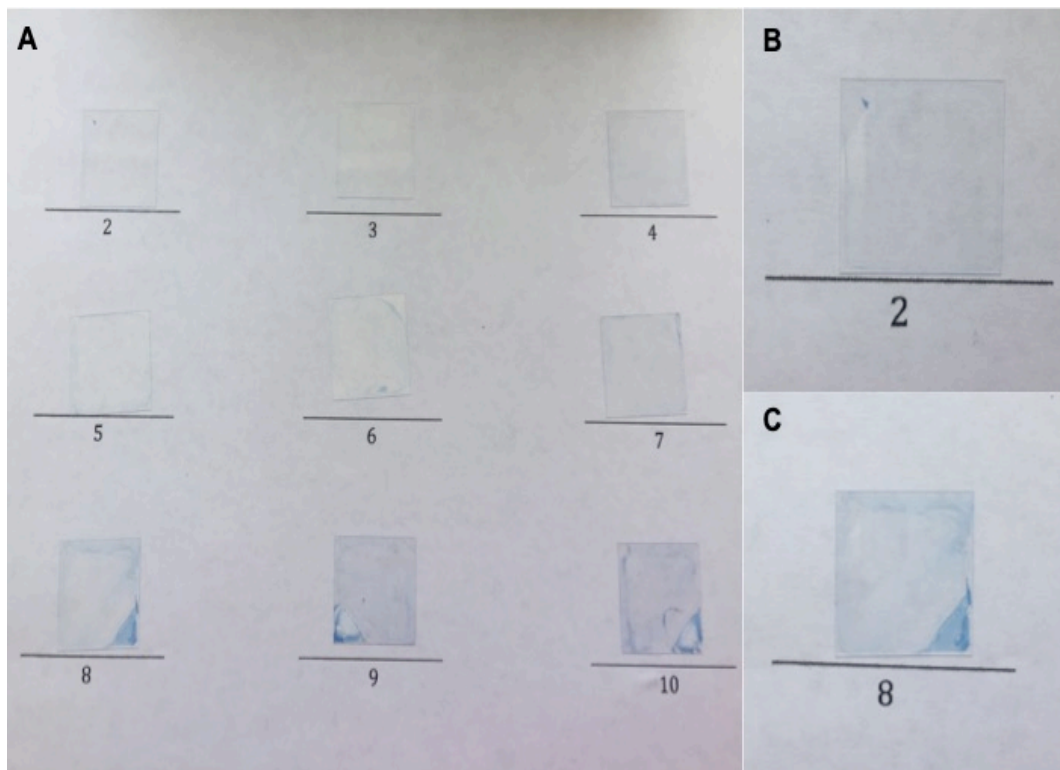
Figure 4.1 Films loaded with 1 mM BPEI loading solution, a delay time of 5 minutes, at various drain speeds. A) Films drained at each different setting on the pump from 2 to 10. This corresponds to speeds of 0.67, 0.78, 0.87, 0.99, 1.10, 1.17, 1.25, 1.36, 1.41, and 1.50 cm/sec, respectively. Mechanical disruption can be seen most clearly on the corner that is first in contact with the BPEI loading solution (see Figure 1.7) and on the edges of the films nearest that corner. B) Close-up of slowest drain speed film, showing very faint visible blue color and very little mechanical disruption. C) Close up of the final chosen drain speed (1.36 cm/sec), showing more intense visible blue color, but at the expense of more mechanical disruption at the corner and edges.

deformation at the corner and edges of the film. A drain speed of 1.36 cm/sec was chosen for further testing as it resulted in a very visible amount of loading with the least amount of mechanical disruption at the edge.

4.4.1.3   Delay Time

Delay times in drain coating affect the extent of polycondensation in the thin film when it is introduced to the dopant.[36] A less evolved silica network can entrap guest molecules more effectively as more uncondensed TEOS is available to grow around the dopant. However, that same uncondensed TEOS can also react with BPEI and prevent the growth of the silica network into a stable thin film. Indeed, testing of delay times showed that longer delay times produced more mechanically sound films with noticeably less pronounced corner and edge deformation, supporting the notion that BPEI reacts with TEOS in the films that has not completed condensation.

Figure 4.2A shows the results of loading BPEI with a variety of delay times from 5:00 to 7:30 minutes and a 1 mM BPEI loading solution. Figure 4.2B shows a film with a 5:00 minute delay time. There are notable structural defects in the film, mostly around the corner and edges of the film and especially on the lower right corner, where a portion of the film was clearly detached from the glass coverslip and was subsequently washed away. Figure 4.2C shows a film with a delay time of 7:30 minutes. Structural defects in the film are less notable at this longer delay time. Delay times beyond those illustrated in Figure 4.2 were also tested (8:00, 8:30, and 9:00 minutes, as seen in Figure 4.3), but they progressively produced less loading, despite showing improved mechanical stability over
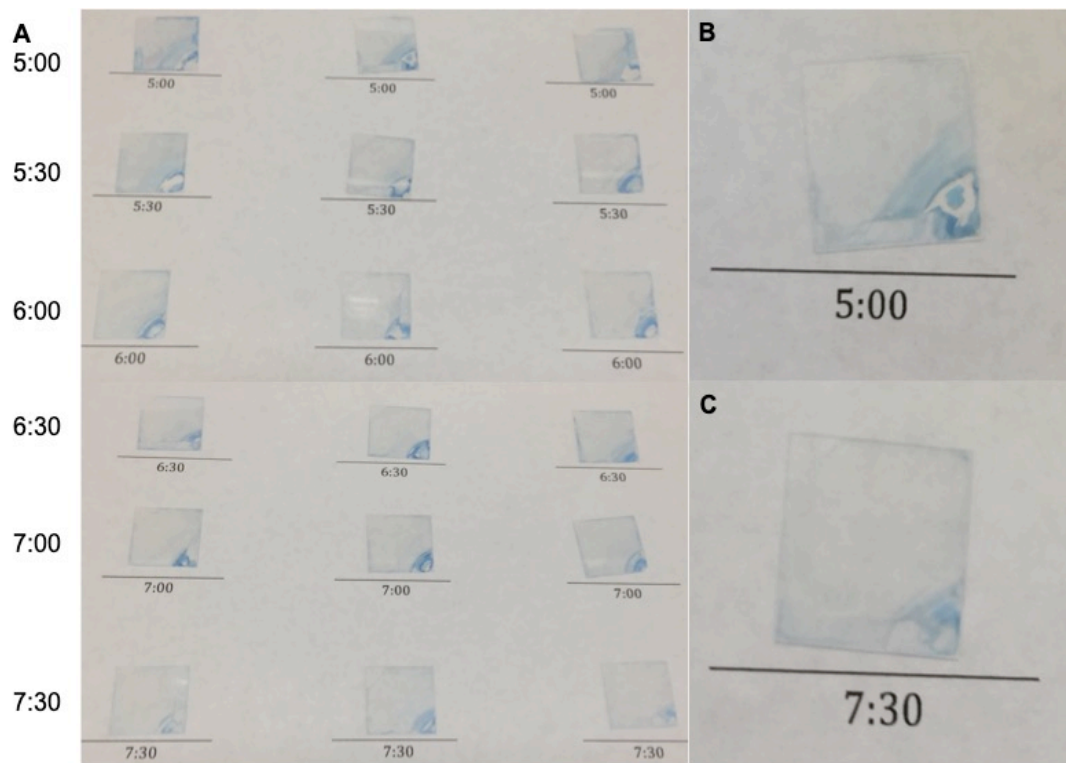
Figure 4.2 Films loaded with 1 mM BPEI loading solution, at 1.36 cm/sec drain speed, with varying delay time, in triplicate. A) Delay times ranging from 5 minutes (top row) to 7 minutes and 30 seconds (bottom row), in 30 second increments. B) Close-up of one of the 5 minutes delay time films, showing the large mechanical defects caused by the early introduction of BPEI, especially on the lower right corner. Part of the film at the lower right hand corner was obviously removed during the washing step, as it had detached from the substrate. C) Close-up of one of the 7 minutes 30 seconds films, showing much less mechanical disruption than the shorter delay time periods but with a slightly lower loading capacity as indicated by the fainter blue color.

the 7:30 minutes delay film. This seems to indicate the kinetic doping window is closing, as very little uncondensed TEOS remains to effectively entrap the BPEI. On the other hand, the more condensed silica network in the longer delay time films seems to better resist the mechanical disruption caused by BPEI, due to the very same lack of uncondensed TEOS.
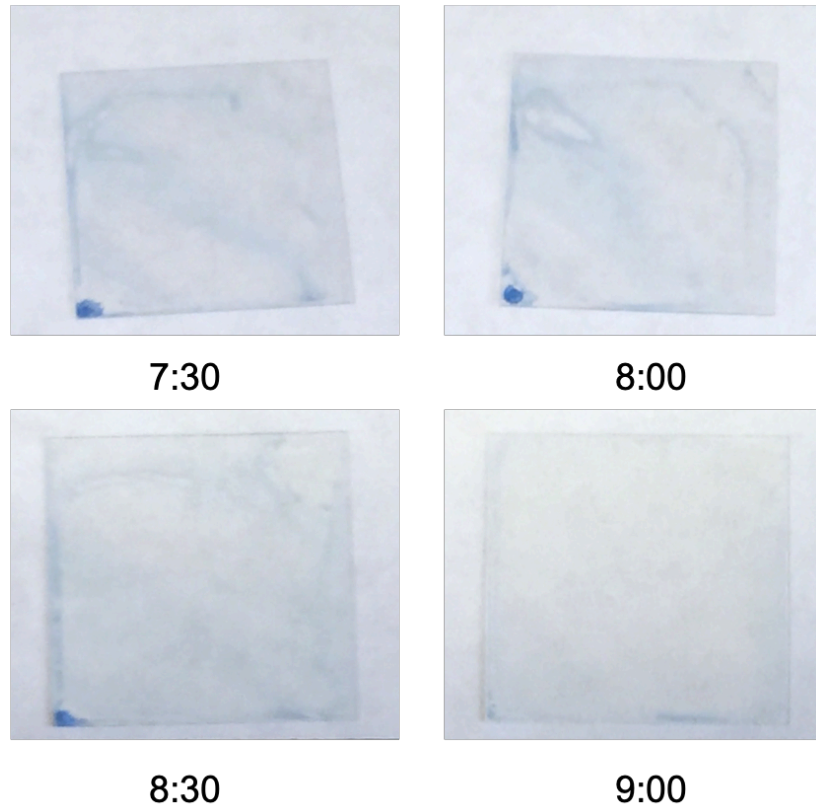
Figure 4.3 Delay times from 7:30 minutes to 9:00 minutes, with a 1 mM BPEI loading solution and drain speed of 1.36 cm/sec.

Thicker films and shorter delay times seem to favor the competing process of nanoparticle formation with TEOS molecules that have not completed condensation, resulting in more severe mechanical defects. This is further supported by the results with the 600 MW BPEI, where silica particle formation out-competed kinetic doping at all delay times we examined. Thinner films and longer delay times allow the film to reach a higher level of condensation and develop sufficient mechanical strength whereupon, when it is introduced to the basic BPEI, it has built sufficient scaffolding to stay structurally sound on the macroscopic level, unfortunately at the expense of BPEI loading.

4.4.2   Quantification of Doped BPEI in Thin Films

The molarity of the doped BPEI was examined using a method based on Wen et al.[35] A standard curve was constructed by using a varying amount of BPEI to complex with a constant 1 mM copper (II) solution. This standard curve showed high linearity and an extinction coefficient of 429 mM^{-1} cm^{-1}, as shown in Figure 4.4.
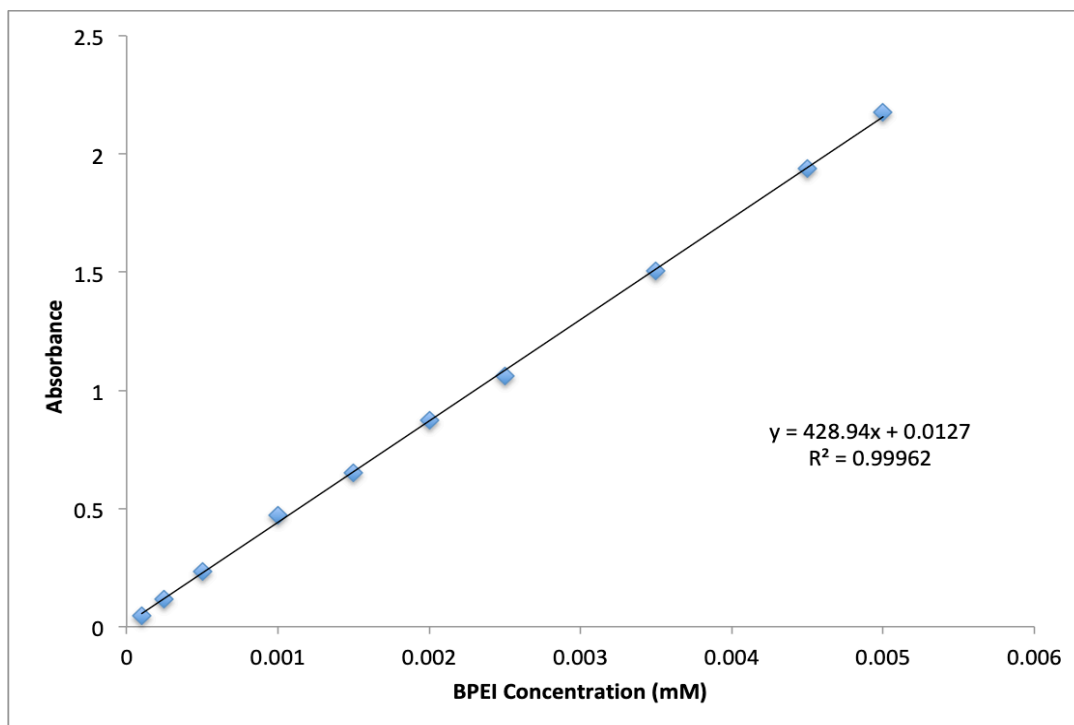
Figure 4.4 Concentration curve using 1 mM copper (II) chloride solution and varying concentrations of 25000 MW BPEI at a wavelength of 276 nm.

The dopant solution for the thin films, diluted to the linear range of the 276 nm standard curve, was then combined with copper (II) chloride to quantify the concentration of the remaining BPEI. The difference between the concentration of the solution prior to loading (pre-loading) and after loading was taken as the amount of BPEI loaded. Figure 4.5 shows the absorption spectra of six replicates and the pre-loading solution. The

average number of moles of BPEI loaded for films with a 7:30 minutes delay time, 1.36

cm/sec drain speed, and 1 mM dopant solution was 0.7 ± 0.2 μmoles. To then calculate

the concentration of BPEI in the films, the thickness of the film was measured via SEM.
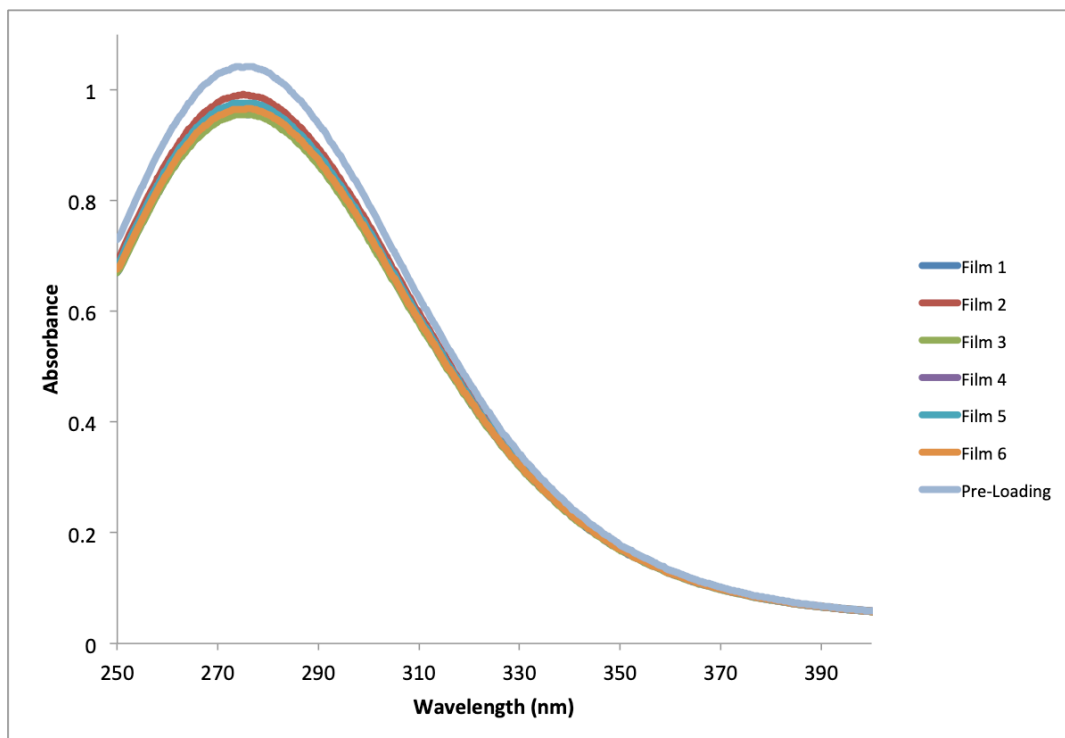
Figure 4.5 Absorption spectra of BPEI loading solutions with 1 mM copper (II) chloride. The labeled "Pre-Loading" is an aliquot of the 1 mM BPEI loading solution that was set aside without interaction with films. Films 1-6 are loading solutions from individual films, where the film was removed after 1 week of loading and the solution left was tested for BPEI concentration.

Scanning electron microscopy (SEM) images were obtained via a JEOL JSM-880

instrument with a 5 nm Au−Pd sputter-coated layer to examine the morphology of the

dip-coated thin film and measure the film thickness. Thirteen separate films were

examined, 6 with 1 mM dopant solutions and 7 without any loaded BPEI. It was observed

that the thickness of the film was highly variable over a single film. Films with BPEI had

a wider range of thickness from as low as 53 nm up to 1.93 μm on one film, as can be

seen in Figure 4.6. This seems to partly be a result of the drain-coating set-up, as a slightly lower variance was seen in the unloaded films, with thicknesses ranging from 1 μm to 1.79 μm in a single film. The angle of loading in drain and dip coating is known to affect the thickness and shape of the resultant film, which is not a perfect 90˚ in our drain coating apparatus. An angle other than a perfect 90˚ between the substrate and the surface of the liquid sol results in a film with a wedge shaped, linearly changing thickness across the direction of coating [42] and could explain some of the variance seen.
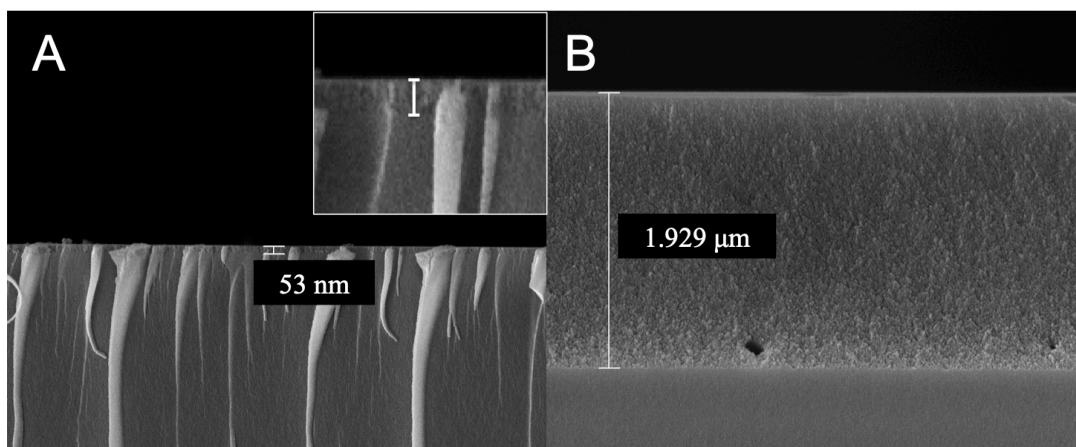
Figure 4.6 SEM images taken from a single thin film loaded with BPEI. A) Image from the edge of the film. The film is only ~50 nm thick. Inset is an enlarged portion of the interface between the glass substrate and film. B) Image from the same film. This is the middle of the cross-section, where the film is ~1.9 μm thick.

Additionally, drain coating at high drain speeds, like those used for our films, can result in varying thickness across a single film,[36] also contributing to the shape seen in the SEM images. A diagram of the drain coating set-up is depicted in Figure 4.7, with the loading angle of the film labeled. The variance across the film in both the loaded and unloaded films suggests that both the angle and drain speed contributes to the thickness variation. While a commercial dip-coating set-up may enable a perfect 90˚ angle of loading, the drain speed would have to be lowered drastically to enter the coating regime that might

produce a film with even thickness. The resultant film would be too thin for our desired

high capacity BPEI loading.
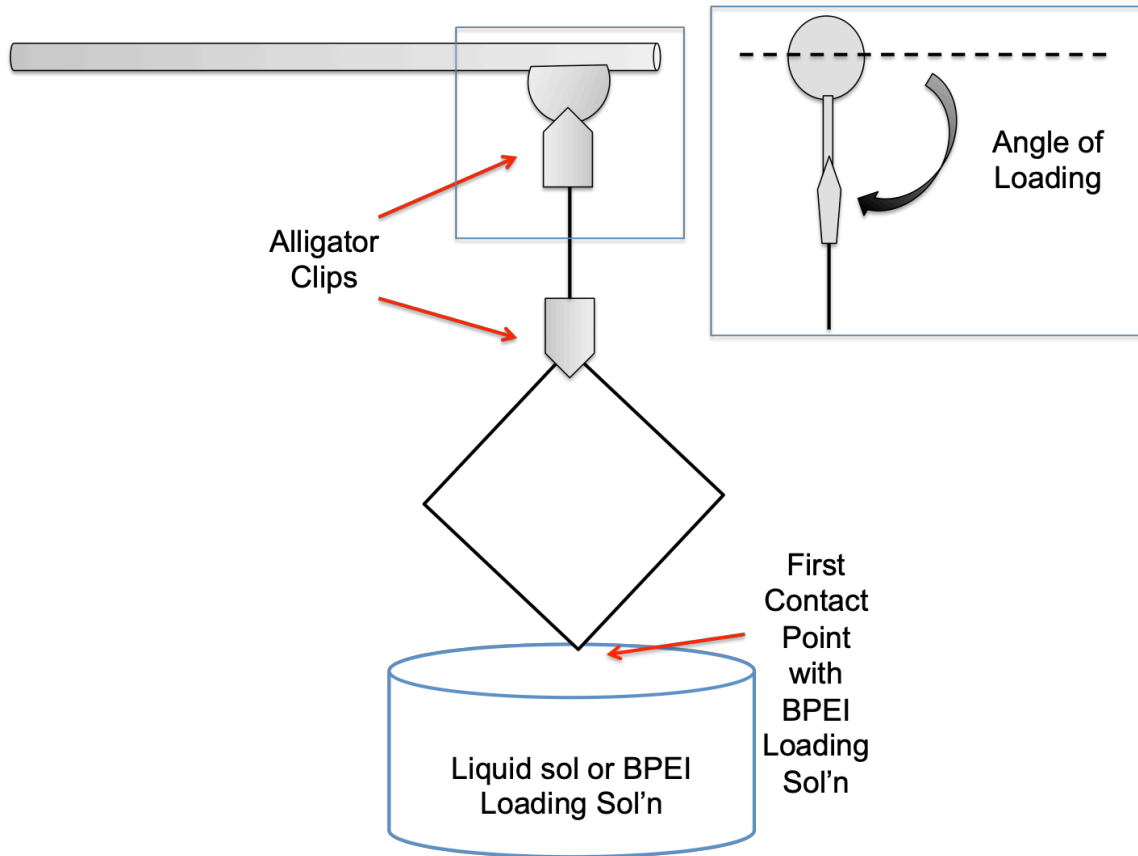
Figure 4.7 Diagram of the laboratory drain coating set-up with a magnified side view inset. The glass substrate is suspended above the sol using a wire with two alligator clips at either end. This can lead to an angle of loading (the angle labeled in the side view inset) deviated from a perfect 90˚. While this change may not drastically affect the thickness of extremely thin films, it does have a large effect on the micrometer thickness films presented here. This diagram also demonstrates which edge of the film comes into contact with BPEI first, where most of the mechanical disruption to the film can be seen.

However, it is important to note that the variance across films loaded with BPEI was

consistently much greater. This is most likely due to the interaction of BPEI with the

film. The SEM images seem to suggest that the interaction with BPEI causes the edges of

the film to thin, but most of the middle portion stays intact. The edges of the film are

where BPEI first comes into contact with it (see Figure 4.7). PEI is known to etch silica nanoparticles,[43] so this may be a similar phenomenon at the edges. This potential etching doesn't extend to the majority of the film, which remains at the same thickness as the unloaded films. However, given this variance in thickness, only an approximation of the final molarity of the film can be made. If we use an average thickness of 1 μm across the film, the average molarity of the loaded BPEI would be ~ 0.5 M, an approximately 500X increase over the loading solution.

0.5 M is in line with concentrations previously reported with kinetic doping, but is a lower percent increase over the loading solution than achieved with proteins or rhodamine 6G (R6G) dye.[29-30] This is most likely due to the competing reactions of silica/BPEI particle formation and kinetic doping. The dyes and proteins do not have any competing reactions, meaning all molecules that enter the film should stay there, in their original state, unlike BPEI. In addition, R6G is capable of hydrogen bonding with small pores inside the silica network to further enhance its loading relative to that of BPEI. Nevertheless, the increase in molarity of the film over the loading solution still means that the very dilute solutions of BPEI can be used to make more concentrated films, reducing the need for larger amounts of BPEI, the most expensive chemical used for producing these films.

Additionally, the SEM images were compared to identify any morphology differences between the BPEI loaded and unloaded films. Figure 4.8 shows a cross-sectional and top-down image of a loaded film, while Figure 4.9 shows the same for an unloaded film. The

morphology does not seem to change drastically in the cross-sectional images between loaded and unloaded films, but the grain size seems to be slightly larger in the loaded films versus the unloaded. The top-down view does show noticeable differences: the film surface in Figure 4.8C appears to be much smoother and devoid of major dents relative to that shown in Figure 4.9C, suggesting that BPEI does alter the surface morphology of the films to a certain degree. The surface of the film in 4.9C, the unloaded film, has both small and large 'dimples,' with an orange peel effect texture on the surface. Figure 4.8C, the loaded film, does not show this texture, and the bright spots are only glass fragments. The samples must be cut down to fit in the SEM instrument, causing some glass fragments to appear in sample images due to the glass coverslip the films are coated on.
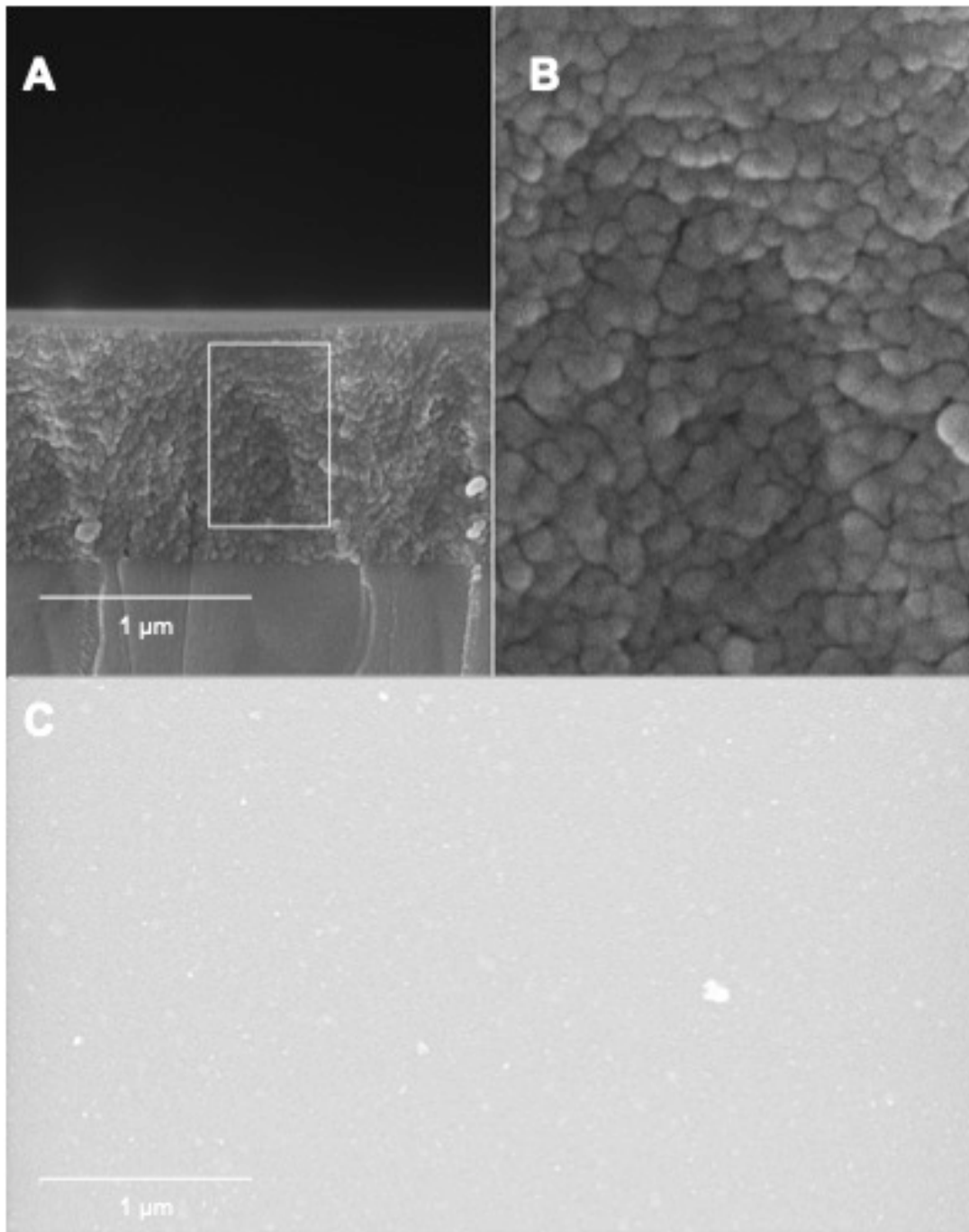
Figure 4.8 SEM images of BPEI loaded films. A) A cross-sectional image of a loaded film at 25X magnification. B) An inset of the same image with 100X magnification. C) A top-down image of a loaded film at 25X magnification. The bright white spots seen are glass fragments caused by sample preparation for use with the SEM instrument.
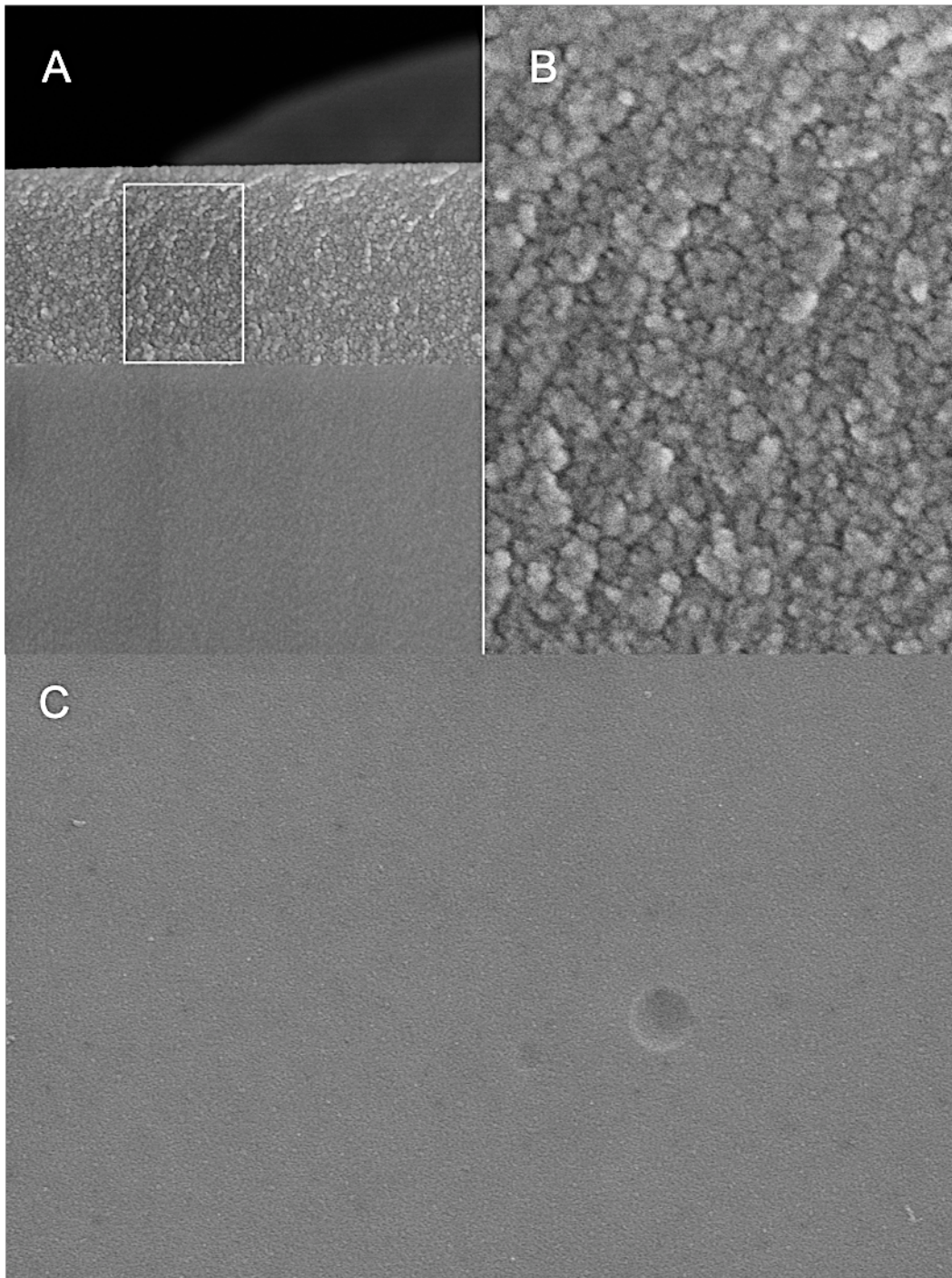
Figure 4.9 SEM images of unloaded films. A) A cross-sectional image of an unloaded film at 25X magnification. B) An inset of the same image with 100X magnification. C) A top-down image of an unloaded film at 25X magnification. The texture seen on the film includes both the large and smaller 'dimples' and the more general orange peel texture of the film.

Figure 4.10 also compares an unloaded film to a loaded film, showing dark patches or a 'mottled' effect on the SEM image of the loaded film that is most likely due to the presence of BPEI. This 'mottled' effect occurs on all BPEI loaded samples, but none of the unloaded samples, suggesting that it is due to the interaction of BPEI with the electron beam. It is unlikely to be simply organic contamination, as it does not show the characteristic dark square that is the hallmark of hydrocarbon contamination.[44] If these darker patches on the SEM images are indeed caused by BPEI, this suggests that the BPEI is distributed fairly evenly throughout the entire thin film, not just localized on the surface. Elemental analysis through energy-dispersive X-ray spectroscopy (EDS) was attempted to confirm this, but the signal from the glass coverslip substrate was so dominant that no discernible signal was observed for the thin films for a meaningful determination of elemental composition.
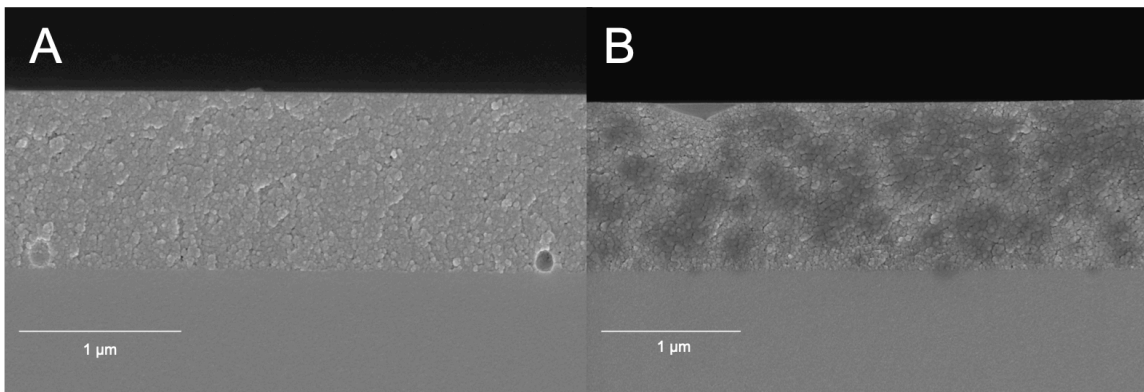
Figure 4.10. Cross-sectional images of an unloaded (A) and loaded (B) film, both at 25X magnification. There is a distinct mottling pattern that can be seen in loaded films, but was never observed in the unloaded films. It does not have the characteristic square pattern of hydrocarbon contamination. It is most likely due to the BPEI itself, which seems to be distributed throughout the film.

4.4.3 Stability of BPEI in Doped Films

BPEI doped films were tested for leaking over the course of one week. Films can be stored dry with no degradation and show no leaking when tested in a copper (II) solution for up to two hours, but more advanced applications, like heavy metal remediation or anti-bio-fouling coatings, may require films to be submerged or stored wet for an extended period of time. To test the leaking of BPEI, films were (i) untreated and stored in DI water, (ii) annealed at 100 ˚C for approximately 18 hours and stored in DI water, or (iii) untreated and stored in 0.01 mM BPEI solution. Untreated films in DI water were expected to release the most BPEI, while untreated films in a dilute BPEI solution were expected to release less BPEI due to the reduced concentration difference between the film and the storage solution. Annealed films were also expected to release less BPEI due to morphological changes induced by the annealing process. Annealing is expected to cause silica pore collapse, making it more difficult for BPEI to leave or leach from the film. The results of this study are summarized in Table 4.1. Over the course of 1 week, the untreated films stored in DI water show the most loss, with a 0.6% loss of BPEI. Storing the films in a 0.01 mM BPEI solution, even without treatment, decreases this loss to 0.4%. Annealing the film further reduces this loss, even when stored in DI water, to 0.1%. Collectively speaking, these results suggest that BPEI doped films could be used for an extended period of time in solution.

	Untreated in DI Water	Heat Annealed in DI Water	Untreated in 0.1 mM Storage Sol'n
BPEI Lost (nmoles)	4.5 ± 0.7	0.8 ± 0.3	2.69 ± 0.03
Percent of Original BPEI Lost	0.6%	0.1%	0.4%

Table 4.1. Comparison of BPEI lost after being stored in DI water/solution for one week.

4.4.4   Copper (II) Uptake and Reusability

Copper (II) ion uptake by the films was tested, to obtain preliminary data on the suitability of this technology for heavy metal remediation. On average, films were able to sequester 10 ($\pm$ 6) mmol of copper ions per gram of film. In comparison, the best commercial resin documented so far for copper (II) uptake is 2.06 mmol/g.[31] Our thin film also outperforms newer, more expensive ion imprinting technology, made with an amino-functionalized silane precursor, with our copper (II) loading capacity an order of magnitude higher than that reported (39.82 mg/g or ~0.6 mmol/g) and with comparable regeneration capabilities.[12, 45] The film also outperforms several other technologies that use (B)PEI; a PEI/silk fibroin hydrogel has a copper (II) uptake of 163.9 mg/g (~2.6 mmol/g),[46] silica bound BPEI has a copper (II) capacity of less than 5 mmol/g,[32] and even a PEI-functionalized ion imprinted hydrogel had a similar uptake to the other hydrogel cited (40.00 mg/g or ~0.6 mmol/g).[12]

This enhanced uptake per mass makes sense, as the resin or bulk materials are likely only able to sequester ions on the surface, whereas most of its bulk remains inaccessible to metal ions. According to our SEM data, BPEI is likely loaded throughout the film and

much of it is expected to be accessible to the copper (II) ions, due to the highly porous nature of silica versus the other polymers that have been used, making it highly efficient at sequestering metal ions from solution. Additionally, the concentration of BPEI loaded into the film is approximately 0.5 M, which is a higher concentration than other methods are able to achieve, which means that there are more amine groups present in our film to interact with the copper (II) ions. The only material with a similar loading capacity reported in the literature is the copper (II) adsorption capacity of silica shell microspheres with magnetic cores, a material that is much more expensive and produced via a much more involved synthesis.[47]

Reusability of the films was also examined, as regeneration of the metal adsorption capacity is highly desirable in heavy metal remediation technology. By the third use of the film, adsorption capacity of the films had only decreased by 6%. However, it was observed that copper (II) sequestration efficiency of the film reduced non-linearly and by the fourth use, adsorption capacity had decreased by 20%, to 8 (± 5) mmol/g. Despite the dramatic decrease, this is still a much higher capacity for copper (II) sequestration than most amine-functionalized gels.

4.5 Conclusions

Using kinetic doping, we were able to produce an amine rich thin film by loading BPEI into silica thin films at approximately 0.5 M concentration, a 500X increase from the loading solution, without any need for pre-doping precursor synthetic chemistry or post-doping surface modification reactions. This is a facile, green, and inexpensive procedure

for introducing amines to silica thin films. To our knowledge, this is the first time BPEI has been doped into silica thin films.

Additionally, these films were preliminarily shown to sequester copper (II) ions at 10 mmol/g, a much higher capacity than most technology found in the literature. They also proved to be fairly reusable, with only a 6% decrease in efficacy after three uses, and were stable in solution over the course of a week with less than 1% loss of BPEI from the film. BPEI loaded films are a promising technology that could sequester heavy metal ions from solution, accomplished by more efficient, less expensive, and 'greener' practices.

Thin films loaded with BPEI present untapped possibilities for a wide range of applications. This is made possible via kinetic doping to load guest molecules into silica thin films, which has been considered one of the major challenges for more advanced thin film technology. SEM images suggest that loaded BPEI is distributed throughout the entire 3D silica network inside a film. Due to its ability to sequester copper (II) ions, this presents an intriguing possibility of the construction of transparent and conductive films if the copper (II) can be reduced to metallic copper. Additionally, BPEI in solution has shown antibacterial properties,[40] making BPEI-doped silica thin films a potential platform to develop surface coatings for medical implants to suppress bacterial infection, as seen in Chapter 5.

4.6 References

1.   Barczak, M., Functionalization of mesoporous silica surface with carboxylic groups by Meldrum's acid and its application for sorption of proteins. *Journal of Porous Materials* **2019,** *26* (1), 291-300.

2.   Hruby, S. L.; Shanks, B. H., Acid-base cooperativity in condensation reactions with functionalized mesoporous silica catalysts. *Journal of Catalysis* **2009,** *263* (1), 181-188.

3.   Hurel, C.; Bignon, C.; Said-Mohamed, C.; Amigoni, S.; Devers, T.; Guittard, F., Functionalized and grafted TiO2, CeO2, and SiO2 nanoparticles-ecotoxicity on Daphnia magna and relevance of ecofriendly polymeric networks. *Environmental Science and Pollution Research* **2018,** *25* (21), 21216-21223.

4.   Rosen, J. E.; Gu, F. X., Surface Functionalization of Silica Nanoparticles with Cysteine: A Low-Fouling Zwitterionic Surface. *Langmuir* **2011,** *27* (17), 10507-10513.

5.   Sevimli, F.; Yilmaz, A., Surface functionalization of SBA-15 particles for amoxicillin delivery. *Microporous Mesoporous Materials* **2012,** *158*, 281-291.

6.   Zhang, X.; Wang, J.; Wu, W.; Liu, C.; Qian, S., Preparation of amino-functionalized mesoporous silica thin films with highly ordered large pore structures. *Journal of Sol-Gel Science and Technology* **2007,** *43* (3), 305-311.

7.   Tauhardt, L.; Pretzel, D.; Gottschaldt, M.; Schubert, U. S. In *Surface coating of sensor materials using poly(2-ethyl-2-oxazoline) based polymers for the prevention of biofilm formation*, American Chemical Society: 2013; pp COLL-459.

8.   Aguado, J.; Arsuaga, J. M.; Arencibia, A.; Lindo, M.; Gascón, V., Aqueous heavy metals removal by adsorption on amine-functionalized mesoporous silica. *Journal of Hazardous Materials* **2009,** *163* (1), 213-221.

9.   Bagheri, H.; Babanezhad, E.; Khalilian, F., A novel sol-gel-based amino-functionalized fiber for headspace solid-phase microextraction of phenol and chlorophenols from environmental samples. *Analytica Chimica Acta* **2008,** *616* (1), 49-55.

10.   Shabir, J.; Garkoti, C.; Surabhi; Sah, D.; Mozumdar, S., Development of Amine Functionalized Wrinkled Silica Nanospheres and Their Application as Efficient and Recyclable Solid Base Catalyst. *Catalysis Letters* **2018,** *148* (1), 194-204.

11.   Thakur, A. K.; Nisola, G. M.; Limjuco, L. A.; Parohinog, K. J.; Torrejos, R. E. C.; Shahi, V. K.; Chung, W.-J., Polyethylenimine-modified mesoporous silica adsorbent for simultaneous removal of Cd(II) and Ni(II) from aqueous solution. *Journal of Industrial and Engineering Chemistry (Amsterdam, Neth.)* **2017,** *49*, 133-144.

12.   Wang, J.; Li, Z., Enhanced selective removal of Cu(II) from aqueous solution by novel polyethylenimine-functionalized ion imprinted hydrogel: Behaviors and mechanisms. *Journal of Hazardous Materials* **2015,** *300*, 18-28.

13.   Zhang, W.; Liu, H.; Sun, C.; Drage, T. C.; Snape, C. E., Capturing CO2 from ambient air using a polyethyleneimine–silica adsorbent in fluidized beds. *Chemical Engineering Science* **2014,** *116*, 306-316.

14.   Gibney, K.; Sovadinova, I.; Lopez, A. I.; Urban, M.; Ridgway, Z.; Caputo, G. A.; Kuroda, K., Poly(ethylene imine)s as antimicrobial agents with selective activity. *Macromolecular Bioscience* **2012,** *12* (9), 1279-1289.

15.   Foxley, M. A.; Friedline, A. W.; Jensen, J. M.; Nimmo, S. L.; Scull, E. M.; King, J. B.; Strange, S.; Xiao, M. T.; Smith, B. E.; Thomas, K. J., III; Glatzhofer, D. T.; Cichewicz, R. H.; Rice, C. V., Efficacy of ampicillin against methicillin-resistant Staphylococcus aureus restored through synergy with branched poly(ethylenimine). *Journal of Antibiotics* **2016,** *69* (12), 871-878.

16.   Stoeber, W.; Fink, A.; Bohn, E., Controlled growth of monodisperse silica spheres in the micron size range. *Journal of Colloid Interface Science* **1968,** *26* (1), 62-9.

17.   Zhu, M.; Lerum, M. Z.; Chen, W., How To Prepare Reproducible, Homogeneous, and Hydrolytically Stable Aminosilane-Derived Layers on Silica. *Langmuir* **2012,** *28* (1), 416-423.

18.   Al-Oweini, R.; El-Rassy, H., Synthesis and characterization by FTIR spectroscopy of silica aerogels prepared using several Si(OR)4 and R"Si(OR')3 precursors. *Journal of Molecular Structure* **2009,** *919* (1-3), 140-145.

19.   Kursunlu, A. N.; Guler, E.; Dumrul, H.; Kocyigit, O.; Gubbuk, I. H., Chemical modification of silica gel with synthesized new Schiff base derivatives and sorption studies of cobalt (II) and nickel (II). *Applied Surface Science* **2009,** *255* (21), 8798-8803.

20.   Cuoq, F.; Masion, A.; Labille, J.; Rose, J.; Ziarelli, F.; Prelot, B.; Bottero, J.-Y., Preparation of amino-functionalized silica in aqueous conditions. *Applied Surface Science* **2013,** *266*, 155-160.

21.   Jimenez-Gonzalez, C.; Ponder, C. S.; Broxterman, Q. B.; Manley, J. B., Using the Right Green Yardstick: Why Process Mass Intensity Is Used in the Pharmaceutical Industry To Drive More Sustainable Processes. *Organic Process Research & Development* **2011,** *15* (4), 912-917.

22.   Collino, R.; Therasse, J.; Chaput, F.; Boilot, J.-P.; Levy, Y., Biological activity of functionalized SiO2 thin films prepared by sol-gel method. *Journal of Sol-Gel Science and Technology* **1996,** *7* (1/2), 81-85.

23.   Zajickova, L.; Manakhov, A.; Skladal, P.; Elias, M.; Necas, D.; Cechal, J., Plasma polymerization of amine-rich films aimed at their bioapplications. *Bulletin - Society of Vacuum Coaters* **2014,** (Summer), 26-30.

24.   Reis, R.; Dumée, L. F.; He, L.; She, F.; Orbell, J. D.; Winther-Jensen, B.; Duke, M. C., Amine Enrichment of Thin-Film Composite Membranes via Low Pressure Plasma Polymerization for Antimicrobial Adhesion. *ACS Applied Materials & Interfaces* **2015,** *7* (27), 14644-14653.

25.   Allen, J. J.; Rosenberg, E.; Johnston, E.; Hart, C., Sol-Gel Synthesis and Characterization of Silica Polyamine Composites: Applications to Metal Ion Capture. *ACS Applied Materials & Interfaces* **2012,** *4* (3), 1573-1584.

26.   Rosenberg, E.; Pang, D. System for extracting soluble heavy metals from liquid solutions, especially aqueous solutions. WO9922933A1, 1999.

27.   Avnir, D.; Levy, D.; Reisfeld, R., The nature of the silica cage as reflected by spectral changes and enhanced photostability of trapped Rhodamine 6G. *Journal of Physical Chemistry* **1984,** *88* (24), 5956-9.

28.   Reisfeld, R.; Manor, N.; Avnir, D., Transparent high surface area porous supports as new materials for luminescent solar concentrators. *Solar Energy Materials* **1983,** *8* (4), 399-409.

29.   Campbell, A. L. O.; Lei, Q.; Tak Yip, W., Kinetic approach to hyper-doped optical quality thin films. *Chemical Communications (Cambridge, U. K.)* **2014,** *50* (66), 9321-9324.

30.   Crosley, M. S.; Yip, W. T., Silica Sol-Gel Optical Biosensors: Ultrahigh Enzyme Loading Capacity on Thin Films via Kinetic Doping. *Journal of Physical Chemistry B* **2017,** *121* (9), 2121-2126.

31.   Marshall, W. E.; Wartelle, L. H., Chromate (CrO(4)(2-)) and copper (Cu2+) adsorption by dual-functional ion exchange resins made from agricultural by-products. *Water research* **2006,** *40* (13), 2541-2548.

32.   Laatikainen, M.; Sirola, K.; Paatero, E., Binding of transition metals by soluble and silica-bound branched poly(ethyleneimine). *Colloids and Surfaces, A* **2007,** *296* (1-3), 191-205.

33.   Da'na, E., Adsorption of heavy metals on functionalized-mesoporous silica: A review. *Microporous Mesoporous Materials* **2017,** *247*, 145-157.

34.   Crosley, M. S.; Yip, W. T., Kinetically Doped Silica Sol-Gel Optical Biosensors: Expanding Potential Through Dip-Coating. *ACS Omega* **2018,** *3* (7), 7971-7978.

35.   Wen, T.; Qu, F.; Li, N. B.; Luo, H. Q., A facile, sensitive, and rapid spectrophotometric method for copper(II) ion detection in aqueous media using polyethyleneimine. *Arabian Journal of Chemistry* **2017,** *10*, S1680-S1685.

36.   Brinker, C. J.; Scherer, G. W., *Sol-Gel Science: The Physics and Chemistry of Sol-Gel Processing*. United States: Academic Press: 2013.

37.   Bauer, C. A.; Chi, G.; Likens, O. Q.; Brown, S. M., A convenient, bio-inspired approach to the synthesis of multi-functional, stable fluorescent silica nanoparticles using poly(ethylene-imine). *Nanoscale* **2017,** *9* (19), 6509-6520.

38.   Kunath, K.; von Harpe, A.; Fischer, D.; Petersen, H.; Bickel, U.; Voigt, K.; Kissel, T., Low-molecular-weight polyethylenimine as a nonviral vector for DNA delivery: comparison of physicochemical properties, transfection efficiency and in vivo distribution with high-molecular-weight polyethylenimine. *Journal of Controlled Release* **2003,** *89* (1), 113-125.

39.   Wagner, M.; Rinkenauer, A. C.; Schallon, A.; Schubert, U. S., Opposites attract: influence of the molar mass of branched poly(ethylene imine) on biophysical characteristics of siRNA-based polyplexes. *RSC Advances* **2013,** *3* (31), 12774-12785.

40.   Gibney, K. A.; Sovadinova, I.; Lopez, A. I.; Urban, M.; Ridgway, Z.; Caputo, G. A.; Kuroda, K., Poly(ethylene imine)s as Antimicrobial Agents with Selective Activity. *Macromolecular Bioscience* **2012,** *12* (9), 1279-1289.

41.   Hoshino, T.; Sato, K.; Oaki, Y.; Sugawara-Narutaki, A.; Shimizu, K.; Ozaki, N.; Imai, H., Plant opal-mimetic bunching silica nanoparticles mediated by long-chain polyethyleneimine. *RSC Advances* **2016,** *6* (2), 1301-1306.

42.   Bottein, T.; Loizillon, J.; Grosso, D., Full Investigation of Angle Dependence in Dip-Coating Sol-Gel Films. *Journal of Physical Chemistry B* **2017,** *121* (25), 6220-6225.

43.   Islam, M. S.; Choi, W. S.; Lee, H.-J., Controlled Etching of Internal and External Structures of SiO2 Nanoparticles Using Hydrogen Bond of Polyelectrolytes. *ACS Applied Materials & Interfaces* **2014,** *6* (12), 9563-9571.

44.   Postek, M. T.; Vladár, A. E.; Purushotham, K. P., Does your SEM really tell the truth? How would you know? Part 2. *Scanning* **2014,** *36* (3), 347-355.

45.   Ren, Z.; Zhu, X.; Du, J.; Kong, D.; Wang, N.; Wang, Z.; Wang, Q.; Liu, W.; Li, Q.; Zhou, Z., Facile and green preparation of novel adsorption materials by combining sol-gel with ion imprinting technology for selective removal of Cu(II) ions from aqueous solution. *Applied Surface Science* **2018,** *435*, 574-584.

46.   Godiya, C. B.; Cheng, X.; Deng, G.; Li, D.; Lu, X., Silk fibroin/polyethylenimine functional hydrogel for metal ion adsorption and upcycling utilization. *Journal of Environmental Chemical Engineering* **2019,** *7* (1), 102806.

47.   Yuan, Q.; Li, N.; Chi, Y.; Geng, W.; Yan, W.; Zhao, Y.; Li, X.; Dong, B., Effect of large pore size of multifunctional mesoporous microsphere on removal of heavy metal ions. *Journal of Hazardous Materials* **2013,** *254-255*, 157-165.

CHAPTER 5 - Effects of Branched Polyethylenimine Molecular Weight on Kinetic Doping and Antibiofilm Efficacy

5.1 Abstract

Bacterial biofilms are associated with up to 80% of human bacterial infections and pose a significant threat to public health. Medical devices and implants can be especially susceptible to biofilm infection, with *S. epidermis* being the most common clinical isolate from these devices. Implant coatings have gained attention in recent literature for their ability to combat biofilm infections. Here, parameters for the kinetic doping of 1800 and 750000 MW branched polyethylenimine (BPEI) into silica sol-gel thin films are developed based on previous successful loading of 25000 MW BPEI. Using a ninhydrin assay, the solvent accessible amines of 25000 and 750000 MW BPEI doped films are found to be similar (a Ruhemann's purple absorbance of 1.8 and 1.6, respectively) while 1800 MW BPEI doped films have less (an absorbance of 1.1). SEM images of the films reveal drastic morphology differences between the films loaded with different molecular weights. The films' efficacy against *S. epidermis* biofilms are tested with a crystal violet assay, and all films proved to be effective in inhibiting biofilm formation (p-value < 0.05). The best dopant, 25000 MW BPEI, caused an 89% reduction in biofilm growth and surpassed the performance of the clinical antibiotic gentamycin (p-value < 0.003).

5.2 Introduction

Biofilms are a protected mode of bacterial growth that are still not fully understood,[1] yet they are associated with up to 80% of human bacterial infections.[2] In addition, over 65% of human infections are associated with bacterial biofilms that are often resistant to antibiotics and host immunity.[3] Medical device and implant infections are a major health concern and are mainly caused by *staphylococci*, aided in their infectious capacity by their ability to form biofilms.[4] *S. epidermis* is the most common clinical isolate from medical devices,[5-6] a normally benign bacterium that has gained recent attention due to the rise of nosocomial infections associated with it, resulting in an economic burden of approximately $2 billion per year.[7]

To combat these types of infections, localized treatment with antibiotics has become a common practice, especially for biofilm forming bacteria,[8-9] as bacteria in biofilms generally show enhanced resistance to antibiotics. The biofilms sometimes have a minimum inhibitory concentration of 100-1000 times that of the same planktonic bacteria,[10] making it extremely difficult to eradicate them completely with systemic antibiotics and causing reoccurring infection.[11-12] The interest in local antibiotic treatments has led to the development of beads[13] or coatings[14] that can be used with implantable medical devices. Due to silica's biodegradability and biocompatibility many researchers are interested in coatings made from silica sol-gel,[15-18] including thin film orthopedic implant coatings for controlled release of antibiotics to combat *staphylococcus* bacteria.[19] While this local release of antibiotics can help, other strategies are also needed

as the prevalence of antibiotic resistance continues to increase, and antibiotics becoming increasingly ineffective.[20]

Branched polyethylenimine (BPEI) in solution is known to inhibit the growth of methicillin-resistant staphylococcus epidermis (MRSE) biofilms, especially in synergy with β-lactams.[21] Different weights of BPEI are known to have different antibiotic activity and cytotoxicity toward mammalian cells, with higher molecular weights generally showing better antibiotic activity, but higher cytotoxicity.[22-23] This cytotoxicity prohibits the more effective higher molecular weight BPEI from being administered systemically. However, a previous study of kinetically-doped BPEI silica thin films has shown no evidence of BPEI release from the films and a significant retention of amine activity.[24] This could make it a promising coating for preventing biofilm formation on medical implants with limited cytotoxicity, as BPEI would be localized to the implant and not present a systemic danger. Additionally, BPEI has been shown to disrupt the extracellular polymeric substances (EPS) that allow biofilms to establish, instead of targeting specific proteins,[21] making resistance possibly harder to develop.

Using kinetic doping to load BPEI into silica sol gel thin films is a fast, inexpensive, and efficient way to produce surface coatings. Kinetic doping takes advantage of a stage of sol-gel film development where poly-condensation has progressed enough to produce a stable thin film, but not so much that molecules are unable to diffuse into the nascent film. This allows the introduction of a dopant molecule to the still-developing film by emerging it in a loading solution and allowing the dopant molecules to diffuse into the

film as it fully sets. This generally results in very high loading efficiency, with improved loading over the traditional methods of pre- and post-doping.[25-26] However, a previous study on the kinetic doping of BPEI has shown that molecular weight has a major impact on kinetic doping, with 600 g/mol or MW BPEI disrupting film formation completely.[24] To study different molecular weights of BPEI and their efficacy against biofilms, parameter optimization was needed. In this work, silica sol-gel thin films loaded with BPEI of three different molecular weights were produced via kinetic doping and the effect of molecular weight on loading parameters was observed. The films were then tested for anti-biofilm activity.

5.3   Methods

5.3.1   Materials and General Methods

Tetraethylorthosilicate (TEOS); 1800, 25000, and 750000 MW Branched Polyethylenimine (BPEI); crystal violet dye; gentamycin; and bacterial growth media were purchased from Sigma-Aldrich. Methicillin-resistant *Staphylococcus epidermidis* (MRSE) bacteria were purchased from the American Type Culture Collection (ATCC 35984). Phosphoric acid was purchased from EMD Millipore. Premium grade glass coverslips (22 mm × 22 mm × 170 μm) were purchased from Fisher Scientific. All chemicals and materials were used as received, with the exception of the glass coverslips, which were cleaned prior to use. All UV−vis spectra were obtained via a Shimadzu UV-2101PC UV−vis spectrometer. Scanning electron microscopy (SEM) images were obtained via a JEOL JSM-880 instrument with a 5 nm Au−Pd sputter-coated layer to examine the morphology of the thin film and measure the film thickness.

5.3.2   Preparation of Glass Coverslips

To remove any organic contaminants on the glass coverslip surface, the coverslips were sonicated in an acetone bath for 30 minutes and rinsed with Millipore water three times to remove all residual acetone. The coverslips were then sonicated in 10% w/v NaOH for another 30 minutes and rinsed with Millipore water five times to remove all residual NaOH. The coverslips then went through a final sonication in Millipore water for 30 minutes. The coverslips were then stored in Millipore water until use.

5.3.3   Preparation of Silica Sol

Silica sol was prepared by mixing a 1:8:7 molar ratio of TEOS:ethanol:water with phosphoric acid acting as a catalyst. A mixture of 55.9 mL of TEOS, 111.8 mL of ethanol, 31.7 mL of deionized water and 0.62 mL of 1% v/v phosphoric acid at room temperature were prepared for most coatings. The sol was then allowed to age for 20 hours at room temperature before use.

5.3.4   Preparation of BPEI-Doped Silica Sol-Gel Thin Films

Thin films were prepared by drain coating with a sol solution in accordance with our previous work.[24] After aging for 20 hours, the silica sol solution was transferred to a 250 mL beaker, elevated by a jack stand. A clean coverslip was dried with compressed air before it was immersed in the aged silica sol-gel coating solution while suspended from above. The sol solution was then drained at a rate of 1.36 cm/sec; the entire drain coating

is complete in less than 2 seconds. Immediately after the silica sol solution was drained, the jack stand was lowered until the newly coated coverslip was completely exposed to ambient air. The nascent thin film was allowed to age in ambient air for 7, 7.5, and 9.5 minutes for 750000, 25000, and 1800 MW BPEI, respectively, before it was transferred to a loading solution, where BPEI was allowed to load into the film via kinetic doping. The loading time was five days for 1800 MW BPEI, seven days for 25000 MW BPEI, and fourteen days for 750000 MW BPEI. The loading solution consisted of 1 mM 1800 or 25000 MW BPEI in 10 mM phosphate buffer, adjusted to pH 7.4 with phosphoric acid or 0.01 mM 750000 MW BPEI, adjusted to pH 7.4 with phosphoric acid. A lower concentration of 750000 MW without a buffer was used due to solubility issues with the larger molecular weight. Unloaded films were made by using a loading solution of 10 mM phosphate buffer adjusted to pH 7.4 with phosphoric acid.

5.3.5   Determination of BPEI Uptake Into Films

Detection of BPEI in the film was done qualitatively with a procedure based on the method for copper detection with BPEI by Wen et al.[27] using the sequestration of copper (II) by BPEI. This produced a dark blue color that could be seen on the film with the naked eye. Quantification of BPEI was performed by measuring BPEI depletion in the loading solution. BPEI uptake was determined by measuring the difference in absorbance of the loading solutions at 638 nm before and after kinetic doping.

5.3.6 Determination of Solvent Accessible Amines

Solvent accessible primary and secondary amines were quantified via the ninhydrin method of amine quantification, based on the procedure developed by Kaiser et al.[28] Briefly, solutions of 500 mg of ninhydrin dissolved in 10 mL of absolute ethanol, 80 mg of phenol dissolved in 20 mL absolute ethanol, and 2 mL of 0.001 M KCN in 100 mL pyridine were prepared. The loaded films together with the coverslips were broken into shards to reduce the solvent needed to cover the surface area and quantitavely transferred to a test tube. 750 μL of each of the three test solutions were added to the test tube and it was then stoppered and placed into a boiling water bath where the reaction was allowed to proceed for 5 minutes. The absorbance of this solution was then measured at 571 nm and compared across the different BPEI molecular weights.

5.3.7 Biofilm Inhibition of BPEI Films Assay

Biofilm inhibition was measured based on previous protocols,[10, 29-30] especially the protocol by Lam et al.[21] A subculture of MRSE 35984 was grown from the cryogenic stock on an agar plate overnight at 35 °C. Coverslips with BPEI loaded films were sterilized in 95% ethanol and placed in pre-sterilized 6-well plates with 1 film per well. Each well was then inoculated with 2.0 mL Cation-adjusted Mueller Hinton broth, plus 20 μL of a stock MRSE 35984 culture ($\sim 5 \times 10^5$ CFU/mL). Unloaded films and gentamycin (10μg/mL) were used as negative and positive controls, respectively. The plates were incubated at 35 °C for 24 h to form biofilms. Media and planktonic bacteria were removed by washing the thin films five times with water. Crystal violet solution

(0.1%) was used to stain the biofilm by adding 2.0 mL of the solution to each well for 15 min. The stained films were washed with water and 10% ethanol to get rid of excess crystal violet. The biofilms on each thin film were redissolved in 5.0 mL of 95% ethanol and absorbance at 550 nm was measured. Each assay was done in triplicate.

5.4   Results and Discussion

5.4.1   Loading of Different Molecular Weight BPEI

Different molecular weights of BPEI behave differently when kinetic doping is attempted. 25000 MW BPEI, but not 600 MW, has previously been successfully kinetically doped.[24] 600 MW BPEI proved disruptive to film formation at all delay times studied, leading us to postulate that molecular weight governed the rate of an unknown side-reaction while the nascent film is forming. This side reaction caused silica particle formation and destroyed the nascent film. To examine this phenomenon further, kinetic doping of 1800 and 750000 MW BPEI was tested. Parameters were optimized in order to produce films with a similar visual quality to 25000 MW films. Keeping the structural stability of the films similar sheds light on the extent of poly-condensation needed before the nascent film is allowed to come into contact with different BPEI dopants.

To keep the thickness of the films the same, the same drain speed was used for all three molecular weights. The delay time, defined at the time between coating of the substrate with the sol gel and introduction of the sample to the loading solution, is the major parameter under investigation. Delay time controls the extent of hydrolysis and condensation in the nascent film before the BPEI dopant comes into contact with it. With

a very short delay, BPEI can interact with the unreacted precursors in the film, forming

particles in solution instead of allowing the film to continue growing. On the other hand,

at long delay times, the cross-linking of the film is too extensive to allow dopant

molecules to diffuse in, leading to little to no doping.

We postulated that the side reaction of BPEI with the sol gel precursors that had

remaining alkoxide side-groups increased with decreasing molecular weight, which is

why the loading of 600 MW BPEI was always unsuccessful. If true, 1800 MW would

need longer delay times than 25000 MW, whereas 750000 MW would need shorter delay

time to produce films of similar visual quality. This proved to be true, with 1800 MW

BPEI needing an optimal delay time of 9.5 minutes, 25000 MW needing 7.5 minutes, and

750000 MW needing 7.0 minutes to produce films of similar visual quality. Figure 5.1

shows the similarity in visual quality of the films with these different delay times.
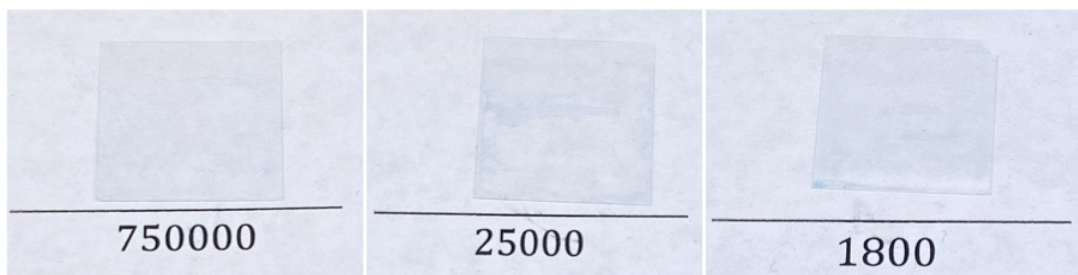
Figure 5.4 Thin films loaded with various molecular weights of BPEI using
different delay and loading times. Parameters were chosen to generate films with a
similar structural quality. Films have been loaded with copper (II) ions to help
visualize them.

5.4.2 Molecular Weight and Solvent Accessible Amines

A previous study has shown kinetic doping likely traps some of the BPEI inside of the thin film, rendering amines from deeply trapped BPEI solvent inaccessible.[24] Consequently, a modified ninhydrin test was used to compare the solvent accessible primary and secondary amines at each molecular weight by comparing the resulting absorbance measurements at 571 nm. If all the molecular weights are loaded at approximately the same molar concentration, more amines should be found on the highest molecular weight (750000) as compared to the medium molecular weight (25000) or the lowest molecular weight (1800). However, 25000 MW BPEI films have the highest amount of solvent accessible primary and secondary amines, with an absorbance measurement of 1.8 ± 0.3. 750000 MW BPEI films have a similar amount of amines, with an absorbance of 1.6 ± 0.6. 1800 MW BPEI films have the lowest amount, as predicted, with an absorbance of 1.1 ± 0.2.

The lower than expected loading for 750000 MW is likely due to a difference in BPEI loading concentration. Neither the 750000 MW nor the 1800 MW films had depleted enough of the polymer from the loading solution to have their concentration quantified by a copper test, as had been previously performed on 25000 MW.[24] This suggests concentrations of 750000 MW and 1800 MW BPEI in the films are lower than that of 25000 MW, most likely due to the dilution of the 750000 MW loading solution due to its high viscosity and the longer delay time needed for the 1800 MW BPEI to avoid complete thin film degradation. However, it is expected that the amount of solvent accessible amines should determine the efficacy of the films in biofilm inhibition. We

predicted that 25000 MW and 750000 MW films would behave similarly, with a negligible difference in the amount of solvent accessible amines between the two types of films. The 1800 MW films, with a much lower quantity of solvent accessible amines, should still inhibit biofilm formation, but to a lower extent than either of the higher molecular weights.

5.4.3   Molecular Weight and Effect on Film Structure

Loading conditions were chosen to produce visually similar films, with approximately the same minimal amount of damage to the film from interaction with the BPEI loading solution. SEM images were then taken to determine the thickness of the films and examine their morphology on a microscopic scale. The SEM images revealed drastic differences in thickness and morphology between the different molecular weights of BPEI and unloaded silica films.

In previous work, small morphology differences in unloaded films and 25000 MW BPEI loaded films were observed. Additionally, 25000 MW BPEI was shown to cause additional etching on the edge of the films, leading to very thin edges.[24] Examining cross-sectional SEM images, 1800 MW BPEI exhibits the same sort of etching on the edges, with the thinnest portion of the film measuring approximately 46 nm. However, the morphology of the film is very different than an unloaded film, being much smoother and showing less distinct colloidal formations, as can be seen in Figure 5.2. This is possibly due to a chemical reaction between the 1800 MW BPEI and any unreacted alkoxide side-groups in the nascent film. As lower molecular weights seem to react more quickly than

higher molecular weights with the nascent film, even a delay time that seemed to protect the film visually may not have eliminated enough unreacted alkoxide side-groups to prevent a reaction.

As reported in previous work, there are very small morphology differences between the
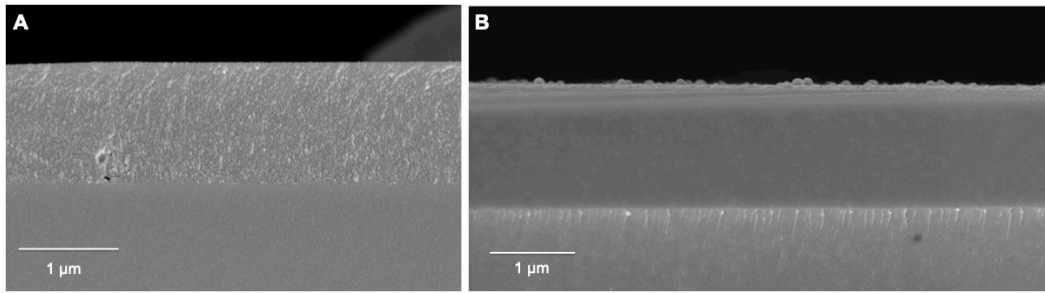
Figure 5.2 SEM images of A) unloaded silica thin film at 25000X magnification and B) silica thin film loaded with 1800 MW BPEI at 30000X magnification. The texture of the loaded film is much smoother, with less distinct colloidal particles

unloaded films and the films loaded with 25000 MW BPEI, which can be seen in Figure 5.3. While there is some difference in the appearance of the colloidal particles that make up the thin films, they are still distinct in the 25000 MW film. The only difference seems to be slightly larger particles in the loaded film.
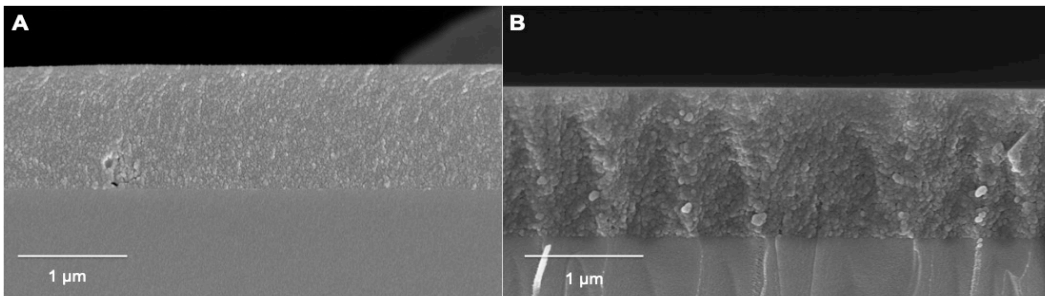
Figure 5.3 SEM images at 25000X magnification of A) unloaded silica thin film and B) silica thin film loaded with 25000 MW BPEI. The texture of the loaded film shows small changes in the colloidal particles as compared to the unloaded film, with slightly bigger particles in the loaded film.
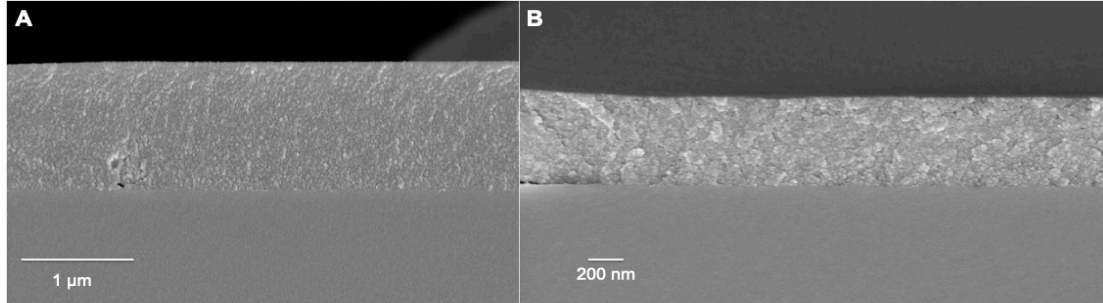
Figure 5.4 SEM images of A) unloaded silica thin film at 25000X magnification and B) silica thin film loaded with 750000 MW BPEI at 50000X magnification. The texture of the loaded film is very similar to that of the unloaded film, with distinct colloidal particles.

Finally, 750000 MW BPEI loaded films also demonstrated small morphology differences with the unloaded film. These differences can be seen in Figure 5.4. Distinct particles can be seen in the loaded film, but they seem to be fairly similar to the unloaded film. However, the 750000 MW films did not show etching at the edges to the same extent as the 1800 or 250000 MW films, with a measured thickness at the edge of the film of 409 nm. The unloaded films have an edge thickness of approximately 1 μm, which indicates that 750000 MW BPEI does etch the film, but much less vigorously than the other molecular weights. The films did, however, show an increased brittleness. Large portions of the films seem to have peeled back or broken off from the substrate in the middle, where it is thickest, during sample preparation. This either leaves no film behind to measure, shattered pieces of the film that are unattached or barely attached to the substrate, or film that seems to have been damaged but is still attached. This can be seen in Figure 5.5.

The damage to the 750000 MW loaded films seems to be limited to that molecular weight, as no unloaded films or other molecular weights exhibited the same extensive

damage from sample preparation. Additionally, no other films broke apart from sample preparation. (B)PEI is known to effect mechanical properties of complexes and gels, including increasing the brittleness depending on the concentration.[31-33] This may be a molecular weight dependent phenomenon, with 750000 MW BPEI creating much more brittle films.
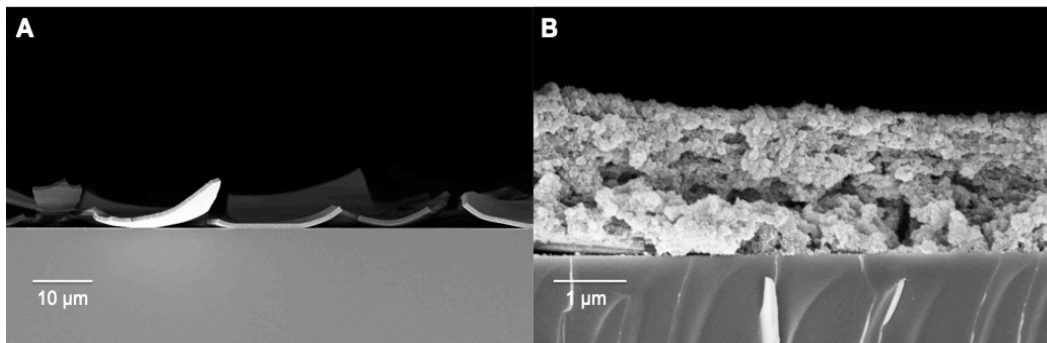
Figure 5.5 SEM images of A) fragments of silica thin film loaded with 750000 MW BPEI at 2500X magnification and B) damaged silica thin film loaded with 750000 MW BPEI at 30000X magnification. The damage occurred when samples were cut with a diamond tip knife in preparation for collecting SEM images.

Top-down images of the films were also taken to examine the surface morphology. These can be seen in Figure 5.6. The surface texture of the 25000 MW BPEI loaded film is closest to that of the unloaded film, in line with the cross-sectional morphology, with only a slight smoothing of the surface. Both 1800 MW and 750000 MW loaded films show a drastic change in surface texture. The colloidal particles are less distinct in the 1800 MW film, with what looks like connected groups of the particles and smooth groups interspersed with holes and divots. The 750000 MW film seems to be more textured, with a lot of the colloidal particles on the surface spaced apart. This may be the effect of etching on the surface, as 750000 MW BPEI is introduced to the film much earlier in its reaction process than the other molecular weights. It does not etch as much of the film, as

evidenced by the edge thickness, but it does still cause a decrease in film thickness. This

could be the cause of the surface morphology, with scattered colloidal particles remaining

after contact with BPEI.
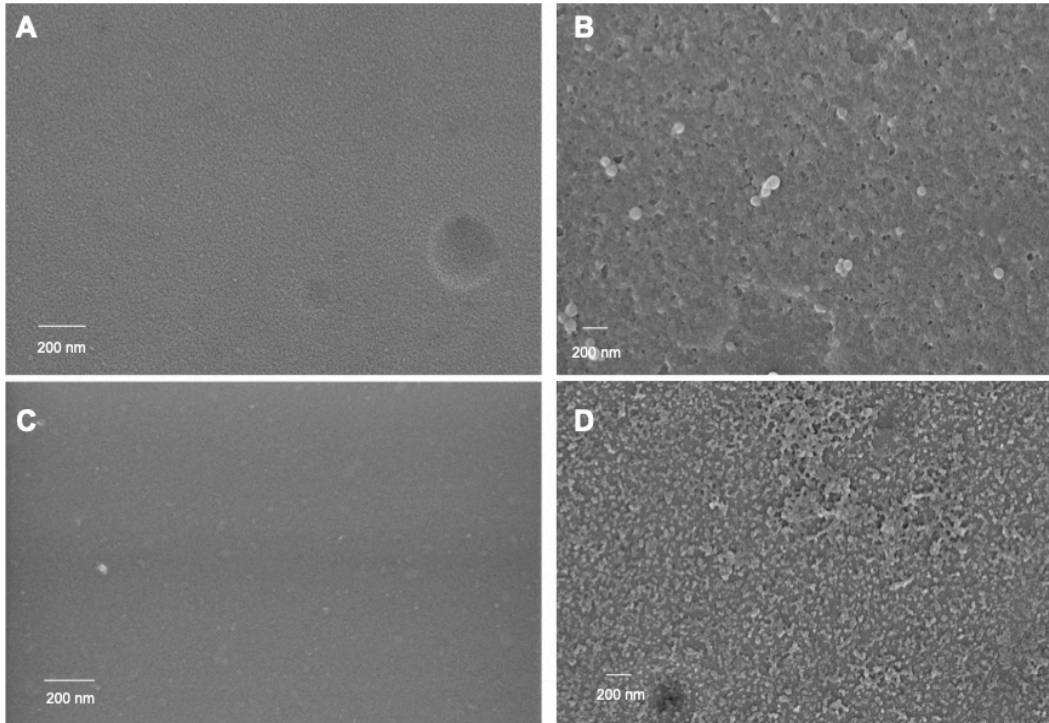
Figure 5.6 Top-down SEM images taken at 50000X magnification of films that are A) unloaded, B) loaded with 1800 MW BPEI, C) loaded with 250000 MW BPEI, and D) loaded with 750000 MW BPEI. The morphology of the 25000 MW BPEI film most closely resembles that of the unloaded film, with the other molecular weights exhibiting drastic deviations.

5.4.4   Molecular Weight and Biofilm Inhibition

The ability of the loaded films to inhibit the formation of MRSE 35984 biofilms was

studied *in vitro*. MRSE was inoculated into wells containing films loaded with different

molecular weights (with unloaded films to serve as controls). The results of a Student's t test indicate all molecular weights of BPEI inhibit biofilm formation ($n=3$ and p-value $<$ 0.01 for all molecular weights), as expected. 25000 MW BPEI shows the most biofilm inhibitory activity, a Student's t test indicating that it out-performs even gentamycin, the negative control ($n_{gentamycin} = 8$, $n_{25000} = 3$, p-value < 0.003). Images of biofilms grown on different molecular weight thin films with crystal violet staining and the OD 550 of the dissolved films are shown below in Figure 5.7.

The percent decrease in biofilm formation compared to the unloaded positive controls is highest for the 25000 MW film at 89%. The 750000 MW films perform equally with the antibiotic gentamycin, both resulting in a percent decrease of 76%. The 1800 MW films show the lowest biofilm inhibition with a 71% decrease. The ability of the films to inhibit biofilm growth follow the same trend as the available amines, with 25000 MW having the most solvent accessible amines and the greatest biofilm inhibition. The difference in efficacy between 25000 MW and 750000 MW is 57%, but this does not prove to be statistically significant in a Student's t test ($n = 3$, p-value > 0.05). The cause of the biofilm inhibition seems to be closely related to the number of solvent accessible amines, with statistically insignificant effect from molecular weight.
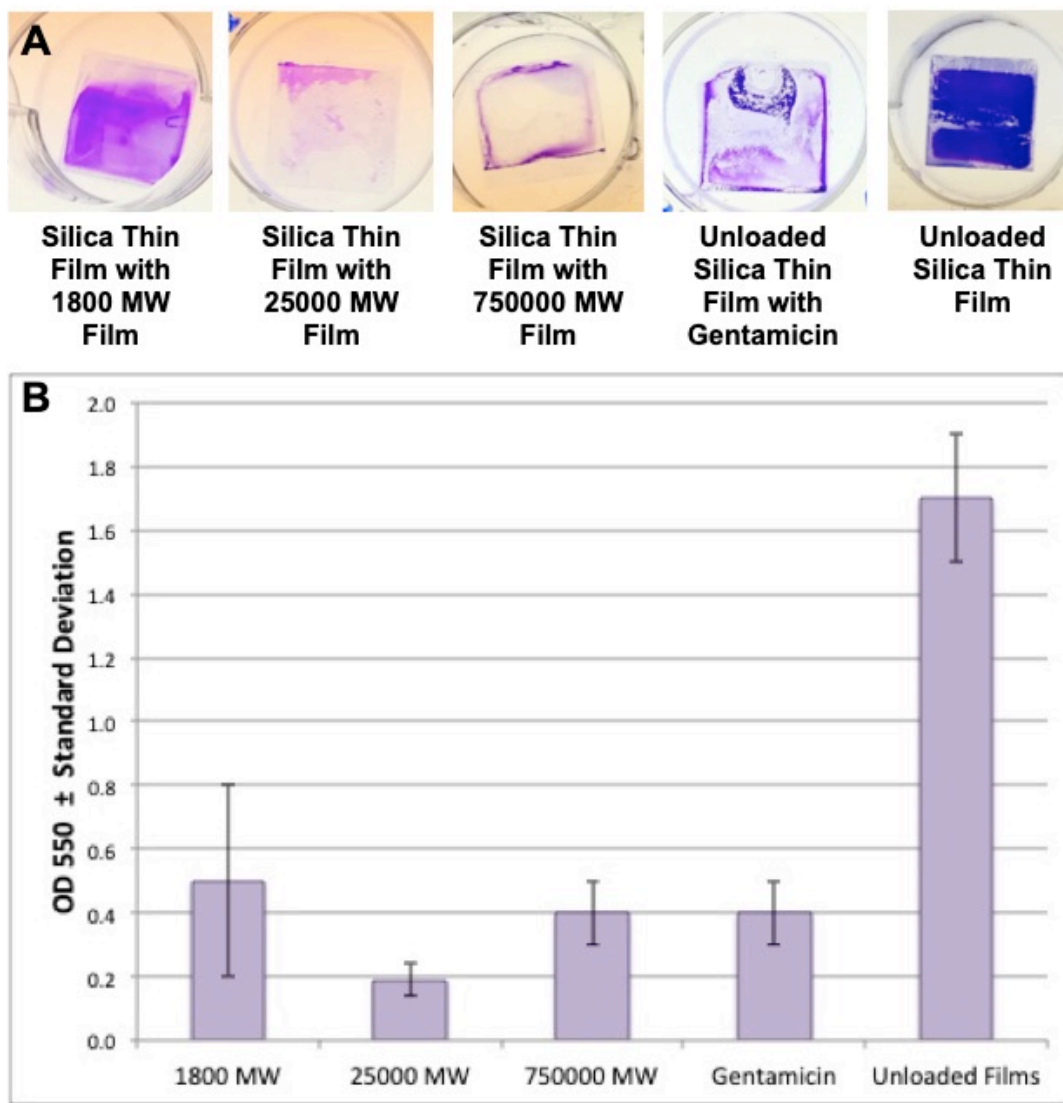
Figure 5.7 A) Films incubated with MRSE for 24 hours, then stained with crystal violet to visualize biofilm formation. B) The mean OD 550 of the dissolved biofilms formed on loaded thin films ($n \geq 3$), error bars denote standard deviation.

The standard deviation of the 1800 MW BPEI films is the highest in the biofilm inhibition assay, but the lowest in the ninhydrin assay for solvent accessible amines. Conversely, 25000 and 750000 MW BPEI films exhibit higher standard deviation in the ninhydrin assay than in the biofilm assays. This may be caused by low surface saturation of 1800 MW BPEI. Because the 1800 MW BPEI seems to cause the most change in

surface morphology, some of the amine groups could be reacting with the remaining TEOS precursor or unreacted alkoxide side-groups. The colloidal particles thought to create pores that entrap molecules could become fused, reacting with the amines on the 1800 MW BPEI so they can no longer serve as antibacterial cations and decreasing accessibility to amines that are already trapped. This would create portions of the film that have less solvent accessible amines than others, allowing biofilms to form more easily. The longer delay time is also expected to cause lower overall loading, which would also explain the decreased amount of amines. The higher molecular weights seem to react less with the silica itself, which may leave more unreacted amines on the surface to interact with the bacteria. However, the shorter delay time could create a more varied film environment during loading, which would explain the higher standard deviation in the amine amount. Nevertheless, the loading would be concentrated and even enough to consistently inhibit biofilm formation, explaining their high efficacy and lower standard deviation in the crystal violet assay.

Previous solution studies have shown molecular weight effects the antibiotic or anti-biofilm efficacy of BPEI,[22-23, 34] with higher molecular weights generally being more effective. This is likely due to the hydrophobicity difference between molecular weights of BPEI, with higher molecular weights having hydrophobic interiors that lead to membrane penetration and damage to both bacterial and human cells.[22] With the BPEI loaded into a solid substrate, this penetration would be limited, if it could occur at all. Instead, the antibacterial mechanism would likely be the amine covered, cationic surface. The measured solvent accessible amines predict the antibiofilm efficacy of the films,

regardless of the molecular size of the polymer. This indicates that the surface accessible amines are the major cause of the biofilm inhibition in the films.

5.5 Conclusions

Biofilms pose a large threat to human health, with antibiotic resistance on the rise.[2, 11-12, 30] Utilizing kinetic doping, BPEI, a polymer known to disrupt biofilms, can be loaded into silica sol-gel thin films. The larger molecular weight BPEIs examined exhibit better biofilm inhibition, but require a longer loading time. The different molecular weight loaded films also exhibit much different cross-sectional and surface morphology, giving some insight into how they may interact with the silica sol gel. The anti-biofilm efficacy of the BPEI loaded films appears to be a function of the solvent accessible amines on the silica thin films. The 25000 MW films showed greater anti-biofilm efficacy than the antibiotic gentamycin, showing a reduction in biofilm formation of 89%, but showed no statistical difference with the 750000 MW films. The 1800 MW films showed the worst performance, but still reduced biofilm formation by 71%. Kinetic doping allows fast, inexpensive, and facile functionalization of BPEI loaded silica sol-gel thin films that are proven to be effective in the fight against biofilm formation.

5.6 References

1.   Hall-Stoodley, L.; Costerton, J. W.; Stoodley, P., Bacterial biofilms: From the natural environment to infectious diseases. *National Reviews Microbiology* **2004,** *2* (2), 95-108.

2.   Roemling, U.; Balsalobre, C., Biofilm infections, their resilience to therapy and innovative treatment strategies. *Journal of Internal Medicine* **2012,** *272* (6), 541-561.

3.   Olwal, C. O.; Ang'ienda, P. O.; Onyango, D. M.; Ochiel, D. O., Susceptibility patterns and the role of extracellular DNA in Staphylococcus epidermidis biofilm resistance to physico-chemical stress exposure. *BMC Microbiology* **2018,** *18*, 40/1-40/13.

4.   Arciola, C. R.; Campoccia, D.; Speziale, P.; Montanaro, L.; Costerton, J. W., Biofilm formation in Staphylococcus implant infections. A review of molecular mechanisms and implications for biofilm-resistant materials. *Biomaterials* **2012,** *33* (26), 5967-5982.

5.   Nery, P. B.; Fernandes, R.; Nair, G. M.; Sumner, G. L.; Ribas, C. S.; Menon, S. M.; Wang, X.; Krahn, A. D.; Morillo, C. A.; Connolly, S. J.; Healey, J. S., Device-related infection among patients with pacemakers and implantable defibrillators: incidence, risk factors, and consequences. *Journal of Cardiovascular Electrophysiology* **2010,** *21* (7), 786-90.

6.   Percival, S. L.; Suleman, L.; Vuotto, C.; Donelli, G., Healthcare-associated infections, medical devices and biofilms: risk, tolerance and control. *Journal of Medical Microbiology* **2015,** *64* (Pt 4), 323-34.

7.   Otto, M., Staphylococcus epidermidis - the 'accidental' pathogen. *National Reviews Microbiology* **2009,** *7* (8), 555-567.

8.   Izakovicova, P.; Borens, O.; Trampuz, A., Periprosthetic joint infection: current concepts and outlook. *EFORT open reviews* **2019,** *4* (7), 482-494.

9.   Metsemakers, W.-J.; Fragomen, A. T.; Moriarty, T. F.; Morgenstern, M.; Egol, K. A.; Zalavras, C.; Obremskey, W. T.; Raschke, M.; McNally, M. A.; Fracture-Related Infection consensus, g., Evidence-Based Recommendations for Local Antimicrobial Strategies and Dead Space Management in Fracture-Related Infection. *Journal of orthopaedic trauma* **2020,** *34* (1), 18-29.

10.   Ceri, H.; Olson, M. E.; Stremick, C.; Read, R. R.; Morck, D.; Buret, A., The Calgary biofilm device: new technology for rapid determination of antibiotic susceptibilities of bacterial biofilms. *Journal of Clinical Microbiology* **1999,** *37* (6), 1771-1776.

11.   Stewart, P. S.; William Costerton, J., Antibiotic resistance of bacteria in biofilms. *The Lancet* **2001,** *358* (9276), 135-138.

12.   de la Fuente-Núñez, C.; Reffuveille, F.; Fernández, L.; Hancock, R. E. W., Bacterial biofilm development as a multicellular adaptation: antibiotic resistance and new therapeutic strategies. *Current Opinion in Microbiology* **2013,** *16* (5), 580-589.

13.   Howlin, R. P.; Brayford, M. J.; Webb, J. S.; Cooper, J. J.; Aiken, S. S.; Stoodley, P., Antibiotic-loaded synthetic calcium sulfate beads for prevention of bacterial

colonization and biofilm formation in periprosthetic infections. *Antimicrobial agents and chemotherapy* **2015,** *59* (1), 111-120.

14.   Jang, C. H.; Park, H.; Cho, Y. B.; Choi, C. H., Effect of vancomycin-coated tympanostomy tubes on methicillin-resistant Staphylococcus aureus biofilm formation: in vitro study. *The Journal of Laryngology & Otology* **2010,** *124* (6), 594-598.

15.   Ciriminna, R.; Fidalgo, A.; Pandarus, V.; Beland, F.; Ilharco, L. M.; Pagliaro, M., The Sol-Gel Route to Advanced Silica-Based Materials and Recent Applications. *Chemistry Review (Washington, DC, U. S.)* **2013,** *113* (8), 6592-6620.

16.   Owens, G. J.; Singh, R. K.; Foroutan, F.; Alqaysi, M.; Han, C.-M.; Mahapatra, C.; Kim, H.-W.; Knowles, J. C., Sol–gel based materials for biomedical applications. *Progress in Materials Science* **2016,** *77*, 1-79.

17.   Martínez-Ibáñez, M.; Juan-Díaz, M. J.; Lara-Saez, I.; Coso, A.; Franco, J.; Gurruchaga, M.; Suay Antón, J.; Goñi, I., Biological characterization of a new silicon based coating developed for dental implants. *Journal of Materials Science: Materials in Medicine* **2016,** *27* (4), 80.

18.   Romero-Gavilan, F.; Araújo-Gomes, N.; Sánchez-Pérez, A. M.; García-Arnáez, I.; Elortza, F.; Azkargorta, M.; de Llano, J. J. M.; Carda, C.; Gurruchaga, M.; Suay, J.; Goñi, I., Bioactive potential of silica coatings and its effect on the adhesion of proteins to titanium implants. *Colloids and Surfaces B: Biointerfaces* **2018,** *162*, 316-325.

19.   Bhattacharyya, S.; Agrawal, A.; Knabe, C.; Ducheyne, P., Sol-gel silica controlled release thin films for the inhibition of methicillin-resistant Staphylococcus aureus. *Biomaterials* **2014,** *35* (1), 509-517.

20.   Dadgostar, P., Antimicrobial Resistance: Implications and Costs. *Infection and drug resistance* **2019,** *12*, 3903-3910.

21.   Lam, A. K.; Wouters, C. L.; Moen, E. L.; Pusavat, J.; Rice, C. V., Antibiofilm Synergy of β -Lactams and Branched Polyethylenimine against Methicillin-Resistant Staphylococcus epidermidis. *Biomacromolecules* **2019,** *20* (10), 3778-3785.

22.   Foxley, M. A.; Wright, S. N.; Lam, A. K.; Friedline, A. W.; Strange, S. J.; Xiao, M. T.; Moen, E. L.; Rice, C. V., Targeting Wall Teichoic Acid in Situ with Branched Polyethylenimine Potentiates β -Lactam Efficacy against MRSA. *ACS Medicinal Chemistry Letters* **2017,** *8* (10), 1083-1088.

23.   Gibney, K. A.; Sovadinova, I.; Lopez, A. I.; Urban, M.; Ridgway, Z.; Caputo, G. A.; Kuroda, K., Poly(ethylene imine)s as Antimicrobial Agents with Selective Activity. *Macromolecular Bioscience* **2012,** *12* (9), 1279-1289.

24.   Jensen, J. M.; Yip, W. T., Amine Functionalization of Silica Sol–Gel Thin Films via Kinetic Doping: A Novel, Green Approach. *ACS Omega* **2019,** *4* (20), 18545-18554.

25.   Crosley, M. S.; Yip, W. T., Silica Sol-Gel Optical Biosensors: Ultrahigh Enzyme Loading Capacity on Thin Films via Kinetic Doping. *Journal of Physical Chemistry B* **2017,** *121* (9), 2121-2126.

26.   Campbell, A. L. O.; Lei, Q.; Tak Yip, W., Kinetic approach to hyper-doped optical quality thin films. *Chemical Communications (Cambridge, U. K.)* **2014,** *50* (66), 9321-9324.

27.   Wen, T.; Qu, F.; Li, N. B.; Luo, H. Q., A facile, sensitive, and rapid spectrophotometric method for copper(II) ion detection in aqueous media using polyethyleneimine. *Arabian Journal of Chemistry* **2017,** *10*, S1680-S1685.

28.   Kaiser, E.; Colescott, R. L.; Bossinger, C. D.; Cook, P. I., Color test for detection of free terminal amino groups in the solid-phase synthesis of peptides. *Analytical Biochemistry* **1970,** *34* (2), 595-598.

29.   Ceri, H.; Olson, M.; Morck, D.; Storey, D.; Read, R.; Buret, A.; Olson, B., The MBEC assay system: multiple equivalent biofilms for antibiotic and biocide susceptibility testing. *Methods Enzymol.* **2001,** *337* (Microbial Growth in Biofilms, Part B), 377-385.

30.   Olson, M. E.; Ceri, H.; Morck, D. W.; Buret, A. G.; Read, R. R., Biofilm bacteria: formation and comparative susceptibility to antibiotics. *Canadian Journal of Veterinary Research* **2002,** *66* (2), 86-92.

31.   Duan, Y.; Wang, C.; Zhao, M.; Vogt, B. D.; Zacharia, N. S., Mechanical properties of bulk graphene oxide/poly(acrylic acid)/poly(ethylenimine) ternary polyelectrolyte complex. *Soft Matter* **2018,** *14* (21), 4396-4403.

32.   Ding, Y.; Wang, J.; Wong, C. S.; Halley, P. J.; Guo, Q., Synthesis, characterization and biocompatibility of novel biodegradable cross-linked copolymers

based on poly(propylene oxide) diglycidyl ether and polyethylenimine. *Journal of Biomaterials Science, Polymer Edition* **2011,** *22* (4-6), 457-473.

33.   Suhaila, M.; Salleh, A. B., Physical properties of polyethyleneimine-alginate gels. *Biotechnology Letters* **1982,** *4* (9), 611-14.

34.   Foxley, M. A.; Friedline, A. W.; Jensen, J. M.; Nimmo, S. L.; Scull, E. M.; King, J. B.; Strange, S.; Xiao, M. T.; Smith, B. E.; Thomas, K. J., III; Glatzhofer, D. T.; Cichewicz, R. H.; Rice, C. V., Efficacy of ampicillin against methicillin-resistant Staphylococcus aureus restored through synergy with branched poly(ethylenimine). *Journal of Antibiotics* **2016,** *69* (12), 871-878.